LIMITATIONS IN GEOPHYSICAL PROCESSING AND INTERPRETATION: THREE CANADIAN CASE STUDIES

LIMITATIONS IN GEOPHYSICAL PROCESSING AND INTERPRETATION: THREE CANADIAN CASE STUDIES

By

MADELINE DANA LEE, B.Sc.

A Thesis

Submitted to the School of Graduate Studies

in Partial Fulfillment of the Requirements

for the Degree

Master of Science

McMaster University

MASTER OF SCIENCE (2008)	McMaster University
(Earth and Environmental Sciences)	Hamilton, Ontario

TITLE:	Limitations in Geophysical Processing and Interpretation
AUTHOR:	Madeline Dana Lee, B.Sc. (McMaster University)
SUPERVISOR:	Professor W.A. Morris
NUMBER OF PAGES:	xvi , 124

ABSTRACT

With an increasing demand on natural resources, more efficient prospecting techniques need to be developed. One important tool is geophysical methodologies. As technology develops so do these methods and availability of high-resolution information; however if this information is not properly corrected biased results are achieved. This thesis intends to explore common limitations faced by modern geophysical surveys.

Processing and interpreting of geophysical data is often accomplished in frequency domain due to speed and efficiency; however this often leads to non-geologically correct results. A spatial domain filter based on potential field signal curvature analysis is a proposed alternative. By isolating specific curvatures, one is isolating specific frequencies, which are generated by sources at particular depths. The method was applied to synthetic and real-world datasets. Following filtering two analytic routines were applied, which showed that the spatially filtered datasets provided cleaner results.

Terrain corrections have always been applied to gravity datasets, but rarely are terrain corrections implemented as a pre-processing step in magnetic survey interpretation. Therefore, interpretations based on anomalies from non-corrected magnetic data may be of non-geological features. In a magnetic survey conducted in the mid-eighties, magnetic lows were associated with alteration; however, at that time of initial interpretation no terrain correction was applied. This dataset was revisited and terrain corrected, which showed that the magnetic lows were associated with unaccounted bathymetry.

The Bathurst Mining Camp (BMC) is one of Canada's most important base metal mines, but is threatened by a fluctuating mineral resources market. By using high resolution geophysical surveys potential mineral reserves may be located. However, in order to do so a better understanding of geology is necessary, which is often difficult due to limited outcrops. Through the processing and interpretation of recent geophysical datasets, a revised geological map of a selected portion of the BMC has been developed.

ACKNOWLEDGEMENTS

I would first like to thank my supervisor Dr. W. A. Morris and Dr. H. Ugalde, who provided months of advice, support, and guidance throughout this project. Their intellectual contributions to this project are invaluable. They both show a passion for geophysical research, the progression of science, and support of all upcoming geophysicists.

Thank you to S. Underhay, V. Tschirhart, and B. Spicer, members of the McMaster Applied Geophysical and Geological Imaging Center (M.A.G.G.I.C) for their support, laughs, and contributions.

I greatly appreciate the contribution and time set forth by my thesis committee, Dr. J. Boyce and Dr. U. Riller. The overall project was improved courtesy of their constructive criticisms.

Thank you to Xstrata Nickel (Raglan) and Paterson, Grant, and Watson Ltd. (PGW) companies that supported me in my research while I worked part-time. It is industry support of academics that allows for the development of interdisciplinary projects. Furthermore, I would like to thank all industry and government members who either provided datasets, financial support or guidance. These include the Geological Survey of Canada, Energy and Natural Resources of New Brunswick, and Xstrata Zinc. It is my hope that my research may provide insight into new methods and developments of mineral exploration.

Finally, I would like to especially thank my friends and family. Without your continued support, love and listening over the last 12 months, this project would not have been possible.

TABLE OF CONTENTS

LIST OF FIGURES

Chapter 2

Chapter 3

Chapter 4

LIST OF TABLES

Chapter 2

Chapter 3

Chapter 4

PREFACE

Concepts

For Chapter 2 and Chapter 3, W.A. Morris introduced concepts based on involvement in previous related projects. Concept for Chapter 4 was introduced by the Geological Survey of Canada and Energy and Natural Resources of New Brunswick.

Datasets

All real-world datasets were acquired from industry members (Morris Magnetics Ltd.) or government organizations (Geological Survey of Canada and the Department of Energy and Natural Resources of New Brunswick). S. Underhay and V. Tschirhart digitized all magnetic susceptibility, Total Magnetic Intensity and topographic datasets necessary for Chapter 3. All synthetic datasets used in Chapter 2 were generated by M. Lee.

Methodology

Methods were collaboratively developed by M. Lee, W.A. Morris, and H. Ugalde based on previous project involvement or from existing related publications. The processing, forward and inversion models, interpretations were completed by M. Lee. Except in the case of Chapter 3, where W. A. Morris generated the regional scale magnetic susceptibility model in Encom's Modelvision and in Chapter 4, where H. Ugalde completed pre-processing routines on the Bathurst Total Magnetic Intensity and radiometric datasets.

Written Content and Figures

Primary content for each chapter was written by M. Lee. W.A. Morris and H. Ugalde reviewed all final written content and figures. Throughout the entire project, W.A. Morris and H. Ugalde provided intellectual discussion and guidance and had a supervisory role in all completed work.

CHAPTER ONE

Introduction

An increased consumption of natural resources coupled with exhaustion of mineral reserves has placed great amounts of pressure on the Canadian mining sector. As such, new exploration methods are being developed in order to quickly and efficiently locate new economical resources. Critical to these new exploration methods is geophysics. Geophysical acquisition, processing, and interpretation continually develop as technology does. Presently, large amounts of geophysical datasets are being acquired and at times it is difficult to keep up with all associated processing and interpretations. Therefore, new techniques are being developed to efficiently resolve these large geophysical datasets. However, with a quick turnaround often required, these techniques may not be fully processed or properly implemented which will cause final misinterpretation. The limitations of these techniques need to be addressed in order to determine appropriate strategies to minimize them.

This thesis intends to explore limitations imposed by some standard geophysical routines and in some cases strategies in which to minimize these limitations will be discussed. Three studies are presented:

1. Applications of curvature analysis as a spatial domain filter in potential field interpretations as an alternative to Fast Fourier Transforms,

2. The rationale for applying magnetic terrain corrections over a non-homogeneous granitic pluton,

3. Application of high-resolution airborne and ground geophysical surveys over a volcanic massive sulfide deposit.

Chapter 2 of this thesis investigates the limitations imposed by Fast Fourier Transforms on geological interpretations. With a demand for quicker processing routines on larger geophysical datasets, the preferred domain in which to conduct these processing schemes is frequency. However, frequency domain interpretations impose many limitations that produce results which do not necessarily reflect geology. As such, this chapter proposes an alternative approach that implements the curvature analysis of a potential field signal. The curvature of a potential field signal is inextricably linked to an associated frequency and wavelength. Therefore by isolating a specific curvature, one is actually isolating a specific wavelength or frequency. This curvature isolation routine is accomplished through regional-residual separation; the regional (large scale trends) is derived through a coarse grid cell size and the residual (local scale trends) is calculated through the subtraction of the desampled grid from the original full dataset. Not only does the grid cell size routine allow for geologically sound results, but it allows for non-biased results in secondary processing methods. The results produced by analytic routines, such as tilt-depth method (Salem et al., 2007a; Salem et al., 2007b) and Euler deconvolution (Reid, 1990; Keating and Pilkington, 2004) suffer from any limitations that are carried through from initial processing. By first implementing the grid cell segregation routine, these limitations are not carried through and processing may be conducted on filtered data.

Chapter 3 of this thesis explores the effect of source-sensor separation. All geophysical surveys are conducted at some height above surface as such a significant physical interface exists between the source and the air. In the case of magnetics, this interface causes significant anomalous results in the final dataset. When this terrain effect is not taken into consideration, anomalies assumed to be caused by geological sources may in fact be due to this varying source-signal separation. Terrain effects are explored through the results of a ground magnetic survey conducted over a structurally heterogeneous granite pluton near Atikokan, Ontario.

Chapter 4 presents a case study on the Bathurst Mining Camp in New Brunswick, Canada, which is a volcanic massive sulfide deposit and one of Canada's largest contributors to base mineral reserves. The Bathurst Mining Camp is the result of an ancient back-arc basin and displays complex multi-generational folding, faulting, and thrusting of five geological blocks and slivers. Unfortunately, most of this complex geology is lost to significant vegetation and glacial overburden. Therefore, geophysical surveys play a critical role in the assessment of near-surface and subsurface geology. This chapter re-evaluates the existing geological map over a small portion of the Bathurst Mining Camp using high-resolution helicopter-borne magnetic, electromagnetic, and radiometric survey data in conjunction with a ground gravity survey dataset.

The following section provides an overview on geophysical surveying, more specifically airborne magnetics due to the emphasis based on this survey method in all chapters. Furthermore, all applicable processing techniques used in this thesis will be discussed.

Geophysical Surveying

With an increased demand for natural resources, especially metals and oil and gas, geophysical methodologies have been greatly developed through increased detection sensitivity and overall reliability. These developments are further increased with new innovations in technology – more specifically acquisition instruments and computer processing algorithms.

The natural resources mentioned above are controlled by subsurface structure and geophysics is the most time effective and efficient means to gain knowledge on these structures. Since geological physical properties are so variable, there are a number of geophysical methods that can be applied depending on the intended geology being studied. These include: Gravity, magnetic, seismic, electrical, electromagnetics, well logging and radioactivity (Telford, 1976). Each method employs different acquisition and processing methods dependant on the physical property being measured.

Magnetic Surveying

The study of Earth's magnetism is the most versatile and longest studied facet of geophysical research and has been extensively used for locating magnetic ore deposits since the mid-seventeenth century (Telford, 1976; Sharma, 1997). The primary objective in studying a magnetic field is to better understand subsurface geology (Thomson, 2004). This is accomplished through non-invasive magnetic mapping of the distribution of surficial magnetization.

Magnetics and gravity are both potential fields, however magnetic surveying is often chosen over gravitational means due to the cheap, easy and quick acquisition of magnetic field measurements. That being said, precise interpretation of magnetic survey data is by far more difficult than those of gravity (Telford, 1976).

Elementary Theory

All magnetic material will produce a magnetic field, which are invisible lines of force. If this magnetic material is simplified to a generic bar magnetic, the magnetic field will be strongest at the two poles due to an increased magnetic flux (smaller separation between lines of force). Continuing with this simplified bar magnet model, all sources produce a magnetic dipole and it is only under the condition of infinitely separated poles can a monopole exist.

Magnetic force (F) is governed by Coulomb's law where the force is inversely proportional to both the magnetic permeability and physical distance between poles. *Magnetic field strength* (H) is defined by Amperes law and represents the magnitude of the force acting on a magnetic pole in a magnetic field of strength (F) (Sharma, 1997).

Field intensity (J) is a measure of pole strength per volume. When a magnetic field is very weak, J is proportional to the magnetizing field (H):

$$J = \kappa H$$

where *magnetic susceptibility* (κ) acts as the proportionality constant. Magnetic susceptibility (κ) is the ability of a material to become magnetized under an applied magnetic field (H). Magnetic susceptibility is a dimensionless quantity due to J and H having the same units. *Magnetic induction* (B) is the summation of magnetic field strength (H) or inducing field and the induced magnetization J (Sharma, 1997).

$$B = \mu_o(H+J)$$

where μ_o is the permeability of free space and has a value of approximately 1 for air. Magnetic induction is a vector quantity but most magnetometers only measure the amplitude, which is known as the *Total Magnetic Field* (Sharma, 1997).

The typical units for magnetics are either in SI or cgs units. The common SI unit is nanoTesla (nT) while the cgs unit of gamma is used, where 1 gamma = 1nT. Magnetic susceptibility (κ) may be expressed in either SI or cgs units (Sharma, 1997), where:

$$\kappa(SI) = 4\pi\kappa\ (cgs)$$

There are two types of magnetizations: *Induced* and *remanent*. Induced magnetization (J_i) is the alignment of the electron spin axes with the applied direction (H) and also depends on magnetic susceptibility (κ) (Sharma, 1997). Remanent magnetization (J_r) is considered a permanent magnetization and may be acquired in a number of different ways. The most common, thermoremanent magnetization (TRM) occurs when a rock unit cools and acquires the orientation of the ambient (geomagnetic) field prevalent at the time and location of formation (Parasnis, 1962).

Earth's Magnetic Field

Since airborne magnetic surveys depend on the application of an ambient field to highlight surface magnetization, the Earth's field plays a critical role in survey acquisition and processing. The magnetic field has two important directional parameters: *inclination* and *declination*. The inclination of the magnetic of field is with respect to horizontal. This is important to take into consideration when calculating the summation of magnetic vectors in the production of an anomaly. Declination is the angle between direction to magnetic pole and geographic pole (Telford, 1976; Sharma, 1997).

The Earth's magnetic field has three components: Main field, external field, and a crustal field. The *main field* is known as the geodynamo and is the result of convection current in Earth's liquid core coupled with Earth's rotation. The magnitude of this main field is highly variable across the entire surface of the Earth, varying from 25 000nT at the equator to 65 000nT at the poles. The *external* field is caused by the bombardment of the Sun's electromagnetic energy with magnetic field of Earth (solar wind). This external field is highly variable due to Earth's rotation causing diurnal variations. As such it is a necessity that these diurnal variations be recorded by a base station magnetometer for subsequent corrections. Finally, all of Earth's rocks contain some degree of magnetization; however, beyond the *Curie depth* magnetization can no longer occur (Telford, 1976; Sharma, 1997).

Magnetometers

Magnetometers are used in magnetic surveys and measure the magnetic flux density. The three primary types of magnetometers are: fluxgate, proton precession, and alkali-vapour. In the case of this thesis, the acquired data was done so using a cesium vapour magnetometer (Chapter 2 and 4) and a proton precession magnetometer (Chapter 3). The former is a type of alkali-vapour magnetometer. An alkali-metal (in this case cesium) vapour is bombarded by ultraviolet light, which causes a change in energy state of the electrons. The rate at which the electrons return to their initial energy state will be a function of the geomagnetic field. This instrument has the greatest amount of sensitivity (0.001nT). The proton precession magnetometer uses the concept that the Earth's geomagnetic can be measured by the precession frequency or spin of a proton. This achieved through energizing a hydrogen based fluid by an electric current. The sensitivity of this instrument is 0.01nT. (Chapman and Hall, 1962; Sharma, 1997)

Corrections and Enhancement Methods

Reduction-to-Pole (RTP)

The primary objective in reduction-to-pole processing is to remove distortion effects on a magnetic signal that are caused by an inclined magnetic field. It essentially causes the signal to represent what it would have looked like under a perfectly vertical ambient field (Blakely, 1995; Sharma, 1997). This is particularly helpful in locating anomalies over their respective sources and is required in certain analytic routines (i.e. tilt-depth method).

International Geomagnetic Reference Field (IGRF)

The geomagnetic field is recalculated every five years because of secular variations, which is the change in the magnetic pole over time. This calculated geomagnetic field is termed the *International Geomagnetic Reference Field*. The IGRF is taken into account in order to correct a magnetic dataset for normal variations of the geomagnetic field with latitude and longitude (Blakely, 1995; Sharma, 1997).

Terrain Correction

Terrain effects are most commonly taken into consideration during gravity surveys. This is because gravity is very sensitive to the amount of mass under the observation point, which is often a function of topography. Terrain effects are implemented as a last step in gravity corrections as typically Bouguer anomalies are not sufficient enough to correct in very rugged terrains (Sharma, 1997). Terrain corrections are not often utilized in magnetic datasets, however as will be discussed in Chapter 3, terrain effects should not be disregarded in magnetic survey interpretation. Terrain effects in magnetics are primarily due to source-sensor separation; magnetic lows will be generated by an increase in source-sensor separation and magnetic highs will be generated by a decrease in source-sensor separation (Flis and Cowan, 2000). Furthermore, since a magnetic signal is affected by the interface of contrasting magnetic susceptibilities, with the greatest occurring between air and rock. False anomalies may be recorded by the magnetometer due to this strong interface and further exaggerated by source-sensor separation (Ugalde and Morris, 2008).

Levelling and microlevelling

Airborne geophysical surveys are subjected to many changing parameters, including varying ambient fields (diurnal variations), instrument variations, and variations in flying height between flight and tie lines. These effects may cause corrugation effects in the recorded dataset. Levelling corrections may be applied in one of two ways: either conventional or empirical means (Thomson, 2004). Conventionally, corrections are applied by determining an average plane surface at which to correct all flight and tie line variations. Empirical corrections may be conducted using filtering methods that reduce high-frequency noise (Minty, 1991).

Filtering

Sometimes data may need to be filtered, whether one is interested in isolating signal or noise. Noise may be suppressed or signal may be amplified through many data-processing wavelength filter algorithms. A filter may be designed to pass all features of a specific wavelength without distortion while attenuating all other anomalies. Or a filter may be designed to reject all features of a specific wavelength. When the filter is designed to pass all wavelengths below a certain cut off this is deemed a *low-pass filter*. In the case of the opposite where all wavelengths above a certain cutoff are allowed to pass, it is a *high-pass filter*. Finally, one may create an upper and lower cutoff, constraining the passing wavelength from both directions, in essence creating a *band-pass-filter* (Sharma, 1997).

Filters may be conducted in different domains – the reference frame in which a mathematical function exists. The two domains are either space or frequency. Spatial domains, also known as the time domain are where distance is the independent variable while the physical quantity is dependant variable. In the frequency domain, distance has been transformed to some function of frequency, which may either be spatial or a temporal frequency. The dependent variable is the amplitude and phase of the frequency (Blakely, 1995). Both domains share any number of advantages and disadvantages and it relies on the user to make a decision as to which domain to conduct filtering dependent on the dataset undergoing t the filtering.

Regional-residual separation

Regional-residual separation is based on the fundamental concept of specific wavelength isolation. A short wavelength will only be produced by a small or shallow source. On the other hand, a long wavelength is primarily caused by deep or large features. An important point is that a short wavelength can only be caused by near surface features while a long wavelength may be caused by near surface (spatially large) or deep-seated sources. These long wavelength anomalies are termed *regional* anomalies while the short wavelength signals are termed *residual* anomalies. In most geophysical studies, it is the residual anomaly that is of most importance. There is any number of methods in which regional-residual separation may be computed. These include but are not limited to: graphical, analytic (filters), or polynomial fitting (Sharma, 1997).

Derivatives

The derivatives of total-field anomalies aid in resolving near-surface features. The derivative may be directly measured during the survey or calculated post-acquisition from the total-field. The derivative is particularly useful in resolving the edges of sources (Sharma, 1997).

Depth Estimation

The most important parameter to determine about a source is its depth. A quick assessment of the depth can be made from its respective anomaly, if the anomaly is of simple geometry. When this is not the case, or a more definitive quantity is required, there are a number of mathematical functions to determine source depth. These methods include but are not limited to: Half-width (Sharma, 1997), Smith rules (Parasnis, 1962) tilt-depth method (Salem et al., 2007a; Salem et al., 2007b), and Euler deconvolution (Reid, 1990; Keating and Pilkington, 2004).

Gridding

Gridding is the interpolation between survey points onto a regular grid. There is a number of gridding algorithms and if not properly chosen may attenuate high-frequency data or generate gridding artefacts. Ultimately, the way in which the survey data was collected will determine which gridding algorithm should be conducted. For this thesis all gridding was carried out in Oasis Montaj, which offers four different gridding algorithms: minimum curvature, bi-directional gridding, tinning, and kriging. For this thesis, minimum curvature (RANGRID) was used. Minimum curvature generates smooth surfaces by calculating biharmonic difference equations and calculates the total minimum curvature from the second horizontal derivative in both the x and y direction at each survey point. This gridding algorithm was chosen for this thesis for three reasons: a) ability to honour original data, b) produces the smoothest fit and c) quickly and reliably conducts interpolation on very large datasets (Cowan, 2001).

CHAPTER TWO

Applications of curvature analysis in potential field interpretations: Regional-residual separation, tilt-depth, and Euler deconvolution

Summary

Over the past few years there has been a dramatic increase in the volume of available magnetic data, covering wider areas for which there is often limited prior geological information. Coupled with a demand for faster data interpretation there has been an increased interest in the development of semi-automated data processing routines designed to aid in delineating source body locations, geometries, and depths. These semi-automated methods may be applied in either a spatial or frequency domain. Irrespective of processing domain, limitations associated with potential field interpretations constrain the derivation of geologically sound models. These limitations include limited physical property constraints and the infinite magnetic source. Through the application of a spatial domain filter that uses the curvature of a potential field signal, these limitations may be minimised. By varying the grid cell size, thus the solution window, isolation of specific wavelengths may be achieved, which can then be used as a regional-residual separation scheme. Furthermore, the application of curvature based regional-residual separation scheme can act as an important pre-processing tool to any analytic routine. These routines include, but are not limited to tilt-depth method and Euler deconvolution. Often these analytic routines are conducted without any pre-processing which causes imposed limitations to be translated through to the final interpretation results. These analytic routines may be enhanced by first conducting the proposed grid cell regional-residual separation method.

Introduction

With an ever increasing demand for quicker processing routines on larger potential field datasets, more efficient semi-automated processing routines are being developed. These include but are not limited to SPI™, analytic signal, and Euler deconvolution (Thurston and Smith, 1997; Smith et al., 1998; Keating and Pilkington, 2004; Reid et al., 1990). These routines are designed to aid in the delineation of source body locations, geometries, and depths. Most of these routines, such as Euler deconvolution are based on computations that involve gradients of the magnetic or gravity field. A basic assumption of all these methods is that the data within an individual solution window defines a single isolated magnetic or gravity anomaly associated with a single geological source. These conditions are rarely met.

The Total Magnetic Intensity (TMI) signal at any single point represents the magnitude of the vector summation of all sources in proximity of the observation points. The ridges and troughs (anomalies) which characterize all TMI maps are a record of the summation (interference) of the field generated by various sources. Applying a semi-automated processing scheme to this type of mixed source data will produce many solutions that are not geologically meaningful. Utilisation of this information then necessitates some type of solution filter that is able to separate the different magnetic/gravitational sources. Assuming a simple dual-layer structure one could attempt source segregation through a regional-residual separation. This is typically achieved through a Fourier series transform related algorithms.

Fourier series transforms can be regarded as a generic transform that maps space or time functions into wavenumber or frequency based functions. Most often in geophysical processing, Fourier transforms are implemented for the specific conversion between time-domain data to frequency-domain data. A *discrete Fourier transform* is the application of Fourier transformed to a sampled data set. Furthermore, a *Fast Fourier Transform* (FFT) is a type of discrete Fourier transform that implements a method known as 'doubling' which ultimately makes the transform more computationally efficient than the conventional discrete Fourier transform. While the FFT approach has permitted rapid analysis of large data sets it is well known that the methodology can produce geologically invalid outputs when some primary assumptions are violated. The information that can be extrapolated from geophysical data is inherently dependent on the source sampling. Since a Fourier transform is periodic, which has a period that is inversely proportional to sampling interval, the manner in which a dataset is sampled will affect the FFT results. This defines a major limitation of the FFT procedure. Since any potential field signal is defined by a minimum of three points, any measured sampling frequency less than twice the sampling interval cannot be resolved. This is known as *Nyquist frequency* and simply states that the smallest frequency that can be resolved is equal to half the recording frequency. However, if the maximum sampling frequency is less than the Nyquist frequency is used, and then *aliasing* is produced. Aliasing is the repetition of signal often characterized by a 'ringing' effect in other portions of the image (Blakely, 1995).

Methodology

As any continuous curve, a magnetic signal can be described in respect to its curvature and can be defined as the rate of change in the direction of a curve in 2D. Roberts (2007) defines curvature (κ) as

$$\kappa = \frac{\partial \omega}{\partial S} = \frac{2\pi}{2\pi r} = \frac{1}{r} \qquad (1)$$

where $\partial \omega$ and ∂S are the rates of change of angle and arc respectively (Figure 1). Based on the above equation, if the radius is large or the angle subtended by the arc is considerably small then the circle will have a small curvature For example, where the radius is equal to infinity, a straight line is produced. If the radius is small (large angle versus arc rate of change, e.g. a small circle) then a large curvature is achieved.

A number of common semi-automated data processing schemes, such as SPI™ and Horizontal Gradient Magnitude (HGM), use some aspects of the curvature of a signal in order to delineate source geometries and their depth (Thurston and Smith, 1997; Smith et al., 1998; Phillips, 2007).

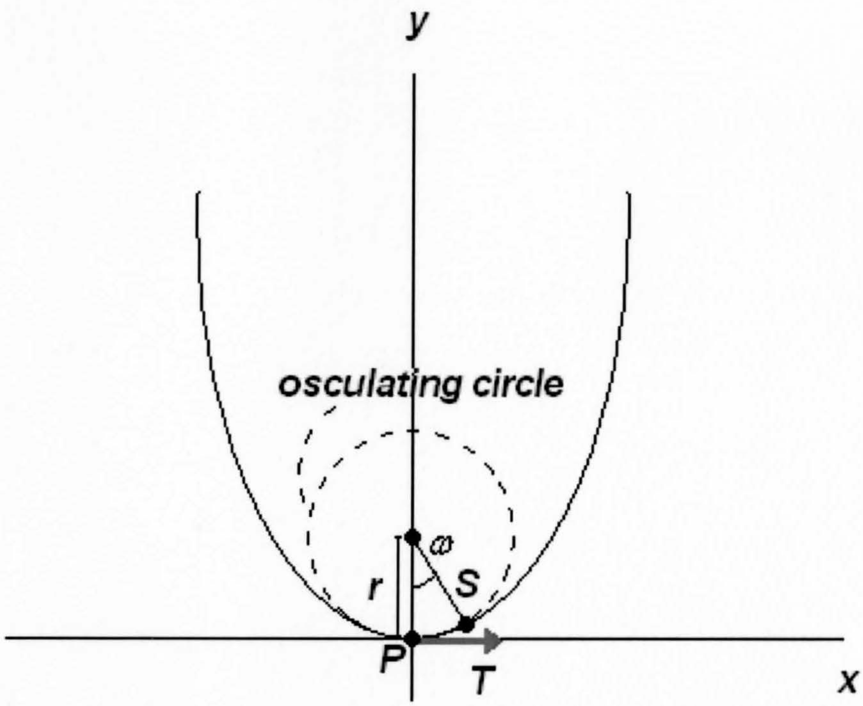
y
osculating circle
ω
r
S
P
T
x

Figure 2-1.

Relationship of radius with curvature. Curvature is the inverse of the radius of the osculating circle, which is the circle that makes the greatest amount of contact with the curve at point P.

Mickus et al. (1991) presented a data processing technique using the minimum curvature gridding method in order to complete regional - residual separation on gravity data. Their proposed minimum curvature technique involved gridding the original dataset at an appropriate grid cell size and then desampling the same dataset at a coarser grid cell size that was based on a feature of interest's size and data spacing. This coarsely gridded interpolation acted as a regional dataset and was subsequently subtracted from the original in order to delineate gravity anomalies (residual field). This method was proposed as an alternative to the typical polynomial surface trend or FFT technique. Through the application of the minimum curvature technique and a polynomial trend surface to a field example, it was shown that the minimum curvature technique was capable of creating a more reliable residual field than the trend surface method. Mickus et al. (1991) discussed that there were still limitations to using minimum curvature and the method was best suited for shallow features at or near surface which had available geologic or geophysical data. The idea of using a varying grid cell size was further developed by Morris et al. (2002), who discussed that it was possible to accentuate circular anomalies by using two grid cell sizes to create a range of the anticipated dimension of a source feature. Morris et al. (2002) successfully isolated pipe-like features through the application of this grid cell size variation.

The minimum curvature methods proposed by Mickus et al. (1991) and Morris et al. (2002) can be further developed in respect to curvature. The wavelength of any signal is inextricably linked to curvature; a high-frequency (short wavelength/high amplitude) signal will be represented by a large curvature while a low-frequency (long wavelength/low amplitude) will be represented by a small curvature. To achieve isolation of a specific frequency or wavelength, curvature identification may be implemented as an alternative to FFT. This curvature identification scheme would act instead as a spatial domain filter and could be accomplished through the regional-residual separation using fine and coarse grid cell sizes. The grid cell size of the original data will have a direct effect on the resultant curvature of the magnetic signal. Through grid cell size variation, one can isolate which portion of a curve is being interpreted. As can be seen in Figure 2, a coarse grid cell size will represent low-frequency (deep) sources and a fine grid cell size will be associated with high frequency (shallow) sources.

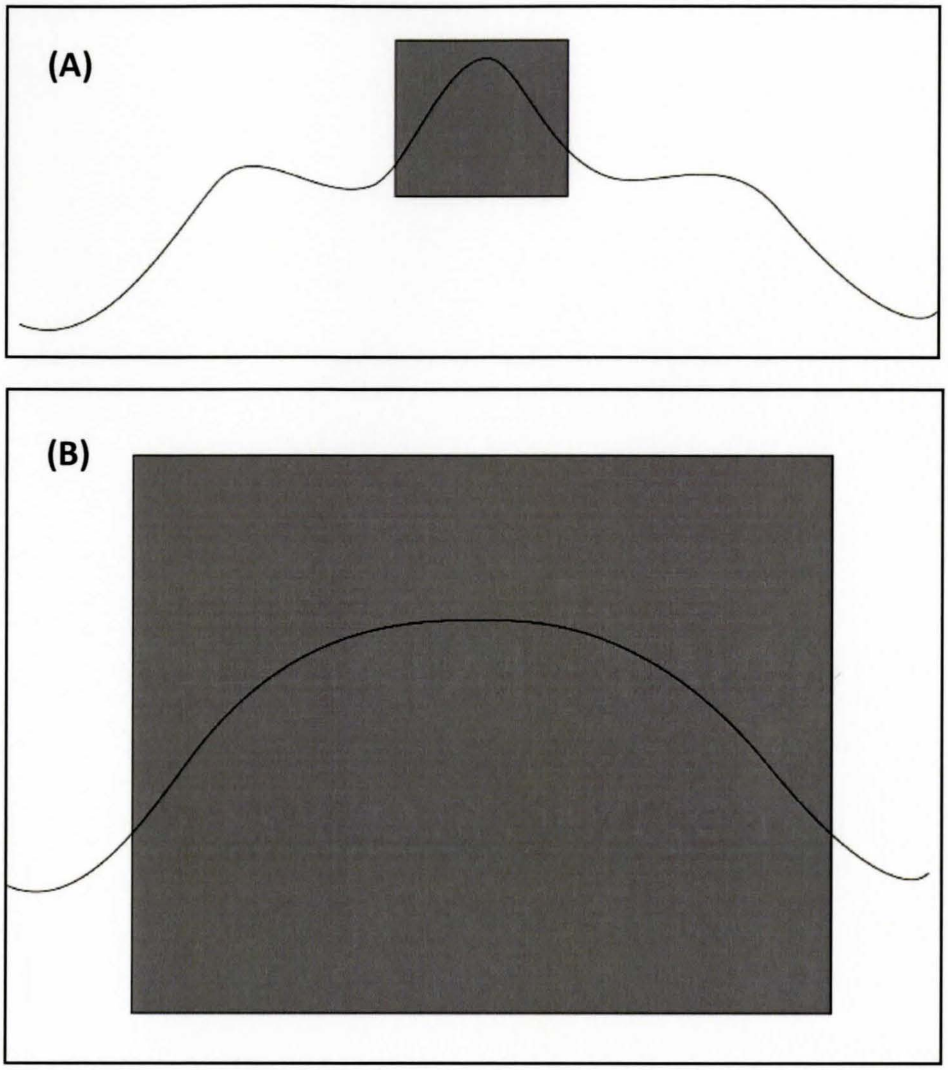
(A)
(B)

Figure 2-2.

Grid cell size comparison. The scale of interpretation needs to be taken into consideration. When a small grid cell size (A) is chosen, higher frequency anomalies will be resolved, while a coarser grid cell size (B) will smooth high frequency signal and only low frequency signals are resolved.

If we consider the total magnetic signal produced by a series of near-surface vertical-sided anomalous source bodies, the geometry of the resulting magnetic anomaly is dominated by the depth to the top of the source and minimally from the bottom of the source (Spector and Grant, 1970). Since a gravity and magnetic field will decay at a rate inversely proportional to source-signal distance squared or cubed respectively, often the signal generated by the bottom of the source has decayed before reaching the sensor. This is true for most cases and as such the depth to bottom is typically not taken into consideration. In isolated instances, such as with very thin, shallow bodies, the depth to bottom does have a significant influence on the resultant anomaly. In this situation, the signal produced by the bottom of the source is readily detectable by the sensor. Again the observed total magnetic field represents a composite of sources. Theoretically one should be able to separate the magnetic anomaly associated with the base of the source body from that associated with the top of the source body by applying a regional - residual approach that separates the influence of top and bottom on the basis of their differing wavelength.

This can be seen as a signal interference reduction algorithm; the high-frequency and low-frequency signal contributions are separated during the initial processing steps, so that all interpretations may be conducted on unbiased data. Over the years a number of different approaches to regional-residual signal separation have been suggested (Hearst and Morris, 2001; Li and Oldenburg, 1996). Most of these procedures invoke some aspect of FFT data processing. While the FFT approach has permitted rapid analysis of large data sets it is well-known that the methodology can produce geologically invalid outputs when some of the primary assumptions are violated. Once again, by implementing a spatial-domain filter, these primary assumptions could be avoided. This methodology can then be used as a pre-processing step to any number of processing and rapid interpretation routines like tilt-depth method and Euler deconvolution.

Analytic routines include depth estimators, such as tilt-angle or Euler deconvolution. These two methods perform a routine on the entire dataset, regardless of signal interference. As such, the results produced by these two methods will likely be biased to complex signal interactions between high- and low-frequencies. The resultant depths will be a combination of short and long wavelength features and not of the true representative depths. This places emphasis on why a reliable pre-processing needs to be put into practice prior to any processing or interpretation method.

Analytic Routines

Tilt-depth Method

The concept of tilt-angle has existed for over four decades and is simply a normalized derivative of the ratio between the vertical and horizontal derivative of a potential field signal. Tilt-angle may be implemented as depth estimation method through contour analysis and is aptly known as *tilt-depth method* (Salem et al., 2007a; Salem et al. 2007b). This method however is still gaining recognition within the geophysical community and is under practiced. Tilt-depth method has been shown to produce reliable and consistent results which may be enhanced in combination with pre-processing steps.

Tilt-angle was first introduced by Miller and Singh (1994) and has since been defined as:

$$\theta = \tan^{-1}\left(\frac{\partial M/\partial z}{\partial M/\partial h}\right) \qquad (2)$$

where $$\frac{\partial M}{\partial h} = \sqrt{\left(\frac{\partial M}{\partial x}\right)^2 + \left(\frac{\partial M}{\partial y}\right)^2} \qquad (3)$$

and $$\frac{\partial M}{\partial x}, \frac{\partial M}{\partial y}, \frac{\partial M}{\partial z} \qquad (4)$$

which are first-order derivatives of the magnetic field (M) in the directions of x, y, and z.

Since tilt-angle is an inverse trigonometric function (arc tan) all resultant values are between -90° and 90°. Miller and Singh (1994) showed that tilt-angle was capable of edge detection and delineation of source body orientation. Tilt-angle will produce a zero value over or near the source edges with positive values over the source and negative values outside the source. This is similar to results produced by vertical derivatives, however unlike vertical derivatives, tilt-angle is insensitive to source depth and can equally resolved deep and shallow sources.

Salem et al. (2007a, 2007b) introduced the concept that tilt-angle could be used as a simple method to delineate the depth to top of source, known as *tilt-depth method*. Salem et al. (2007a, 2007b) extended the tilt-angle expression in order to derive a relationship between the horizontal location of a contact (h) and the depth to top of source (z_T):

$$\theta = \tan^{-1}\left(\frac{h}{z_T}\right) \qquad (5)$$

According to Salem et al. (2007a, 2007b) when the results of tilt-angle are calculated and contoured, it is shown that the physical distance between -45° and 45° is equivalent to twice the depth to top ($2z_T$). Furthermore, that the 0° contour is equivalent to the source body contact (h=0). This depth estimation routine could be further enhanced through the application of the grid cell separation scheme as a pre-processing step.

Euler deconvolution

Tilt-depth method is not the only depth estimation routine gaining ground in geophysical processing. Euler deconvolution has become a standard step in any processed and interpretation geophysical study. Once again, these results produced by Euler deconvolution may be enhanced though a pre-processing routine. Furthermore, an inherent component of Euler deconvolution calculation is the incorporation of a decay constant, which is a measure of the rate at which a potential field signal decomposes. This concept of signal decomposition can be alternatively seen as the amount of curvature a signal possesses at a particular depth. As such, a curvature filter routine becomes even more applicable as a pre-step to Euler deconvolution.

Euler deconvolution is a semi-automated process that utilizes the three directional derivatives of the total magnetic field in order to delineate the source locations of anomalies (Reid et al., 1990; Keating and Pilkington, 2004). The methodology uses Euler's homogeneity equation:

$$(x - x_0)\frac{dT}{dx} + (y - y_0)\frac{dT}{dy} + (z - z_0)\frac{dT}{dZ} = N(B - T) \tag{11}$$

where T is the observed magnetic field at the locations *x, y, z* of the magnetic source with the location x_0, y_0, z_0. The total field has a value of B and the structural index (SI) is N, which is a measure of homogeneity degree. Structural index is the rate of decay of the source's signal with distance of the field. Different source geometries will have a different rate of signal decay. The conventions for structural index are can be found in Table 1. The idea that different geometries will produce either a fast or slow signal decay, relates to the concept addressed previously that the generated wavelength will be a function of source depth and geometry. Thus structural index may be refined through an initial curvature analysis. By first completing curvature analysis and isolating key wavelengths, when Euler deconvolution is conducted the structural index does not carry as much weight and fewer results outside the anticipated parameters will be resolved.

Curvature and aperture (window size) play an important role in the application of Euler deconvolution. In Euler deconvolution, a set of solutions is determined for a specified window size. As such the window size will control the number of solutions that will be generated, including their depth. If the window size is too small, too many redundant solutions will be calculated since the moving window moves at a rate of one grid cell size. However, if the window is too large a smoothing effect is imposed, and too few solutions are delineated.

Geological Model	Magnetic SI	Gravity SI
Sphere	3	2
Pipe	2	1
Horizontal cylinder	2	1
Dyke	1	0
Sill	1	0
Contact	0	NA

Table 2-1.

Structural indices for Euler deconvolution. Accepted structural indices (SI) for magnetic and gravity datasets used Euler deconvolution. Note that the structural indices for different geometries depend on the physical parameter being evaluated. This is due to the difference is potential field decomposition with distance between magnetics and gravity.

In order to control the number of solutions a number of variants on the standard Euler deconvolution routine have been developed. For example located Euler as implemented by Geosoft's Oasis Montaj is calculated on the analytic signal of the original TMI grid. Prior implementations of analytic signal serve to reduce the overall variance of the magnetic signal over a source body generally converting dipolar to monopolar anomalies. As such, the number of solutions is based on the number of peaks calculated in the analytic signal, which is typically very few. If an initial curvature interpretation is conducted to separate long-wavelength features from the short-wavelength features initially, more reliable solutions may be derived once the regional trend is removed.

Both of the above mentioned depth estimation routines produce optimal results in the absence of interference; however, when signals are deformed by complex signal interaction, this causes erroneous effects that translate into all subsequent interpretation methods, tainting final results.

Applications

Synthetic Model

In order to investigate interference effects due to shallow, thin bodies, two synthetic models were generated: both at close proximities to the sensor - one with a shallow depth to bottom (60m below sensor) and one with an infinite depth to bottom (20km below sensor). Both synthetic models comprised of a rectangular, vertical-sided prism, 3km in length and 1km wide occurring in an ambient magnetic field of 60 000nT with an inclination and declination of 90° and 0° respectively. This vertical ambient field was used to maintain control and simplicity in all interpretations. It is important to note that remanence was not used in the synthetic models. A flight line spacing of 100m and a sampling interval of 10m was used. Each prism had a magnetic susceptibility of 0.01emu/cm^3 and a distance of 10m between the top of body and sensor. Figure 3 shows the resultant TMI signals generated by the two models.

(A)

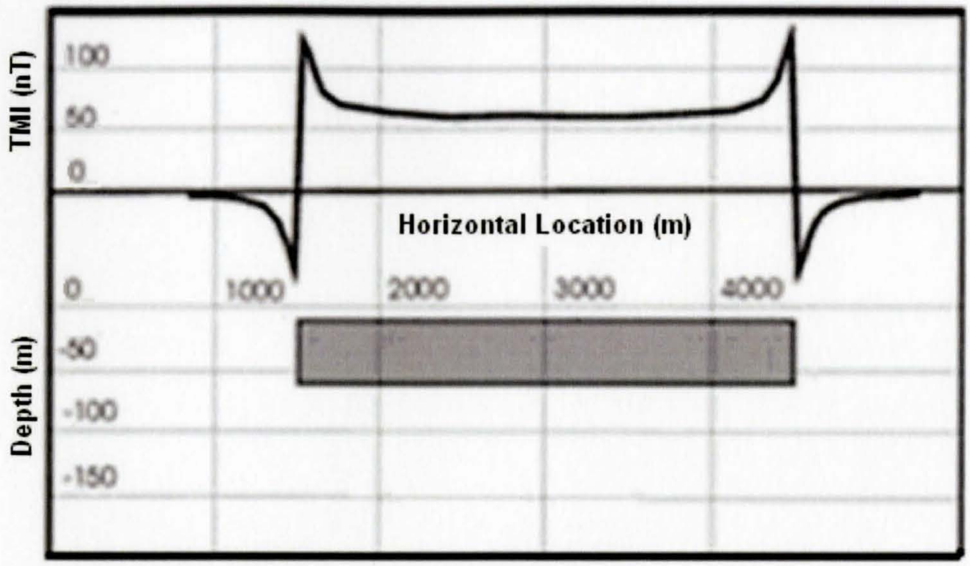
TMI (nT)
100
50
0
Horizontal Location (m)
0
1000
2000
3000
4000
Depth (m)
-50
-100
-150

(B)

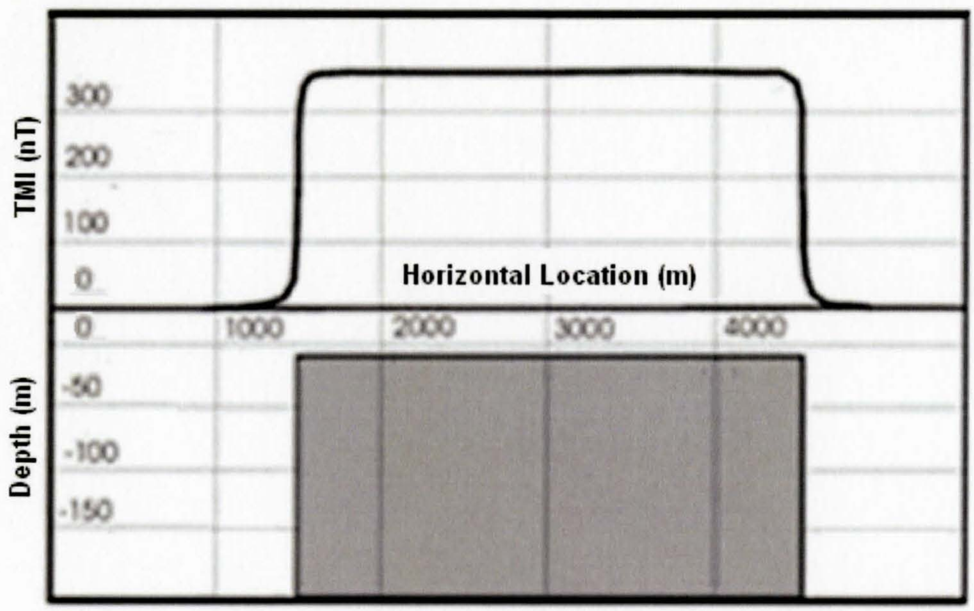
TMI (nT)
300
200
100
0
Horizontal Location (m)
0
1000
2000
3000
4000
Depth (m)
-50
-100
-150

Figure 2-3.

Generated magnetic signal over two rectangular prisms. Both generated synthetic models share the same depth to top and magnetization parameters. The depth to bottom was varied to illustrate its interference on the resultant anomaly: (A) bottom at 60m below surface and (B) bottom at 20km below surface to approximate an infinite-body.

In order to isolate any high-frequency signal generated from the bottom of the source, the grid cell segregation routine was implemented strictly on the shallow, thin vertical prism dataset. The original dataset was gridded with a grid cell size of 100m and then a coarser grid cell size of 1000m was utilized to isolate only the low frequency signal (regional field). It is important to note that standard size for grid cells is ¼ or 1/5 the flight line spacing. However, due to the gridding algorithm used in Oasis Montaj, artificial high-frequency signal is generated in magnetically flat areas when a grid cell size of ¼ the line spacing was used. This ringing effect was reduced by using a larger grid cell size than standard practice. Grids were constructed using a minimum curvature interpolation scheme with a normal distribution colour scheme. Subsequently, the regional grid was subtracted from the original one in order to isolate the high-frequency signal (residual field) which can be seen in Figure 4. It is at this point that secondary processing and interpretation routines may be applied to the unbiased data.

Tilt-depth method was applied to both the full RTP magnetic dataset (unfiltered) and the residual magnetic dataset (filtered). This was to directly compare the produced depths from a filtered dataset to those of a unfiltered dataset. Tilt-angle was calculated both mathematically using the equation from Miller and Sing (1994) and using the tilt-derivative algorithm in Oasis Montaj. The results produced by both methods were identical, therefore for all further tilt-angle calculations the automated tilt-derivative operation in Oasis Montaj was used for efficiency. Since the results produced by tilt-derivative are in radians a final grid calculation was conducted to convert all values to degrees based on the conversion factor of $180^\circ/\pi$. The tilt-angle values were contoured and the spatial separation between the -45° and 45° contours were measured to calculate the supposed depth to top. The results can be found in Figure 5 and Table 2.

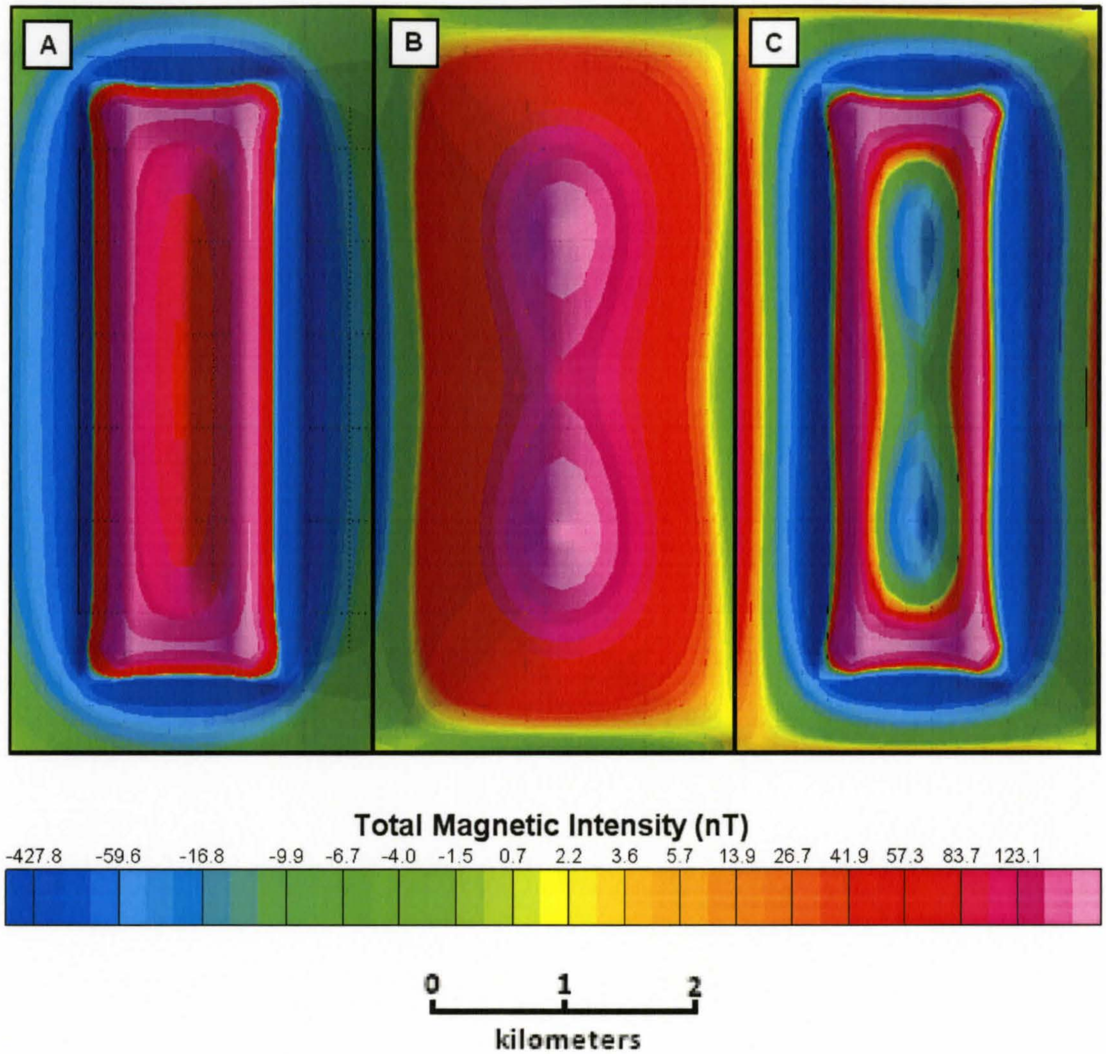
A
B
C
Total Magnetic Intensity (nT)
-427.8 -59.6 -16.8 -9.9 -6.7 -4.0 -1.5 0.7 2.2 3.6 5.7 13.9 26.7 41.9 57.3 83.7 123.1
0 1 2
kilometers

Figure 2-4.

Regional-residual separation on the synthetic TMI dataset. Regional-residual separation was applied to the synthetic dataset seen in Figure 3 using the grid cell separation scheme. (A) Original TMI dataset gridded at 100m. (B) Regional TMI dataset gridded at 1km. (C) Residual TMI dataset produced by the subtraction of (B) from (A).

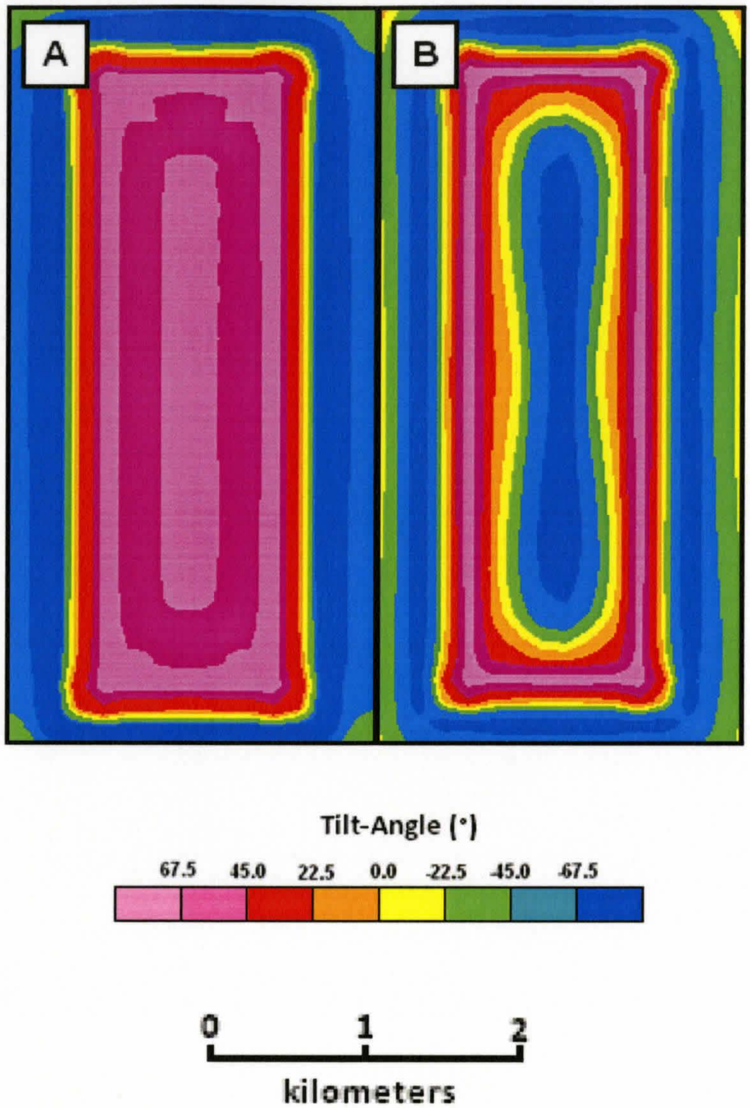
A
B
Tilt-Angle (°)
67.5
45.0
22.5
0.0
-22.5
-45.0
-67.5
0
1
2
kilometers

Figure 2-5.

Tilt-depth method results for synthetic dataset. (A) Full RTP dataset gridded at 100m. (B) Residual dataset produced by the subtraction of a desampled grid (1000m grid cell size) from the full RTP. The high-frequency dipole effects seen in Figure 3 can be seen along all vertical edges of the prism in the residual grid as tilt-degree values greater than 0.

Dataset	h (m)	Depth (m)
Unfiltered	110	55
Filtered	80	40

Table 2-2.

Results of tilt-depth method solution depths. Summary of calculated depths for unfiltered (Full TMI) and filtered (Residual) synthetic datasets.

Finally, Euler deconvolution was applied to both the unfiltered and filtered datasets. Standard Euler deconvolution was chosen over located Euler due to its suitability for geological applications. A structural index of 0 was used to isolate contacts. A window size of 10 with a maximum depth tolerance of 15% was utilized to enable more solutions. These Euler deconvolution parameters were used on both the filtered and unfiltered datasets in order to maintain consistency. Euler deconvolution results can be found in Table 3.

Field Dataset

The data used in this field example has been acquired from a high-resolution Midas horizontal magnetic gradient survey over the Porcupine Destor-Pipestone Faults area near Iroquois Falls and Matheson, Ontario (OGS, 2004). The helicopter survey was flown in 2003 and 2004 by Fugro Airborne Surveys Corporation with a line spacing of 75m and a terrain clearance of 15m above the tallest surface feature. This region is predominantly Archean greenstone, cross-cutted by dykes and faults which produce high frequency signals. A geological map of the area can be seen in Figure 6.

Salem et al. (2007a, 2007b) discussed that depth estimating routines like tilt-depth method should be conducted in a perfectly vertical ambient magnetic field. Since this was not possible due to geographical location of the study area, Reduction-to-Pole (RTP) was applied to the Iroquois Falls dataset. RTP reduces the effect of an inclined magnetic field essentially creating a 'perfectly vertical ambient field'. The simple grid subtraction routine was implemented to filter the high-frequency geologically generated signals from the background signal. Initially, the dataset was gridded at the standard ¼ of the line spacing (20m) and then subsequently gridded at a coarser grid cell size of 640m. This coarse grid represented only the long wavelength features in the study area (regional). When the regional was subtracted from the original dataset, a residual dataset was produced as seen in Figure 7.

Grid	Maximum depth (m)	Mean depth (m)	Standard Deviation
Full TMI	2033	475	571
Regional	682	271	163
Residual	573	104	194

Table 2-3.

Statistics of Euler deconvolution solutions. Maximum, mean, and standard deviations of Euler deconvolution depth solutions calculated for the full TMI, regional and residual grids using the synthetic dataset.

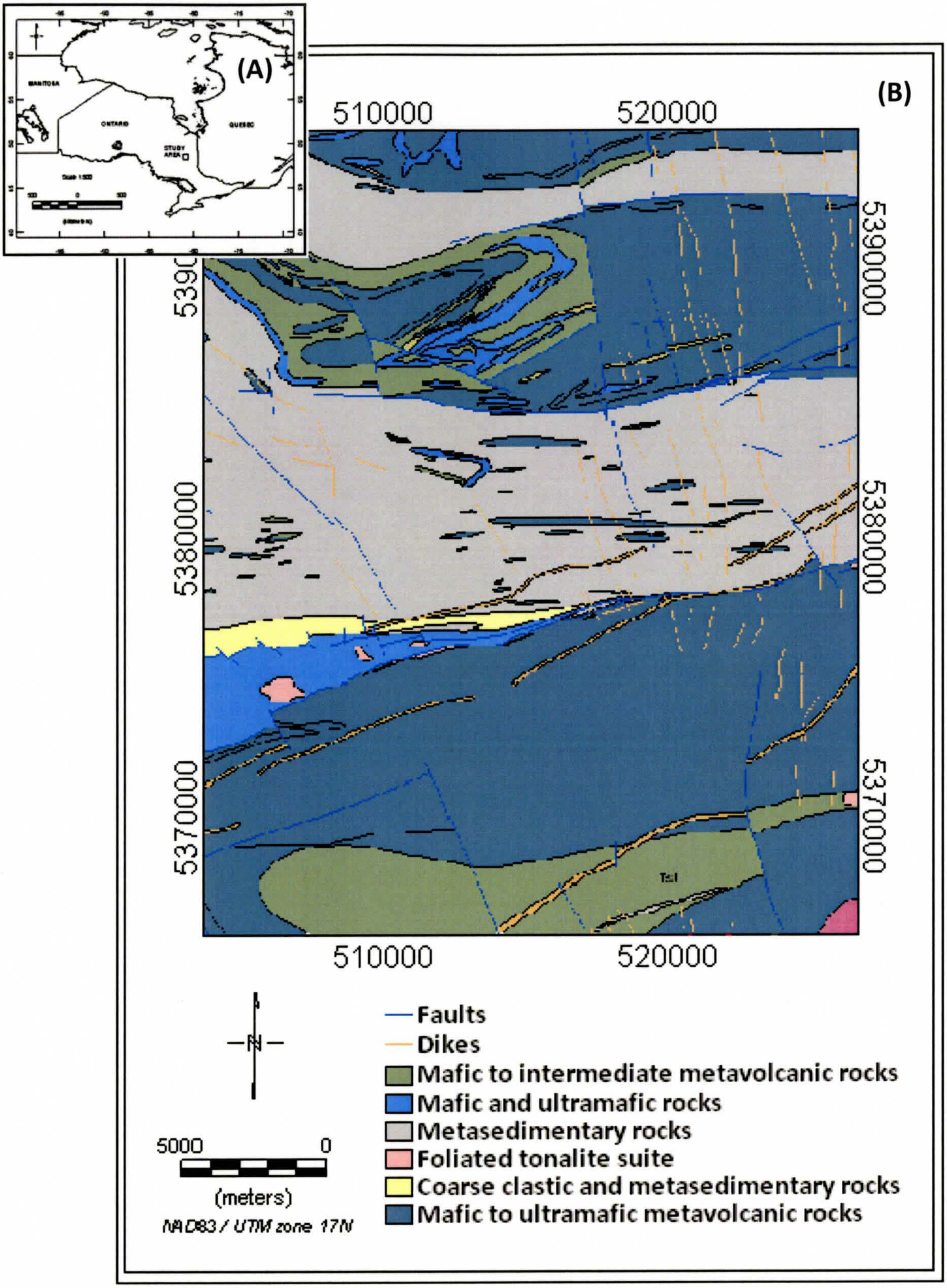
(A)
MANITOBA
ONTARIO
QUEBEC
STUDY AREA
(B)
510000
520000
5390000
5380000
5370000
510000
520000
N
Faults
Dikes
Mafic to intermediate metavolcanic rocks
Mafic and ultramafic rocks
Metasedimentary rocks
Foliated tonalite suite
Coarse clastic and metasedimentary rocks
Mafic to ultramafic metavolcanic rocks
5000
0
(meters)
NAD83 / UTM zone 17N

Figure 2-6.

Geological map of the Pipestone and Porcupine-Destor Faults area. Geological map of the study area within the Pipestone and Porcupine-Destor Faults area near Iroquois Falls, Ontario (A: ESRI, 1997; B: OGS, 2004). Geological units, faults, and dikes have been indicated.

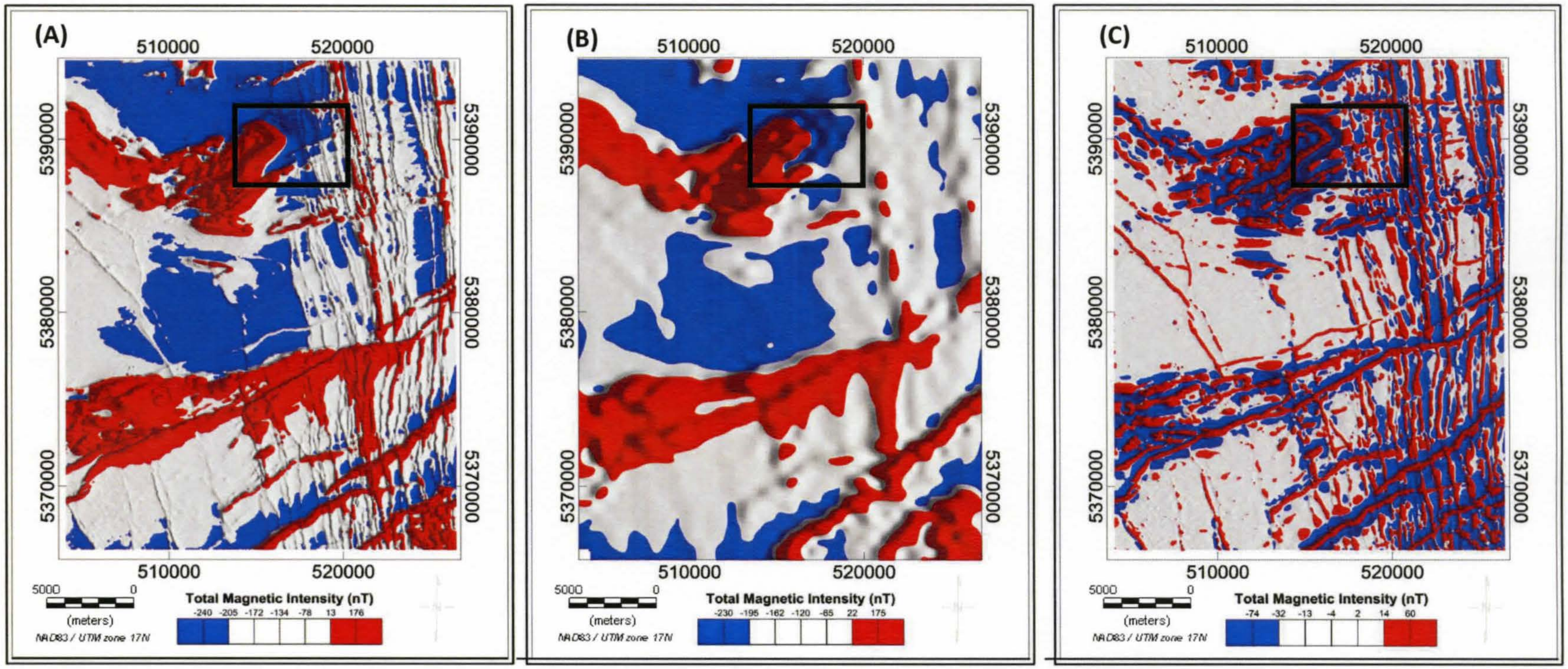
(A)
510000
520000
5390000
5380000
5370000
510000
520000
5000
0
(meters)
NAD83 / UTM zone 17N
Total Magnetic Intensity (nT)
-240 -205 -172 -134 -78 13 176
(B)
510000
520000
5390000
5380000
5370000
510000
520000
5000
0
(meters)
NAD83 / UTM zone 17N
Total Magnetic Intensity (nT)
-230 -195 -162 -120 -85 22 175
(C)
510000
520000
5390000
5380000
5370000
510000
520000
5000
0
(meters)
NAD83 / UTM zone 17N
Total Magnetic Intensity (nT)
-74 -32 -13 -4 2 14 60

Figure 2-7.

Grid plots of total magnetic field from Pipestone and Porcupine-Destor Faults area. (A) Original TMI dataset gridded at 20m. (B) Regional TMI dataset gridded at 640m. (C) Residual TMI dataset produced by the subtraction of (B) from (A). A generated bi-modal colour scheme has been used in all grids to isolate extreme values; blue represents magnetic lows and red represents magnetic highs. An elliptical structure (inset box) of mafic and ultramafic rocks can be resolved in the north section of study area along with local dykes and fault systems.

Subsequently both analytic routines, tilt-depth method and Euler deconvolution, were applied to the above results. Tilt-angle was applied to the original full RTP magnetic grid and the computed regional and residual grids (Figure 8). Following, standard Euler deconvolution was calculated using the three component derivatives of the full TMI, the regional, and the calculated residual from the previous steps. Standard Euler deconvolution was once again chosen over located Euler. A structural index of 1 was chosen to isolate dykes and sill-like features. A window size of 10 with a maximum depth tolerance of 15% was utilized to enable more solutions. These Euler deconvolution parameters were used on all three datasets (full TMI, regional, and residual) in order to maintain consistency. Basic Euler statistical results can be found in Table 4.

Results

Synthetic Dataset

As can be seen in Figure 3 and Figure 4, it is apparent that the depth to bottom does have an influence over the resultant TMI anomaly in specific instances, such as thin, near surface features. The effect of the bottom signal generates a dipole over all edges of the vertical prism. It is this dipole effect that is isolated during the grid cell segregation routine. This emphasizes the idea that in any potential field dataset that a source produces multiple signals that may cause complex interference patterns. It is mandatory that these interference effects be addressed prior to further processing and interpretation.

Taking into consideration the tilt-depth results, there are large inconsistencies between the computed depths and the actual depths (Table 2). In the case of the filtered dataset, according to the applied tilt-depth method the source-signal separation was 40m. Since the filtered dataset only represented the magnetic signal from the depth to bottom, which was 60m below surface, this accounted for a difference of 20m. The unfiltered dataset produced a depth solution of 55m according to tilt-depth; however, since this dataset represents both high- and low-frequency signals, this depth solution is incorrect for the depth to top.

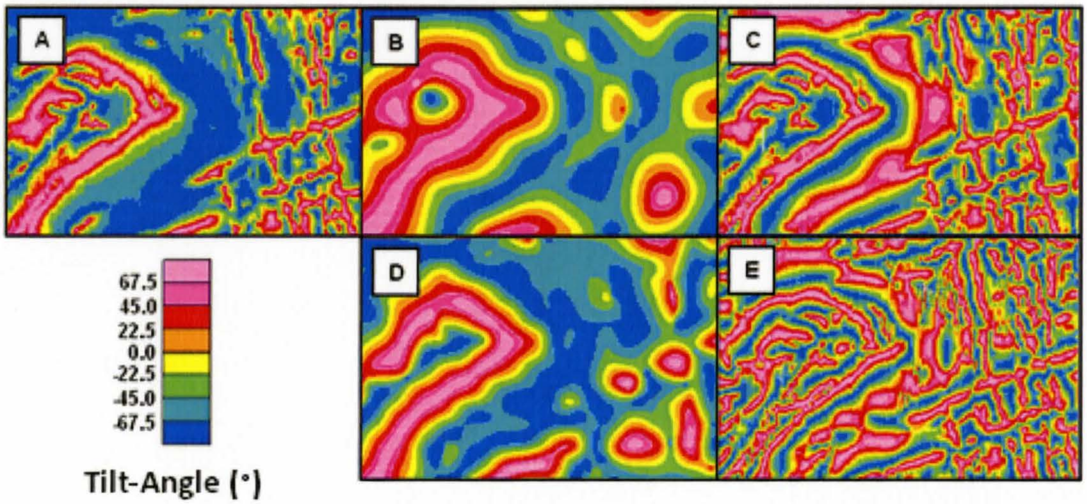
A
B
C
D
E
67.5
45.0
22.5
0.0
-22.5
-45.0
-67.5
Tilt-Angle (°)

Figure 2-8.

Tilt-depth applied to varying grid cell sizes of the Pipestone and Porcupine-Destor Faults dataset. Close-up of elliptical geological structure in north section of study area. (A) Original TMI dataset gridded at 20m. (B) Regional TMI dataset gridded at 640m. C) Residual TMI dataset produced by the subtraction of (A) from (B). (D) Regional TMI dataset gridded at 320m. (E) Residual TMI dataset produced by the subtraction of (D) from (A).

Grid	Maximum depth (m)	Mean depth (m)	Standard Deviation
Full TMI	752	101	56
Regional	837	299	98
Residual	81	24	6

Table 2-4.

Statistics of Euler deconvolution solutions of the Iroquois Falls dataset. Maximum, mean, and standard deviations of Euler deconvolution depth solutions calculated for the full TMI, regional, and residual grids using the field.

A similar depth discrepancy was found when applying Euler deconvolution (Table 3). The depth solutions on the filtered dataset were upwards to 50 times deeper than the actual source-signal separation. In the case of the unfiltered dataset, the depth solutions were in the order of 200 hundred times deeper than the actual depth.

The synthetic model was designed to exemplify what influence the depth to bottom plays in signal generation. It has been shown in more ways than one that the bottom has a very strong influence on the resultant anomaly and therefore needs to be taken into consideration if possible. In this case, the depth to bottom created complex signal interactions over the edges. In this case the signal generated from the bottom created misinterpretations of the depth estimation routines. All depth estimation routines are implemented in order to find the top of the source body. But in this case, since the depth to bottom had such a significant effect on the resultant anomalies, the depth-estimation routines were producing results somewhere between the top and the top bottom, or in the case of Euler deconvolution results that were just complete outliers. This reiterates that in most cases the depth to bottom may be ignored, but under special circumstances that the depth to bottom may have a detrimental effect on all subsequent processing and interpretation routines.

Consistently all depth solutions for the filtered dataset were always closer to the true depth location, which supports the grid cell separation ideology. In all analytic routines, the unfiltered datasets produced greater depths, which in turn increased the amount of associated error. This shows that by not taking into consideration initial signal interaction, the end results will be further from the truth.

Field Dataset

Post grid cell segregation routine, high-frequency features in the study are readily delineated, which includes all faults and dykes. Particular rock units were resolved particularly well, more specifically the mafic and ultramafic units which can be seen as magnetic anomaly highs in Figure 7. This increases the confidence that when tilt-depth and Euler deconvolution were applied, that all analyses would strictly be conducted on local trends.

A qualitative analysis of the tilt-angle depth solutions was completed through spatial separation of tilt-angle pair contours (i.e. -22.5° and 22.5°). As was expected, the regional grid produced tilt-angle solutions at greater depths, while the residual grid produced shallow solutions. When focusing on the elliptical intrusion of mafic, intermediate, and ultramafic metavolcanic rocks located in the north section of the study area, the tilt-angle indicated the signal generated by the mafic and ultramafic rocks had a depth to top of 50m and extended to at least 255m below the sensor according to the tilt-depth solutions. When comparing the solution depths between the original TMI and residual TMI, there was a difference of 25m, which can be accounted for in the deconvolution of signals during the regional-residual separation scheme.

Table 4 displays the Euler deconvolution solution depths obtained for the different grids. As expected, the regional grid produces greater depth solutions while the residual produced significantly shallower depths. The full TMI produced a wide range of depths which would be the result of all produced signals at all frequencies.

Discussion

In each grid produced, a resolution limit has been set by choosing a specific grid cell size. According to the Nyquist frequency principle, the smallest feature that can be resolved is equivalent to twice the sample spacing. Therefore, the smallest geological feature resolved by any of the produced grids will equivalent to twice the grid cell size. This is an important consideration when attempting to resolving specific features or choosing which grid cell size to use for the regional-residual separation scheme.

The idea of isolating a range of geological features, whether it be based on depth or geometric size can be further discussed by attempting to isolate a specific source depth by creating upper and lower curvature bounds. This was accomplished by creating an upper (residual) and lower (regional) extent of interpretation, we are in turn creating a "depth slice", a narrowed perspective of a specific region below surface. By varying the upper and lower extents, we can vary what subsurface slice is being observed. In order to view the effects of changing the lower extent, a regional trend of 320m grid cell size was computed and tilt-angle recomputed. The results over the northern geologic feature can be seen in Figure 8. The thinner depth slice (20m-320m) produced features at shallower depths while the thicker depth slice (20m-640m) delineated the feature at a greater depth (an average depth solution difference between the two depth slices was 10m).

Subsequently, two depth slices were computed using the above mentioned technique to compare the solutions resolved at varying depth slice location below surface. Both slices were equal to 4n, where n is the grid cell size of the original TMI grid. The depth slices using a finer grid cell size (80m-320m), resolved the sources at shallower depths, while the depth slice utilizing coarser grid cells (160m-640m) resolved features at greater depths (Figure 9). The deeper depth slice produced solution depths of 75m for the northern geologic structure, while the shallower depth slice produced a depth of 60m.

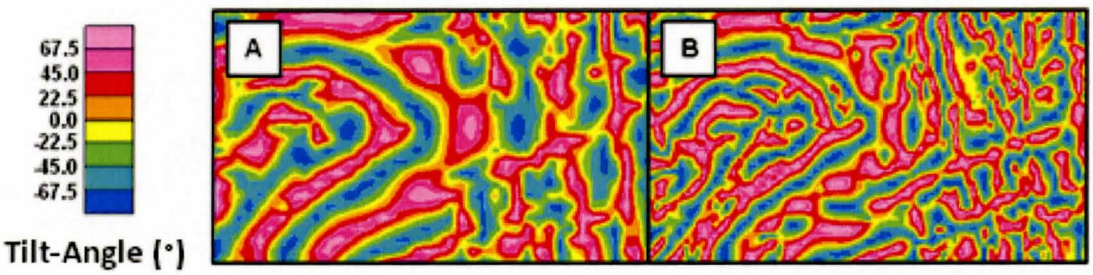
67.5
45.0
22.5
0.0
-22.5
-45.0
-67.5
Tilt-Angle (°)
A
B

Figure 2-9.

Tilt-depth applied to varying depth slices of the Pipestone and Porcupine-Destor Faults dataset. Close-up of elliptical structure of mafic and ultramafic rocks in north section of study area. (A) Residual TMI dataset produced by the subtraction of 640m grid from 160m grid. (B) Residual TMI dataset produced by the subtraction of 320m grid from the 80m grid.

To discuss the extent in which tilt-angle may be applied a sensitivity analysis was performed using a variety of tilt angles. As discussed earlier in this chapter, the distance between -45° and 45° is equal to 2h, where h is the depth to the top of source. Similarly, it should be assumed that the distance between -22.5° and 22.5° is equal to 1h, and the distance between -67.5° and 67.5° is equal to 3h (Figure 10). In theory, if there is no error associated with tilt degree, then the value of all three depths (h) should be the same when determined from a variety of degrees. If they are not, then error bounds may be deduced.

The first step was to create a synthetic model that produces valid results using the original 2h between -45° and 45°. In order to test the ratio relationship, the model designed by Salem et al. (2007a) was implemented (Figure 11). Body A was located at a depth of 4km while Body B was located at a depth of 16km. Both sources were placed in an ambient field of 60 000nT with an inclination of 90°. A line spacing of 1km was used with a sample spacing of 0.5km. TMI was calculated from which tilt-angle was derived. As can be seen from Figure 12 and Table 5, there is little variation between the h calculated from varying tilt-angles. Therefore, the same depth to top should be resolved regardless of whether the it is determined using the distance between -22.5° and 22.5°, -45° and 45°, or -67.5° and 67.5°.

The grid cell separation scheme has been shown to help isolate key wavelengths in order to more accurately describe a source's geometry and depth through any subsequent processing routines. That being said the method is still crude and may be further refined through a more quantitative approach. This may be accomplished through histogram analysis of the curvature grid in order to isolate curvature populations that may be associated with geological sources at particular depths. Furthermore, that regional-residual separation scheme does not enable a fully clean filtered dataset under certain circumstances such as the case discussed earlier when the signal generated from depth to bottom influences the signal generated from the depth to top. In the end, curvature analysis does allow for the successful separation of different wavelengths, now it's just how to specify more accurately which wavelengths those are.

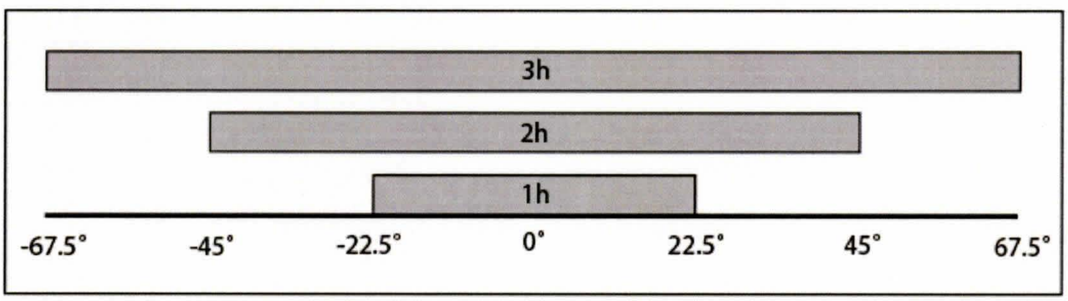
3h
2h
1h
-67.5°
-45°
-22.5°
0°
22.5°
45°
67.5°

Figure 2-10.

The ratio relationship between h and tilt-angle and associated tilt-angle. The distance between h and -22.5° and 22.5°, -45° and 45°, and -67.5° and 67.5° is respectively 1h, 2h, and 3h.

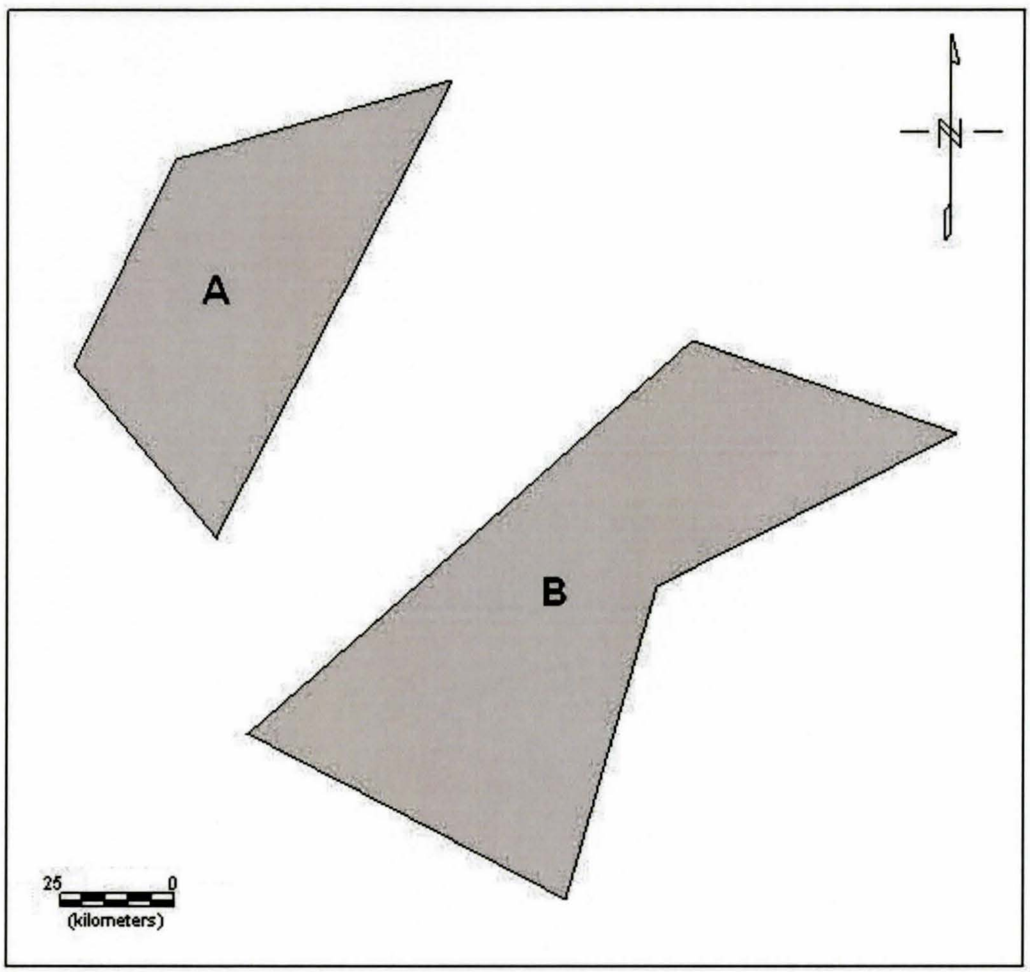
A
B
25
0
(kilometers)

Figure 2-11.

Synthetic model location map. Geometries and spatial location of body A and body B (after Salem et al., 2007a).

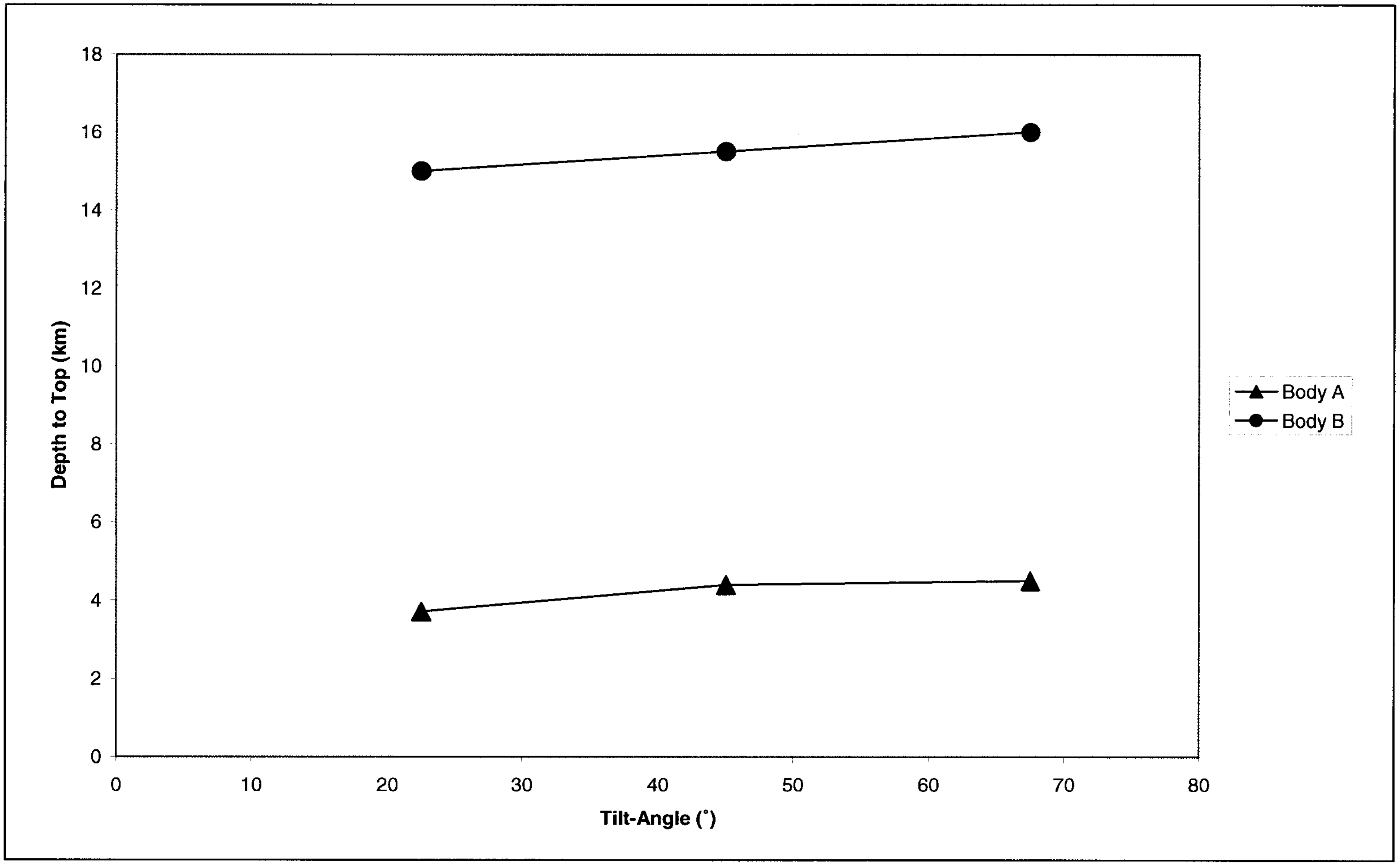
Depth to Top (km)
18
16
14
12
10
8
6
4
2
0
0
10
20
30
40
50
60
70
80
Tilt-Angle (˚)
Body A
Body B

Figure 2-12.

Graphical representation of tilt-angle contour separation. A graph showing the calculated depth solutions to top from varying tilt-angle pair spatial separations.

Body	Tilt-Angle (º)	h (m)	Depth (km)	Standard Deviation
A	22.5	3721	3.7	**0.500**
	45.0	8800	4.4	
	67.5	18000	4.5	
B	22.5	15000	15.0	**0.424**
	45.0	31000	15.5	
	67.5	64000	16.0	

Table 2-5.

Statistics of tilt-depth method solutions. Summary of calculated depths relative to h and tilt-angle.

Conclusion

Curvature interpretation of potential field datasets acts as a simple spatial domain filter; by doing so, many primary assumptions including aliasing conventionally associated with FFT can be avoided. Furthermore, when curvature isolation is implemented in combination with grid cell size, the method allows for a quick regional – residual separation method. In order to efficiently isolate key wavelengths, careful selection of the appropriate grid cell size must be completed. For example the smallest feature that will be resolved by any processing routine will be equal to twice the smallest sample spacing. In the case of this grid cell segregation routine – the smallest feature resolved will be twice the grid cell size. This regional-residual separation scheme was able to isolate the high-frequency signal generated by the special case of a thin prism. The routine was also able to isolate the high-frequency signal generated by local dikes, faults, and ultramafic/mafic rock units in the Pipestone and Porcupine-Destor Faults area. Furthermore, by varying the upper and lower depth boundaries, we are able to isolate source features at specific depths and in combination with depth estimation routines, such as tilt-angle and Euler deconvolution, the subsurface structure may be resolved in a series of depth slices. Finally, the curvature isolation methodology may be implemented as a pre-processing routine to semi-automated processing techniques, including Euler deconvolution and tilt-depth method. Although, the application in analytic routines did show that the grid cell segregation routine is not perfect and that signal interference is still occurring. Ultimately, the concept of signal isolation and more specifically depth isolation is important for accurately resolving the subsurface location of key geological structures which may include potential mineral location, structural water traps for oil, gas, and water.

CHAPTER THREE

A rationale for applying magnetic terrain corrections: A case study from the Eye – Dashwa Lakes Pluton, Atikokan, Ontario

Summary

The Eye-Dashwa Lakes Pluton located near Atikokan, Ontario has been at the center of many nuclear repository studies over the last two decades. Assessments into the suitability of igneous rock as an underground nuclear fuel waste disposal require significant understanding of fault and fracture configurations. This is accomplished through different geoscientific methods, including alteration mapping. Zones of alteration can be mapped through magnetic susceptibility, since alteration leads to a decrease in the occurrence of iron-titanium oxides. In-situ field measurement of magnetic susceptibility is only possible where outcrops exist and these are often limited by the presence of overburden cover and water bodies. An alternative approach to the standard in-situ surveying method is to derive apparent magnetic susceptibility information from a Total Magnetic Intensity (TMI) survey. Unfortunately, when examined in detail the TMI signal is also influenced by topographic morphology and by any changes in the source-sensor distance. As such, the raw TMI dataset contains many apparent anomalies that are predominantly artefacts of the local topography. In order to achieve a valid TMI based estimate of the regional fracture pattern as required for nuclear fuel storage it is necessary to minimize all non-geological sources of magnetic signal. Corrections for topographic morphology effects were computed using known elevation data and source – sensor variations using a Taylor Series expansion approach. The validity of the derived apparent susceptibility map is confirmed through comparison with available in-situ susceptibility data. The fracture pattern derived from the terrain corrected TMI dataset agrees with information provided by borehole magnetic susceptibility surveys.

Introduction

Magnetic anomalies are created through the juxtaposition of rock masses with contrasting physical properties in the presence of a constant applied magnetic field (the present Earth's magnetic field). Genesis of the physical property contrast may be related to either a change in the magnetic susceptibility of the rock unit (for induced field magnetizations), or the occurrence of a remanently magnetized rock mass (for remanent field magnetizations). Given a similar source depth the amplitude of the observed magnetic field is a direct function of the level of contrast between the adjacent rock masses. When this contrast level is high the magnetic field pattern produced by a systematic field survey will directly reflect the distribution of rock masses in the immediate subsurface. This simple observation explains why aeromagnetic surveys have been extremely successful in providing detailed pseudo-geological maps in so many different geological environments worldwide.

The magnetic signal at any point above the Earth's surface is a direct function of the distance between the magnetic sources (rocks at ground level and/or subsurface) and the sensor. In aeromagnetic surveys, an integral part in minimizing the source-sensor distance effects is to fly the survey over the terrain at a constant predefined clearance. Draped surveys are particularly helpful in regions of exaggerated terrain because anomalies in valleys are more properly resolved and anomalies along peaks are not damped. Grauch and Campbell (1984) showed that terrain effects may be reduced or exaggerated depending on the survey ground separation distance. Their results showed that in the end a draped survey over a varying terrain will not produce the same results as a level survey over a constant terrain. They concluded that a draped survey will minimize effects due to terrain survey distance but that anomalies produced by the geometry of any magnetic terrain will always be present. So although variations on the source-sensor separation distance do not account for <u>all</u> the terrain effects on a magnetic survey, source-separation effect should be considered.

During any survey, the pilot attempts to minimize any variation in the height of the aircraft relative to the topographic surface. However, the flight characteristics of individual aircraft and local topographic variability will always result in some source-sensor variations being present in the final data. Attempts at minimizing the influence of these effects are occasionally attempted using drape corrections based on the sub-sampling of multiple continuation surfaces assuming a uniform source-sensor distance during the survey. As noted by Flis and Cowan (2000) when one or more lines are flown at an aberrant height source-sensor differences are erroneously carried through into the final grid. Pilkington and Thurston (2001) introduced a terrain correction procedure based on a Taylor Series expansion approach which can accommodate individual flightline height fluctuations.

While draping can mitigate potential terrain effects there is some debate over whether this methodology fully corrects for terrain effects since draping does not take into consideration the actual morphology of the air / rock interface. For the vast majority of magnetic surveys, whether they are ground based or airborne, the sensor is carried in the air at some elevation above the terrain surface. By definition air has a magnetic susceptibility of zero. Hence, there is always a strong magnetic contrast between the air and the ground. In a uniformly magnetized terrain where all of the observation points lie at the same height above a flat surface there will be no magnetic signal from topography (since there is no topography). In locales with high topographic relief, where adjacent rock masses have similar magnetic mineral characteristics, it is quite probable that the magnetic anomaly pattern will reflect local topographic fluctuations and not the lithological variations.

The concept of magnetic terrain effects is not new, and a number of previous works have discussed this issue in the past. Gupta and Fitzpatrick (1971) developed a simple routine for modelling topographic slopes given knowledge of the aspect and angle of the topographic surface. In this study they showed examples from the Abitibi Greenstone Belt in which the topographic magnetic anomalies are of a similar magnitude to the observed survey data. Few studies have since followed up on this idea. Plouff (1976) and Barnett (1976) introduced the concept that topography can be modelled through the use of a triangular polyhedral. Although there is a recognized problem that terrain effects will always exist, many geological interpretations are conducted without the terrain effects being addressed or corrected in the end (Ugalde and Morris, 2008). One of the few papers to ever implement a topographic anomaly correction to a magnetic dataset was Hildebrand et al. (1993) who provided insight into the magnetic properties of the rocks of Hawaii.

An important contribution to the analysis of terrain induced geophysical anomalies was the 'Nettleton method', first proposed by Nettleton in 1940. Nettleton recognized that spurious anomalies may occur in a gravity survey over a relatively homogeneous surface purely as a consequence of topographic variations. From this, Nettleton realized that it was possible to derive an estimate of the density of the immediate subsurface material. This method used an objective function which sought to minimize the gravity signal over the homogeneous topographic source. While this method was specially developed for gravity surveys, there is no reason why a similar type of approach could not be implemented for deriving magnetic physical property information from ground based TMI surveys. In this chapter I use this approach to obtain localized estimates of magnetic susceptibility.

In the past, a common problem has been accessibility to reliable topographic information. However, with the advent of GPS navigation systems, inertial navigation platforms, radar altimeters and Lidar, most modern aeromagnetic surveys also provide a topographic data set with a resolution that exceeds that produced by earlier aerial photography based stereogrammetry studies. In addition, topographic information is now available from a number of satellite platforms.

The source – sensor distance effect on magnetic signal is not only affected by fluctuations in the flight path of the sensor, but it can also be affected by morphological details of the topographic surface. For example if a water-body is present, the source – sensor distance is controlled by the bathymetry of the lake. Water is non-magnetic so there is no contribution to the overall magnetic signal. An extension of this analogy is the presence of any overburden. Depending on the thickness and magnetic characteristics of the overburden it is possible for this to lead to a diminished magnetic signal (non-magnetic overburden) or create a near surface magnetic anomaly source (magnetic overburden on non-magnetic rocks). Overburden (or regolith) related magnetic anomalies are particularly problematic in areas with deep surface weathering profiles (Pfeiffer et al., 2004).

In order to investigate terrain effects on a magnetic dataset, a magnetic survey from the eighties was revisited. In 1975, the Atomic Energy of Canada Limited (AECL), in collaboration with Natural Resources Canada (formerly Energy, Mines, and Resources – EMR), began an assessment into the suitability of mined igneous rock for the underground disposal of nuclear fuel waste. The Geological Survey of Canada, along with a branch of EMR, conducted a number of drilling and core logging projects in order to obtain geoscientific detail on select locations in the Canadian Shield; one of which included the Eye-Dashwa Lakes Pluton (EDP) 15km north-northeast of Atikokan, Ontario. Various studies were carried out in order to map the EDP and determine its suitability as a potential underground disposal of nuclear fuel waste (Dugal, 1981; Morris, 1985; Lapointe, 1986; Harding, 1988). Central to selection of an area for an underground disposal unit is that the geology be as structurally homogeneous as possible. More specifically, it was recognized that the existence of fractures and faults will invariably affect the stability of the containment and enable subsurface water movement (Kamineni and Stone, 1983). Any potential subsurface water movement is of most concern since it could provide a means of transport for toxic materials to enter the biosphere (Stone and Kamineni, 1981).

The analysis of the configuration of fractures and faults at the EDP was accomplished in the past using a number of geotechnical methods including: aerial photography, aeromagnetic magnetic surveys, airborne VLF-EM and ground geological mapping (Dugal, 1981; Morris, 1985; Lapointe, 1986; Harding, 1988). However, most of these studies were only able to map faults and fractures through indirect inference methods; like the presence of topographic features, ground magnetic geophysical survey and detailed magnetic susceptibility logging of core samples. Geological field mapping of the alteration associated with fractures was, as usual, limited by the extent of rock outcrops. Magnetic susceptibility data indicated that porous / fractures were directly associated with systematic reductions in magnetic susceptibility (Lapointe, 1986; Harding, 1988).

One of the methods used in these previous fracture analyses was a ground-based total magnetic intensity (TMI) survey. Initially all observed magnetic lows were taken as being indicative of a fracture due to reduced magnetic susceptibility. However, no terrain corrections were attempted in the original study. Unfortunately, the magnetic contrast associated with the fractured / unfractured rock is lower than the magnetic contrast associated with the rock / air interface. So it should have been recognized that terrain fluctuations could impact the observed magnetic signal. Further complications are introduced by the presence of numerous lakes in the study area. As the ground magnetic survey was performed in winter, the source – sensor separation over all the lakes was increased by the local water depth. This increased source-sensor separation could have further impacts on the recorded magnetic signal.

In this study, I examine the impact of applying magnetic terrain corrections to this ground magnetic data set and compare fracture patterns derived from the enhanced result with that suggested by the original unprocessed data. In order to minimize the effect of water bodies on the computed magnetic signal, I corrected for terrain effect with bathymetry derived from inversion of the magnetic data with those derived from a splined interpolation of adjacent topographic surface. Estimates of localized susceptibility fluctuations were computed using a modified Nettleton (1940) topographic minimization approach. Finally, the validity of the computed susceptibility fluctuations were tested through a comparison with in-situ susceptibility measurements that were obtained simultaneously with the ground magnetic survey. In summary, this paper shows that it is possible to derive rock – property information from detailed analysis of field magnetic anomalies, and that with surveys reporting sub – 100 nT magnetic anomalies, due consideration must be given to possible topographic effects.

General Geology

The study region is located within the Archean Eye-Dashwa Lakes Pluton (EDP) 15km north-northeast of Atikokan, Ontario (Figure 1), which is south of Forsberg Lake and is part of the Superior Province of the Canadian Shield. This pluton is of Kenoran age (2.5Ga) and is an elliptical shaped massive, medium to coarse grained biotite-horneblende granite (Brown, 1980; Kamineni and Stone, 1983; Lapointe, 1986). The EDP displays three distinct compositional phases: an early coarse-grained syeno-dioritic phase followed by a fine to medium grained leucogranite, and finally by a late medium- to coarse-grained sub-porphyritic granite which represents majority of the mass of the pluton (Brown, 1980).

The Dashwa Gneiss, into which the pluton intruded and exists as xenoliths, is a tonalitic to amphibolitic gneiss complex (Brown, 1980). The gneiss displays banding that is controlled by the contact with the EDP and is sub-parallel with the contact. It has been shown that the gneiss dips away from the pluton in the north and east while to the west the gneiss dips below the pluton (Brown, 1980; Kamineni and Stone, 1983). The Dashwa Gneiss exhibits a complex metamorphic and tectonic history which is not replicated within the pluton indicating the pluton was emplaced post-tectonically.

The Gneiss is shown to have a higher density of lineaments (fractures) than the granite and that these lineaments display more regular patterns. There are no obvious displacements of the contact between the pluton and the gneiss suggesting that this area has not been subjected to any extensive faulting since emplacement of the granite mass. Fractures within the pluton, defined as zones of alteration, are infilled with a variety of materials including chlorite, diabase and lamprophyre dykes, calcite, clay, gypsum, epidote, quartz, granodiorite, and muscovite (Dugal, 1980). Different proportions and combinations of these minerals provide insight into the fluids that have passed through the fractures with time. Early high temperature fracture systems formed during the initial cooling of the pluton are epidote rich (2.6Ga to 2.4Ga), while recent remobilization and rejuvenation of existing fractures are marked by the presence of low-temperature hematite (Kamineni, 1983). Typically epidote, chlorite, or hematite is the dominant infill material (Dugal, 1980).

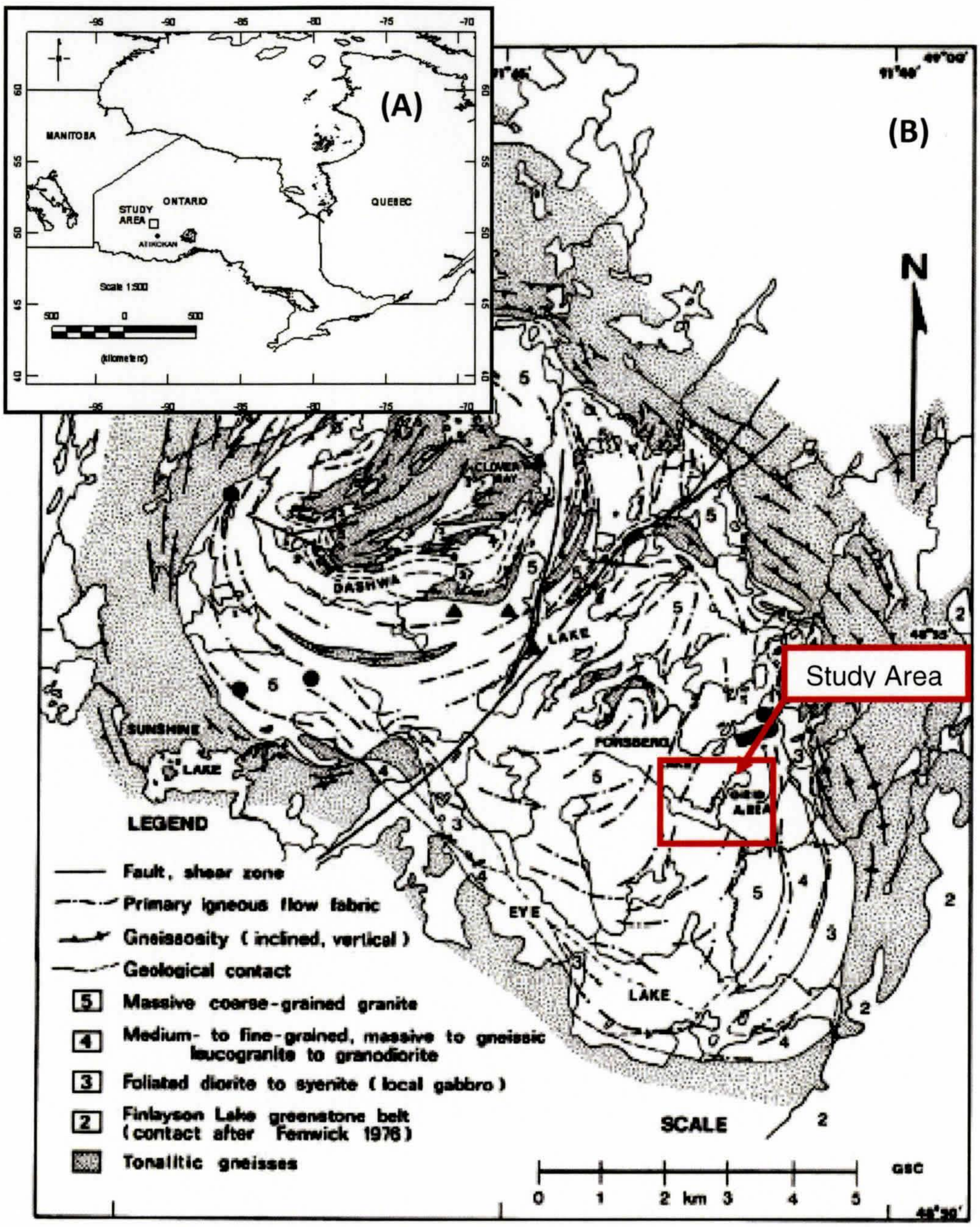
(A)
MANITOBA
ONTARIO
QUEBEC
STUDY AREA
ATIKOKAN
(kilometers)
(B)
N
Study Area
CLOVER BAY
DASHWA
LAKE
SUNSHINE
LAKE
FORSBERG
EYE
LAKE
LEGEND
Fault, shear zone
Primary igneous flow fabric
Gneissosity (inclined, vertical)
Geological contact
5 Massive coarse-grained granite
4 Medium- to fine-grained, massive to gneissic leucogranite to granodiorite
3 Foliated diorite to syenite (local gabbro)
2 Finlayson Lake greenstone belt (contact after Fenwick 1976)
Tonalitic gneisses
SCALE
0 1 2 km 3 4 5
GSC

Figure 3-1.

Map of study area. Location map of study area north northeast of Atikokan, Ontario (A: ESRI, 1997; B: after Stone and Kamineni, 1981).

Since each of these minerals has a significant iron content and is known to have differing specific magnetic susceptibility values their presence in a homogeneous granite should be tied to magnetic anomaly fluctuations. Then the analysis of magnetic susceptibility can be map potential zones of alteration.

According to Brown (1980) all the geoscientific surveys were only capable of in-directly locating discontinuities (faults, fractures) in the rock through anomalous features. Most of the geotechnical mapping methods are identifying surficial lineament features whose geophysical responses are accentuated by water-saturated overburden. However, genesis of surficial lineaments is not restricted to only fracture patterns. Even in the case of geological mapping, direct observations were limited by lack of outcrops. In essence, evidence for the distribution of fractures in a situation which requires careful map detail, like this case study, is somewhat speculative.

Data Sources

All data used in this study were originally collected over two research areas within the Atikokan region during the winter of 1984 and 1985 by Morris Magnetics Inc. These surveys collected total magnetic field (TMI), vertical magnetic gradient of TMI, and magnetic susceptibility variations. The original intention of these surveys was to conduct a quantitative analysis on the distribution of magnetic susceptibility in order to delineate alteration zones in the homogeneous granite.

Magnetic Susceptibility

The ability of a substance to become magnetized under an influencing magnetic field is known as magnetic susceptibility. The magnitude of susceptibility is produced by the occurrence of iron-titanium oxides in a substance, the grain size and the chemical composition of these oxides. Processes like oxidation of magnetite to hematite, a decrease in overall oxide mineral content, or a decrease in grain size of oxide minerals will all lower the magnetic susceptibility of the original sample. The same holds true if secondary mineralization occurs along fractures and alteration zones.

The EDP in the Atikokan region is part of a homogeneous granite in regards to primary mineral content. If this granite is truly homogeneous it should be represented by a uniform magnetic field with random fluctuations associated with the standard deviation of the log-normal susceptibility distribution (Lapointe, 1986; Harding, 1988). Detailed core and in-situ magnetic susceptibility measurements at the ATK site have shown that observed fluctuations in magnetic susceptibility are directly related to systematic changes in the grain size and oxidation state of iron-titanium oxides. Furthermore, it was shown that these systematic susceptibility changes can be directly linked to changes in mineralogy along fracture zones (Coles, 1981; Chomyn et al., 1986). In Lapointe et al. (1986) a quantitative method for identifying these regions of alterations through the application of drill cores from the Atikokan region was discussed. In the same study three observations were discussed: a) the relationship between altered rocks and regions of low magnetic susceptibility; b) inhomogeneous lithologies are associated with highly variable susceptibility; and c) specific types of alterations will be associated with specific magnetic susceptibility levels. Although a reduction in magnetic susceptibility can be attributed to either low iron content in the (original) non-fractured rock reduced susceptibility due to alteration within a fractured rock, this is not a critical problem due to limited extent of oxide-depleted intervals. However, Chomyn et al. (1986) argued that this is not a serious problem due to the limited extent of the oxide-depleted intervals. Table 1 summarizes the relationship between fracture zone characteristics and the mean magnetic susceptibility value. It is obvious that the degree of alteration, fracture frequency and amount of rejuvenation could be consistently correlated to the decrease in magnetic susceptibility (Hillary et al., 1985).

Fracture Zones Type	Fracture-filling Materials	Mean magnetic susceptibility (cgs)
Moderate to subhorizontal dip	Epidote alone	**0.0088**
	Epidote (+ minor chlorite)	**0.0060**
	Chlorite (+ minor epidote)	**0.0049**
	Chlorite (without epidote)	**0.0043**
Steep to subvertical dip	Epidote alone	**0.0082**
	Epidote (+ minor chlorite)	**0.0052**
	Chlorite (+ minor epidote)	**0.0030**
	Chlorite (without epidote)	**0.0027**
Any dip	Any filling of clay or geothite	**0.0028**
Unfractured; unaltered granite		**0.0139**

Table 3-1.

Mean magnetic susceptibilities of common fracture infill materials. Influence of fracture-filling materials and their characteristics on the mean magnetic susceptibility of granite (after Hillary et al., 1985).

All magnetic susceptibility readings were conducted along parallel N-S trending cut-lines with a 100m line spacing. The sampling interval along lines was 100m where outcrops permitted. Susceptibility measurements were acquired in the field using a portable Sapphire Instruments susceptibility bridge. At each location the instrument was first nulled by holding the coil sensor in the air. Then up to six readings were taken at each location. The geometric mean of these six readings was taken as being representative of the susceptibility at that site. The associated standard deviation value gave some indication of the consistency of values at each point. A major limitation of this study was the requirement for a clean outcrop, which was a problem since this study area had swamps with very limited outcrop.

Total Magnetic Intensity (TMI)

Ground magnetic data was collected along a series of parallel N-S trending cut-lines spaced at 100m, different from those of the magnetic susceptibility survey. A proton precession magnetometer, the EDA PPM-400, was used with a resolution of 0.01nT. Individual readings were acquired at 10m intervals along the cut-lines with the sensor 2m above ground surface. A base station magnetometer located at the edge of the grid was used to record "diurnal" (solar) field fluctuations. Simple time-synching between the base station and the field rover magnetometer was used to apply drift and diurnal noise correction.

The line data was gridded using a standard minimum curvature gridding routine with a grid cell size of 25m. As expected the resulting magnetic anomaly map exhibits distinct magnetic lows over the lakes. Another quite definitive feature was the presence of dipolar anomalies at the shore / ice interface (Figure 2A.

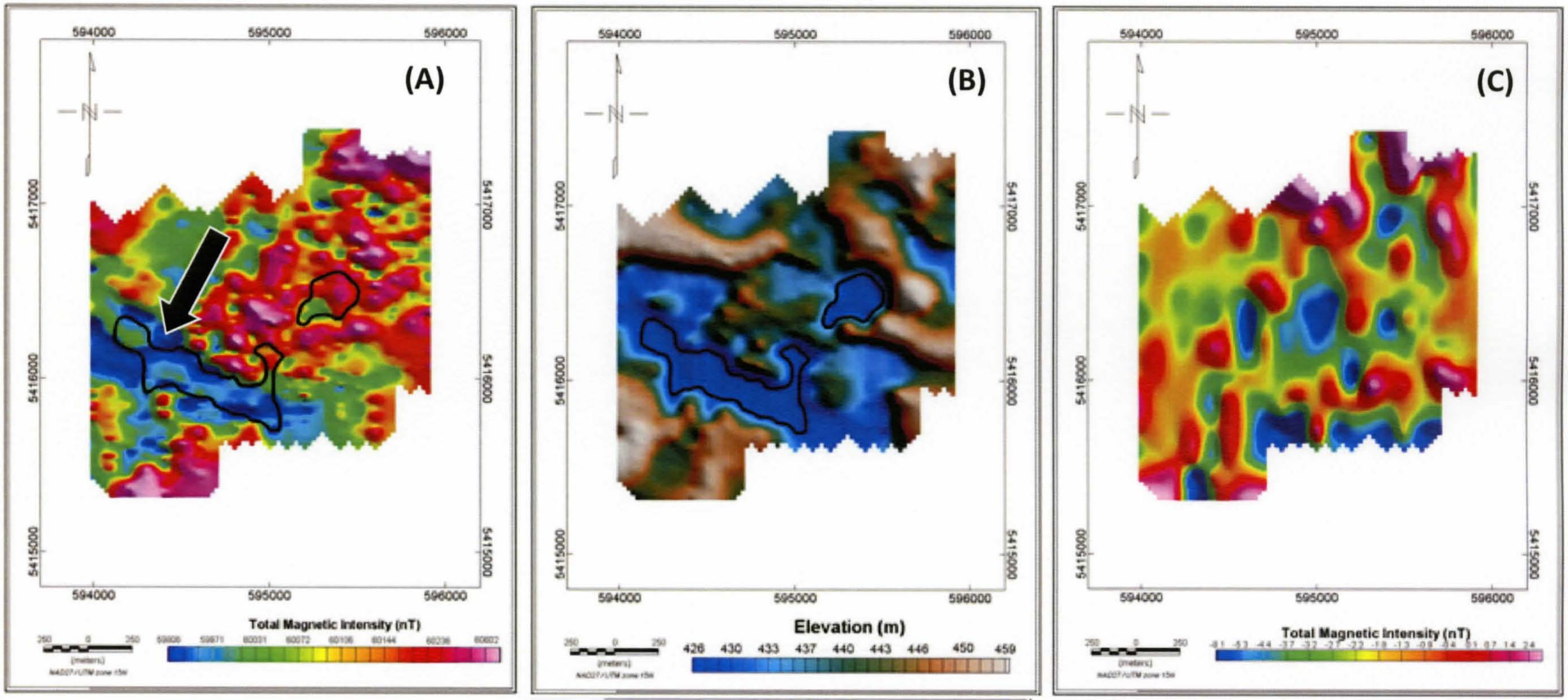
(A)
(B)
(C)
Total Magnetic Intensity (nT)
Elevation (m)
426 430 433 437 440 443 446 450 459
Total Magnetic Intensity (nT)
594000
595000
596000
5417000
5416000
5415000

Figure 3-2.

Grid comparison of original TMI and topography data. Comparison of uncorrected Total Magnetic Intensity (A) and topography (B). Local lakes are indicated in black. A NW-SE running magnetic low can be seen running parallel to a lake (indicated by an arrow).

Topography

The Atikokan field surveys predate the more recent navigational advances made possible with high precision GPS systems. All of the observation points were surveyed in prior to the commencement of the actual survey. The location of each sample point was referenced to a 1:50 000 base map supplied by the Canadian topographic survey. With this information we had two methods of deriving the topographic surface at the time of the study. First, a topographic data base was created by digitizing the position of topographic contour points along each of the cut-lines. Second, knowing the location of the study area, it was possible to verify the topography of the area using more recent SRTM Space Shuttle Topography Mission data. Unfortunately, the 90m spacing of the Space Shuttle imagery is insufficient for the detailed topographic corrections that we required in this study. Topography can be seen in Figure 2B.

Methodology

Bathymetry

Since the magnetic survey was conducted during the winter, all lake surfaces in the study area were frozen. Therefore, for all the magnetic measurements made over the lakes, the source-sensor distance was increased by the bathymetry of the lake possibly creating apparent magnetic lows. In order to see if the increased source-sensor separation over the lakes is in fact generating false anomalies, it is critical to obtain some estimate of the bathymetry of each lake. As these lakes are in a bush environment there is no readily available data source for the bathymetry. Two approaches were used to estimate lake bathymetry.

The first approach is based on the assumption that the topography of the shoreline at each side of the lake can provide some constraint on the overall depth of the lake. This would be especially true if the immediate shorelines were formed by rock outcrops. Assuming there are no sharp discontinuities between opposing outcrops then the bathymetry along each cut line can be estimated by interpolating the topography on either side of the lake using a low order polynomial (B-spline). Like any other polynomial line-fitting approach in a situation with limited data input, it is quite possible to introduce dramatic overshoots which have no real significance. This issue was addressed by careful selection of the tension parameter used in the B-spline calculation. If the tension was too high, then the interpreted bathymetry created unrealistic values that would arise above the known lake surface. The tension which produced the most reasonable bathymetry was 0.3 with a smoothness of 0. Figure 3 presents the observed elevation, draped elevation and the splined elevation.

The second approach to bathymetry mapping was based on simple 2.75D forward magnetic anomaly models of the lake geometry. As input information we know the x, y, z location of each magnetic field measurement. For the survey portions over the lakes, all observations occurred at a constant height above the water (ice) surface, while for the land based portions the ground–based observations had a constant height above the local topography. As an initial step for the purpose of this model calculation we can assume that there are no changes in the susceptibility of the granite below the lake bottom, while the water of the lake can be assigned a magnetic susceptibility value of zero. In this situation the only variable left affecting the calculated magnetic field is the depth of the water (function of source-sensor separation). Hence, computing the optimum model match between the observed and the computed magnetic field provides an estimate of the bathymetry along each cutline.

Apparent magnetic susceptibility

Knowing that magnetic susceptibility at the Atikokan site is a direct indicator of fracture related alteration, obtaining the best estimate of the surficial distribution of magnetic susceptibility became high priority. Unfortunately, as noted by Morris (1985) the idea of obtaining a magnetic susceptibility map through in-situ field sampling is tempered by some practical considerations. While far superior to many other locales, the Atikokan study area only has a limited number of outcrops. Much of the region is covered by lakes and overburden, both of which preclude direct susceptibility measurements. Furthermore, even if outcrop had been more extensive there are practical limitations to an in-situ field mapping program.

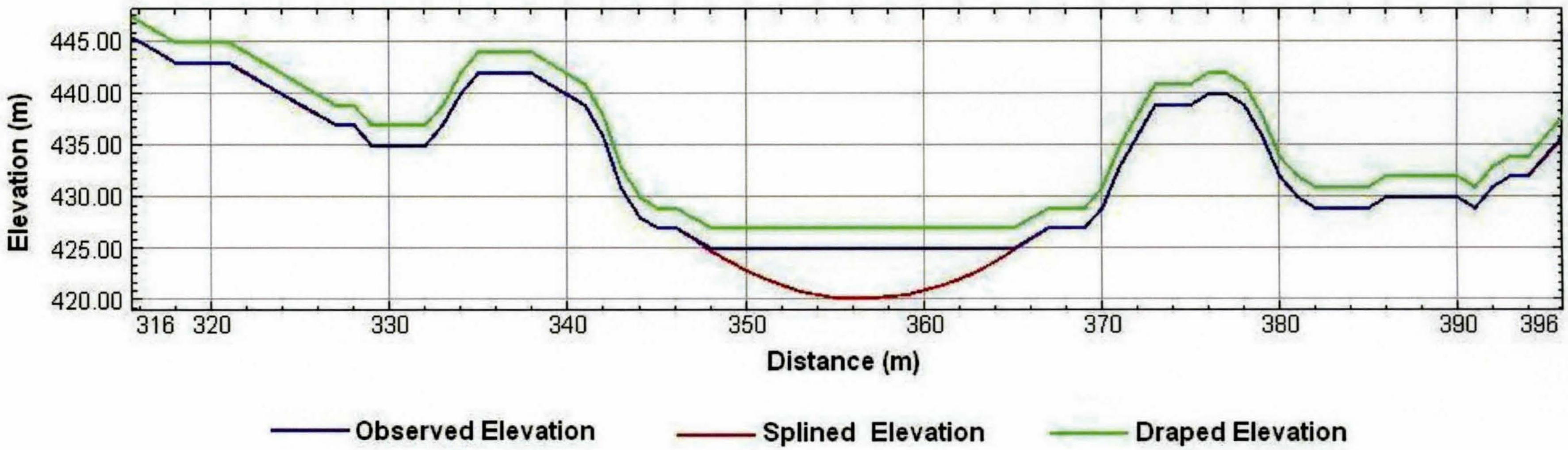
Elevation (m)
445.00
440.00
435.00
430.00
425.00
420.00
316 320 330 340 350 360 370 380 390 396
Distance (m)
Observed Elevation
Splined Elevation
Draped Elevation

Figure 3-3.

Profile section of varying elevations. Profile along line 4200 exhibiting the differences between the observed elevation, the draped (observed + 2m) elevation and splined elevation.

This in-situ magnetic susceptibility survey conducted survey readings every 100m when outcrop was available. However, borecore studies, which used three readings every 2m, suggested the fracture systems have a scale of tens of meters. To adequately map a surficial area would require samples on a 5m scale grid, which was impossible based on the limited availability of outcrops.

An alternative approach is to compute an apparent susceptibility distribution from the measured TMI data. Since the TMI dataset covered a more extensive area with a sample spacing of 10m, fracture zones that were 20m or greater in scale would be resolved. TMI will not resolve all fracture zones, but a greater number than the in-situ magnetic susceptibility survey. These calculated apparent magnetic susceptibility values are subsequently compared with observed magnetic susceptibility values to delineate zones of alteration within the EDP study area. While in essence this involves simple forward modeling of the TMI there are a number of ways of approaching this problem. Each of them involves analyzing the problem with distinct levels of spatial resolution – at both a *regional* and *local scale*.

Taking a regional scale approach - if the EDP granite is indeed truly homogeneous, then the average calculated magnetic susceptibility for the whole study area should be similar to that of non-fractured, unaltered granite. An average bulk magnetic susceptibility value was derived by computing the magnetic variation of a slab of massive granite having a known morphology and uniform physical property. A Taylor Series expansion correction was applied to all of the TMI data over the lakes to ensure that all observation points were at a constant elevation above the topographic surface. The upper surface of the uniform slab was defined by the combined splined bathymetric and topographic surfaces. The lower surface of the slab was defined as a horizontal surface that was positioned just below the minimum surface topographic level. The actual location of this surface is not critical since increased depth would result in a DC shift on the computed magnetic data. Determination of the average bulk magnetic susceptibility of this homogeneous rock slab was accommodated through algorithms defined by Encom's modelling software ModelVision. Using an ambient field of 57400nT with an inclination and declination of 74° and -3° respectively, the magnetic susceptibility of the generated granite slab was varied until the computed TMI matched the observed TMI. For this part of the study I defined match as agreement between the mean and standard deviations of the observed and computed TMI values.

This regional scale approach cannot provide any information on the spatial variation of apparent magnetic susceptibility. It is only capable of determining if the computed average susceptibility is similar to the observed magnetic susceptibility associated with unaltered granite, a value of 0.013cgs (Hilary et al., 1985). To derive more detail (local scale) on the spatial fluctuations of susceptibility, apparent susceptibility was derived by computing 2.75D forward models for each of the cutline TMI profiles using the profile based forward modeling routine Geosoft GM-SYS. Knowing topography, TMI, and the local Earth's magnetic field the only variable remaining is the localized susceptibility distribution. In these models, no magnetic remanence was taken into consideration. Optimized matches between the observed and computed magnetic field for each cut line were derived through the introduction of localized sub-vertical slabs of varying susceptibility, which represented in-filled fractures (Figure 4).

Two issues were addressed in the more detailed modelling approach. First, ground magnetic surveys are notoriously noisy, especially when looking at low amplitude magnetic anomalies. For example, field operators are not non-magnetic and small differences in the proximity of the sensor to the operator are noticeable. To address this issue I applied a low-pass filter (cutoff wavelength of 5 fiducials) to the original profile data and desampled the data to an observation point every 20m. Secondly, it is incorrect to tie the presence of an alteration zone to a single observation point as there is no degree of confidence in this observation. Hence the width of all modelled slabs (alteration zones) was set at a minimum of three observation points, which corresponded to a minimum slab thickness of 40m.

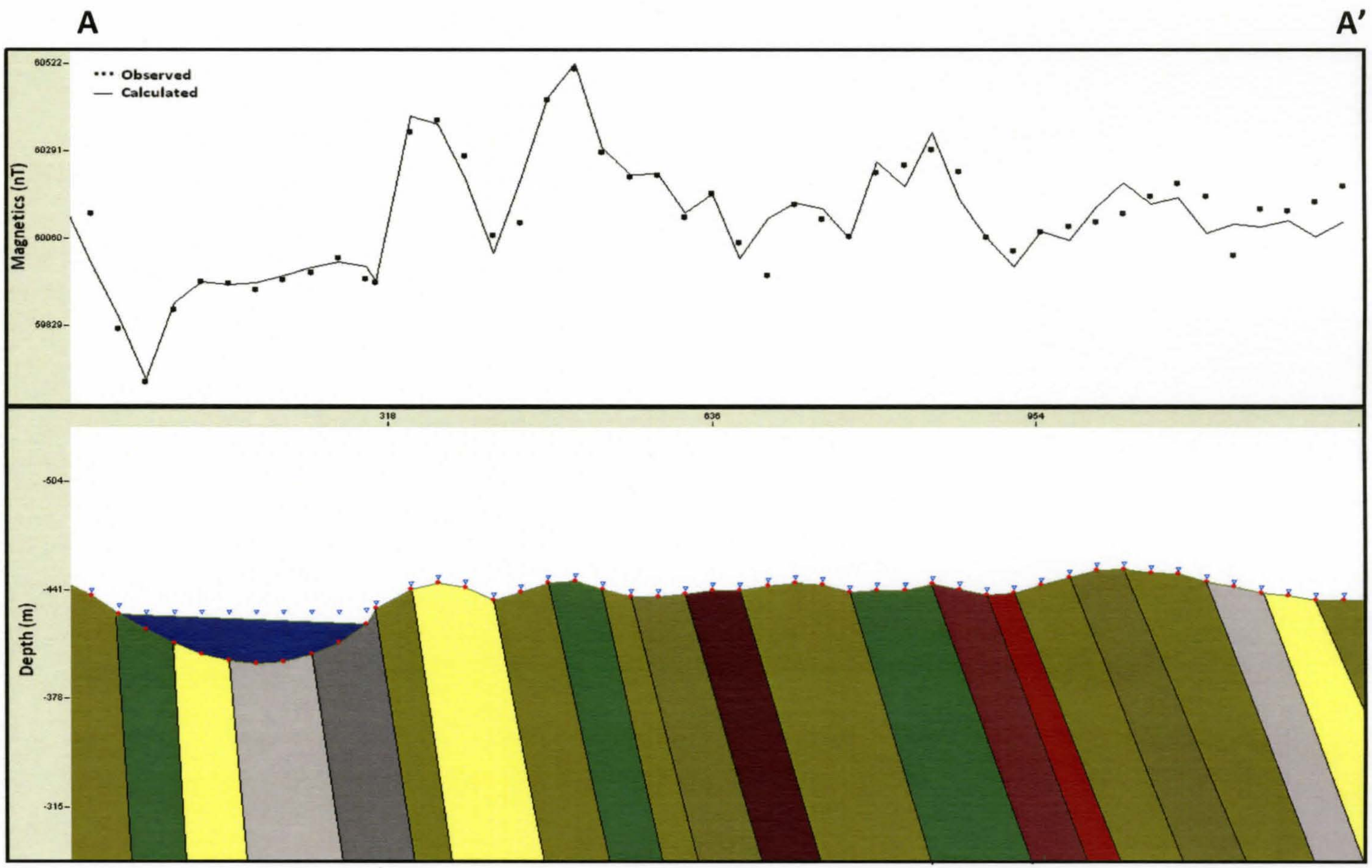
A
A’
Observed
Calculated
Magnetics (nT)
60522
60291
60060
59829
318
636
954
Depth (m)
-504
-441
-378
-315

Figure 3-4.

GM-SYS Profile along line 4800. A cross-section along line 4800 showing the north dipping sub-vertical slabs that represented zones of alteration. Each slab has been randomly coloured and do not represent any specific magnetic susceptibility value.

To obtain more detail of the susceptibility variations requires higher resolution topographic data and a finer spacing magnetic data set. With respect to geology, all alteration zones (modelled as vertical slabs) were sub-vertically dipping to the north, which was the dominant dip direction indicated by Stone (1980) and Morris Magnetics Limited (1985) and only the top 100m below surface were forward modelled. Once again, an ambient field of 57400nT with an inclination and declination of 74° and -3° respectively was used. Following the forward model, an inversion was completed along each cut line. During the inversion process, only the magnetic susceptibility of each slab was allowed to vary. This enabled the determination of more refined magnetic susceptibility values in order to accomplish the closest match possible between the observed and computed magnetic fields.

Results

Bathymetry

The rock slab unit was treated as an unaltered massive, homogeneous rock unit with a constant magnetic susceptibility of 0.013cgs (Hillary et al., 1985) to represent the Eye-Dashwa Lakes Pluton. The data set then underwent inversion allowing the model to vary strictly in the Z (vertical) direction over the lakes based on the assumed subsurface geometry (homogeneous granite) and magnetic susceptibility. A comparison between the interpolated and inverted bathymetry can be found in Figure 5A and 5B. Both computation methods produced similar results for bathymetry. The smaller lake displays shallower depths while the larger lake is consistently deeper, with the central portion at greatest depth. As can be seen in Table 3, the average difference between the two methods was only 0.65m ± 3.67m.

Ideally the two approaches should produce similar bathymetric models. Clearly there are a number of limitations. First, the bathymetry determined by the polynomial fit will be strongly influenced by the topographic gradient at the edges of the lake. If a steep gradient exists at the lake edge, this will result in a bathymetry that is deeper than what is likely the true depth. The contrary would hold true as well, if the lake edge has a shallow gradient, the interpolated bathymetry will be too shallow.

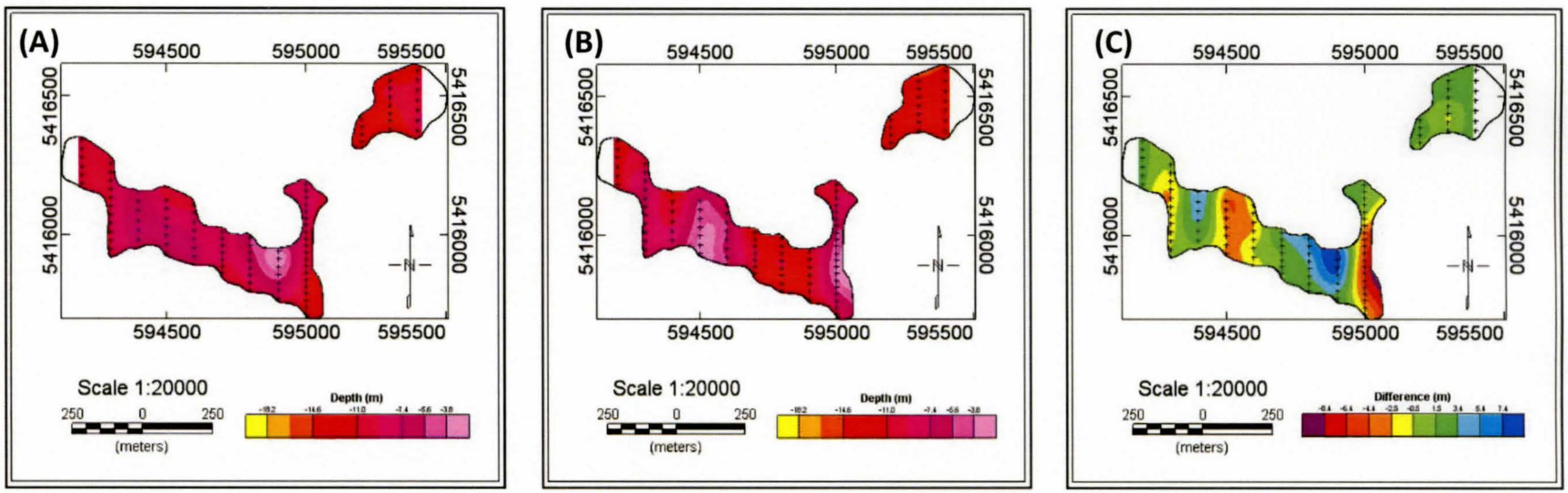
(A)
594500
595000
595500
5416500
5416000
Scale 1:20000
250 0 250
(meters)
Depth (m)
(B)
594500
595000
595500
5416500
5416000
Scale 1:20000
250 0 250
(meters)
Depth (m)
(C)
594500
595000
595500
5416500
5416000
Scale 1:20000
250 0 250
(meters)
Difference (m)

Figure 3-5.

Grids of calculated bathymetry. Splined bathymetry (A); Inverted bathymetry (B); Difference between splined and inverted bathymetry (C) with survey locations (+). Equal area colour scheme used.

	Minimum	Maximum	Mean	Standard Deviation
Difference Statistics	-10.3	9.33	0.65	3.67

Table 3-2.

Bathymetry statistics. Statistics of difference grid between inverted and splined bathymetry (cgs) of both local lakes in the Atikokan study area.

Secondly, it was of prime importance for this study that the magnetic susceptibility under the lake remained constant. Therefore, any observed TMI lows were accommodated through a calculated deeper bathymetry. However, should a portion of the lake actually be underlain by a fracture then the observed TMI signal at that point will be lower as a consequence of the reduced susceptibility level. Thus, previously calculated bathymetric lows in fact represent alteration zones. Therefore by calculating a summary grid that represents the difference between the interpolated and modelled bathymetry, negative differences between the two bathymetry estimates probably suggest the presence of underlying altered fractures (Figure 5C).

Magnetic Susceptibility

Regional Scale

The standard deviations calculated for the magnetic susceptibility of the granite slab were used as an "error envelope" in which the observed maximum and minimum values of the recorded TMI had to occur. Based on Figure 6, if a susceptibility below 0.0019cgs was chosen then the observed minimum would fall outside the error envelope and conversely a susceptibility above 0.0021cgs would result in the observed maximum falling outside the envelope. As such, the optimal average susceptibility lies between 0.0019cgs and 0.0021cgs. This treats the slab as having a uniform magnetic susceptibility. Since the average calculated magnetic susceptibility of the generated granite slab is lower than the measured magnetic susceptibility value of non-fractured, unaltered granite, there is likely some occurrence of alterations within the EDP. Therefore a detailed investigation into the spatial occurrence of magnetic susceptibility should be completed.

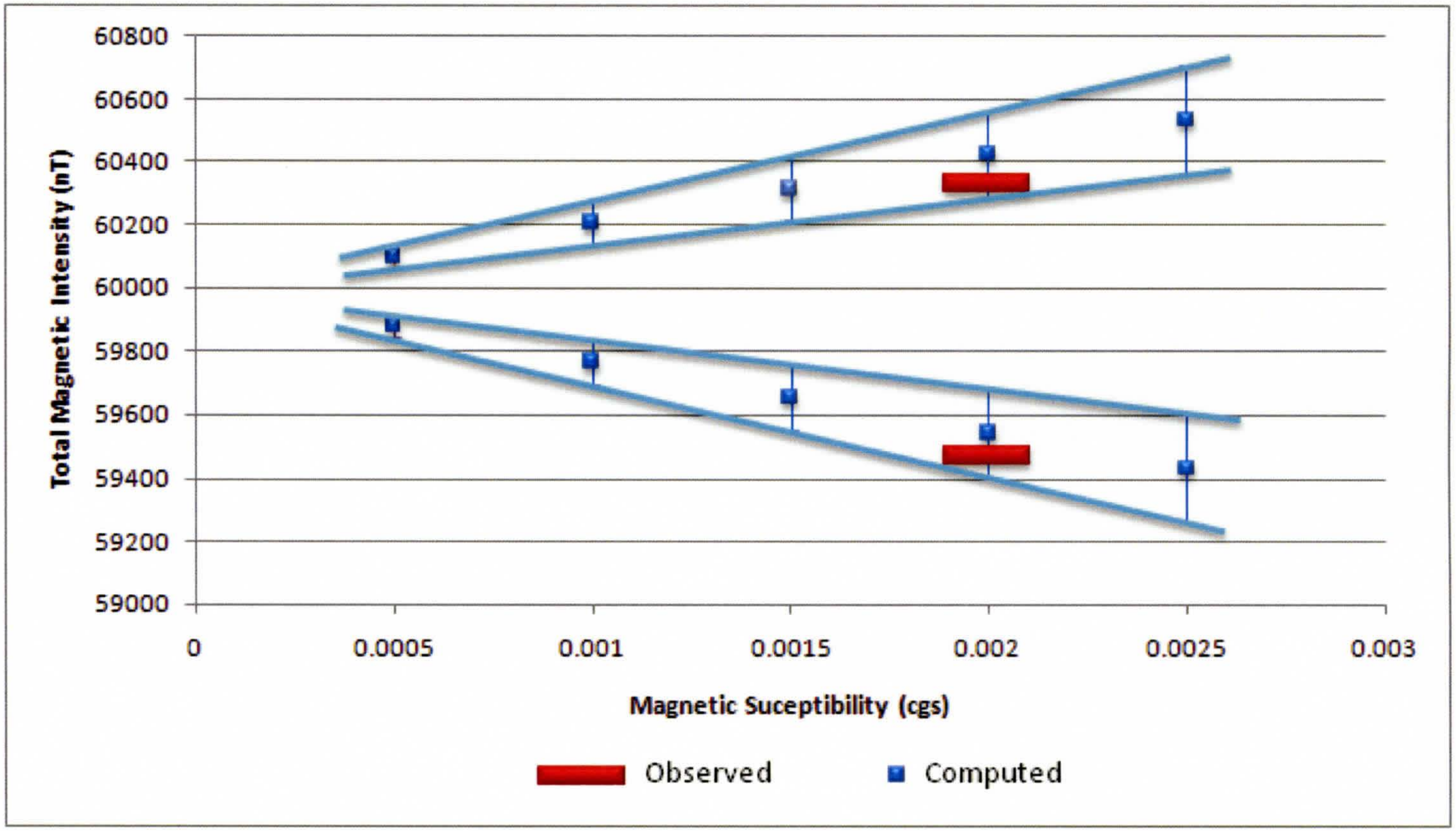
60800
60600
60400
60200
60000
59800
59600
59400
59200
59000
Total Magnetic Intensity (nT)
0
0.0005
0.001
0.0015
0.002
0.0025
0.003
Magnetic Suceptibility (cgs)
Observed
Computed

Figure 3-6.

Observed magnetic susceptibility from computed error bounds. Position of observed minimum and maximum TMI values with respect to the derived computed error envelopes from generated granite slab.

Local Scale

The two magnetic susceptibility grids in conjunction with each other provide more thorough detail into the configuration of alteration zones within the EDP. As can be seen in Figure 7, large and small scale sub-parallel northwest trends scale can be seen in both magnetic susceptibility datasets. The trends display a gradual variation in magnetics. Based on previous insight into the alteration of hydrothermal fluids and their link to magnetic anomaly lows, these lineaments may indicate zones of alteration and fracture in-fill. This general alteration trend of NW-SE agrees with the fracture populations discussed in Dugal (1980) and Morris Magnetics Ltd. (1985). This shows that the EDP is in fact not homogeneous and has undergone fracturing with subsequent in-filling. However, it is important to note that there is an unaccounted for DC shift between the two datasets. The apparent magnetic susceptibility data has overall higher values than the values seen in the observed magnetic susceptibility. A comparison on grid statistics of the two magnetic susceptibilities can be seen in Table 3.

Finally, to confirm that the interpreted local scale magnetic susceptibility variations are independent of topography variation, both the apparent and observed susceptibility grids were draped on the splined terrain and assessed in 3D (Figure 8). Qualitatively, there is little to no correlation between the occurrence of susceptibility anomalies (lows) and topography. This indicates that the magnetic susceptibility values, both apparent and observed, are influenced solely by true surficial geology.

Discussion

As was already well known, all magnetic anomaly records do contain significant topographic signal and that if topographic effects are not taken into consideration prior to any sort of processing and interpretation, then results may be misguided. In the case of EDP, magnetic anomaly lows previously linked with fracture zones were reconfirmed by the results of this case study. In this case, the increased source-sensor separation due to unaccounted bathymetry did not account for the significant magnetic low seen in Figure 2A.

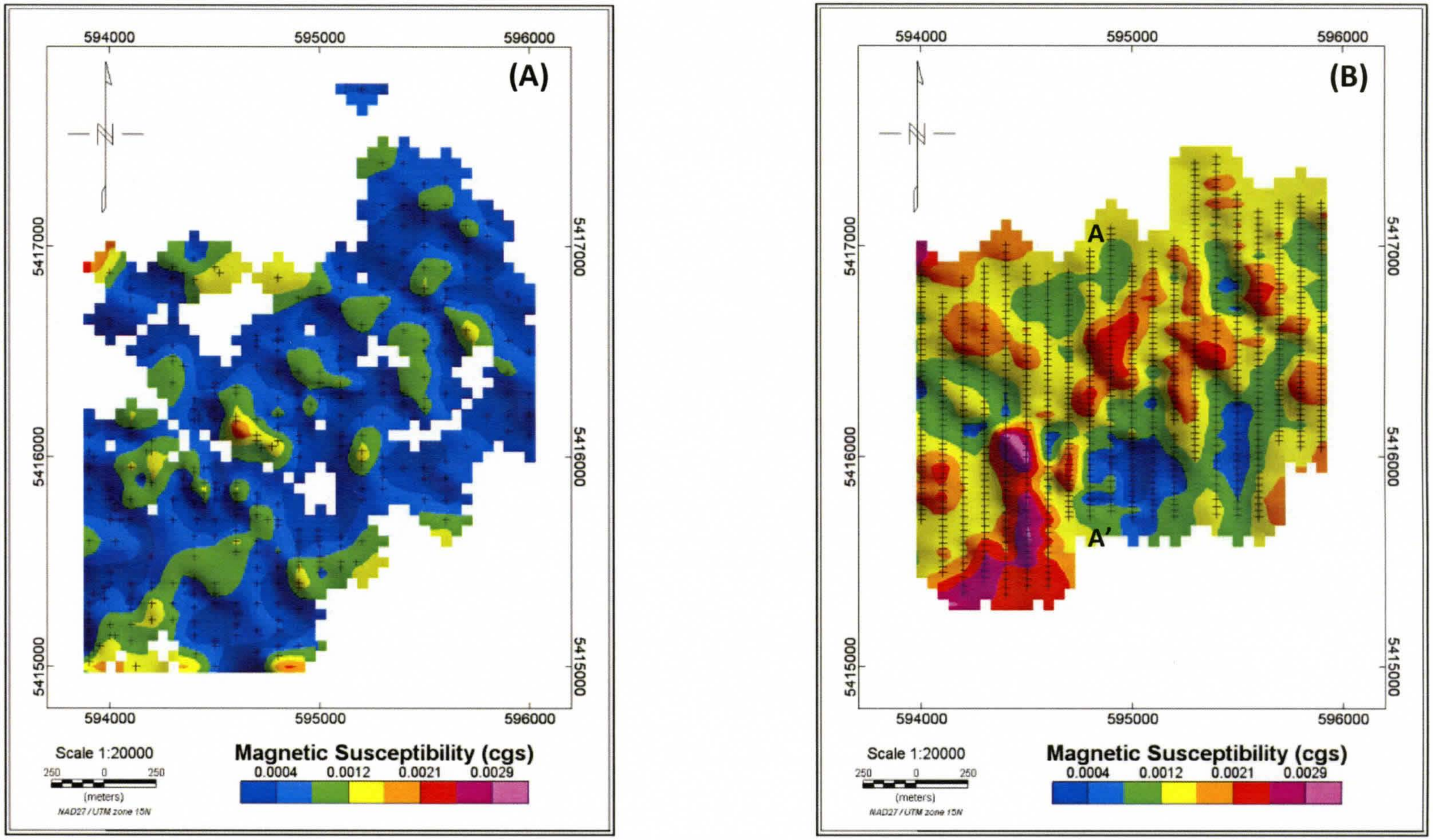
(A)
594000
595000
596000
5417000
5416000
5415000
Scale 1:20000
250 0 250
(meters)
NAD27 / UTM zone 15N
Magnetic Susceptibility (cgs)
0.0004 0.0012 0.0021 0.0029
(B)
A
A'

Figure 3-7.

Distribution of observed and apparent magnetic susceptibilities. Observed (A) and apparent magnetic susceptibility (B) maps with position of readings indicated (+). Even though the average susceptibility is lower in the observed dataset, both datasets display a series of sub-parallel NW-SE running lineaments. A minimum curvature interpolation method and linear colour scheme with identical intervals were used. A DC shift is apparent between the two datasets.

	Minimum	Maximum	Mean	Standard Deviation
Apparent Magnetic Susceptibility	0.0001×10^{-1}	0.0033	0.0012	0.0005
Observed Magnetic Susceptibility	-0.0001	0.0021	0.0006	0.0003

Table 3-3.

Comparative statistics of magnetic susceptibilities. Statistical comparison of apparent and observed magnetic susceptibilities (cgs) of the Atikokan study area.

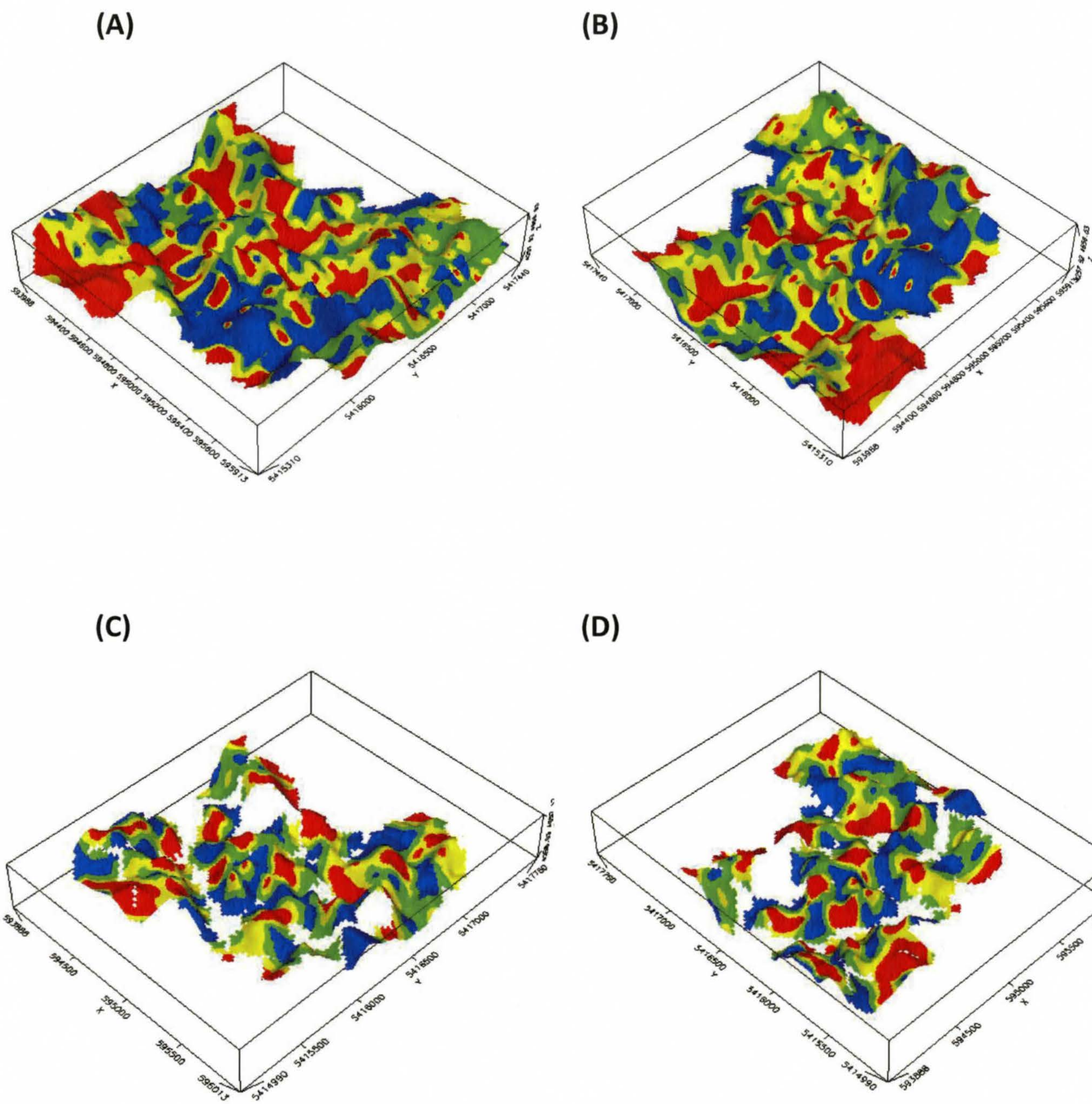
(A)
(B)
(C)
(D)

Figure 3-8.

3D perspectives of apparent and observed susceptibilities draped on splined topography. First perspective (A, C) is from an inclination and declination of 45° and 45° respectively. Second perspective (B, D) is from an inclination of 45° and -45° respectively. Visually, there is a difference in the occurrence of magnetic susceptibility lows and known topographic features.

The shallow lake bathymetry only accounted for a variation in magnetic intensity of less than 10nT when calculating the difference (Figure 2C) between the original TMI and the Taylor Series expansion corrected TMI. Therefore, the large magnetic anomaly seen in Figure 2A represents valid geology. What likely occurred was initially a large NW-SE fracture was emplaced into the granite, which was subsequently in-filled by hydrothermal fluids causing lower magnetic susceptibilities along this fracture. Over time, due to the difference in mineral content of the granite and alteration zone, erosional processes permitted the development of a topographic low in which the lake developed.

Following this idea, it has been shown that the EDP contains fractures and alteration zones. In order to assess quantitatively the number of alteration populations contained in both datasets the log percent frequency histograms for the susceptibility of the study area were calculated (Figure 9). The observed susceptibility displays a bimodal distribution while the apparent susceptibility appears to display only a single normal distribution. These distributions would suggest that the observed data has recorded two discrete magnetic susceptibility populations while the apparent data has only resolved one population. However, transforming both datasets into cumulative frequency probability plots (Figure 10) show there are four distinct cutoffs, resulting in three distinct populations for each dataset in the study area. Note that outliers present in both datasets were removed prior to transformation in order to more readily discriminate specific populations. The method of cumulative frequency probability causes any normal distribution in a dataset to be represented linearly. This is very beneficial with the current datasets, where the occurrence of certain populations shadow the occurrence of smaller populations. This is why only two distributions were resolved in observed susceptibilities and only one was resolved in the apparent susceptibility dataset. With three populations existing in both datasets, this supports the surface susceptibility results of nearby study areas and borecore results discussed by Morris (1985). Furthermore, when regarding the cumulative frequency plots, the DC shift present in the magnetic susceptibility grids causes a shift once again between the average susceptibilities of the individual populations.

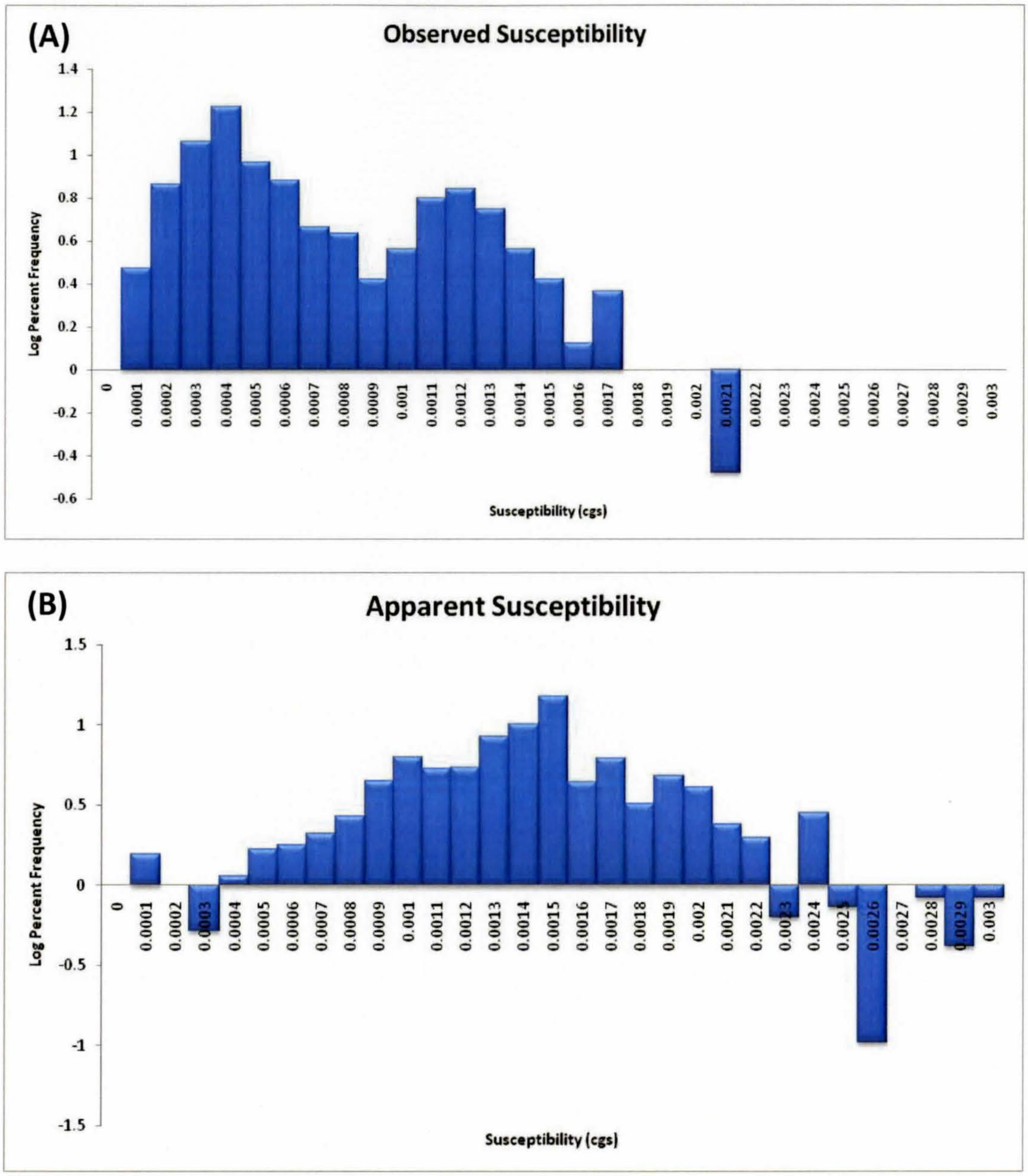
(A)
Observed Susceptibility
Log Percent Frequency
1.4
1.2
1
0.8
0.6
0.4
0.2
0
-0.2
-0.4
-0.6
0
0.0001
0.0002
0.0003
0.0004
0.0005
0.0006
0.0007
0.0008
0.0009
0.001
0.0011
0.0012
0.0013
0.0014
0.0015
0.0016
0.0017
0.0018
0.0019
0.002
0.0021
0.0022
0.0023
0.0024
0.0025
0.0026
0.0027
0.0028
0.0029
0.003
Susceptibility (cgs)
(B)
Apparent Susceptibility
Log Percent Frequency
1.5
1
0.5
0
-0.5
-1
-1.5
Susceptibility (cgs)

Figure 3-9.

Log of percent frequency histograms. Log of percent frequency of observed susceptibilities (A) and apparent susceptibilities (B). Observed susceptibilities display a bimodal distribution while the apparent susceptibilities display a single normal distribution.

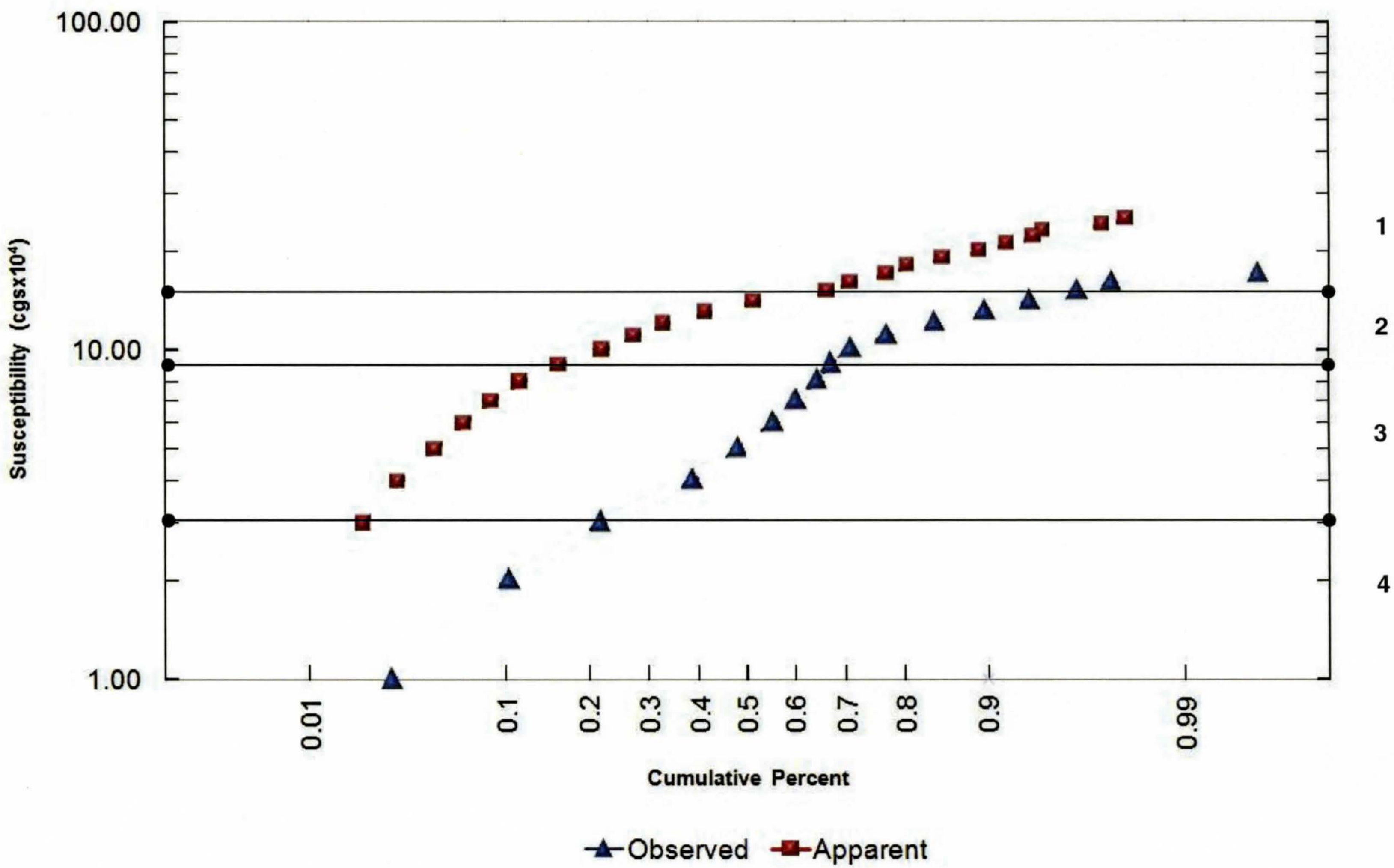
100.00
10.00
1.00
Susceptibility (cgsx10-4)
0.01
0.1
0.2
0.3
0.4
0.5
0.6
0.7
0.8
0.9
0.99
Cumulative Percent
1
2
3
4
Observed
Apparent

Figure 3-10.

Cumulative frequency probability plots. Cumulative frequency probability plot of observed and apparent susceptibilities with outliers removed. Transformation of data resolves three distinct populations in the study area. The cut offs are associated with the following magnetic susceptibilities: 1.>0.0017cgs; 2. >0.0009cgs and <0.0017cgs; 3. >0.0003cgs and <0.0009cgs; 4. <0.0003cgs. Once again, a DC shift can be seen between the two datasets.

Based on the cut offs derived from Figure 9, both the apparent and observed datasets were separated into four discrete groups based on the following cutoffs: 1.>0.0017cgs; 2. >0.0009cgs and <0.0017cgs; 3. >0.0003cgs and <0.0009cgs; 4. <0.0003cgs. Figure 11 shows the resultant apparent and the observed susceptibility grids in conjunction with each other. Visually, there is somewhat of a correlation between the occurrence of cutoffs two and three; however there is less correlation within cut offs one and four. This is expected since according to the cumulative probability plot, cut offs one and four have represented a very limited percentage of the total populations of the two datasets (apparent or observed).

Physical rock properties may be derived from alternative geophysical methods in situations of limited accessibility. This concept is not new, but forgotten in an era of new high resolution aeromagnetic surveys. Both methods for determining magnetic susceptibility distribution display different overall magnetic susceptibility averages. The observed susceptibility dataset has a higher percentage of lower susceptibility values, which would imply increased alteration. If this implication is valid, then there is a higher occurrence of alteration at surface than within the general rock mass. However, validation may be considered through differences in source sampling. The observed magnetic susceptibility survey was collected in-situ, therefore observations were only collected in outcrop areas, which are not consistent across the survey area. Even when outcrops were available, the sampling interval was 100m separation, therefore no feature smaller than 200m could be fully resolved. This places a large biasing effect on whether zones of alteration could truly be resolved. Since previous borecore studies showed that fractures and alterations were on the order of tens of meters (Morris Magnetics Limited, 1985), the resolution of the in-situ magnetic susceptibility survey was insufficient for the purpose of this study. This reiterates the idea that in order to fully evaluate the magnetic susceptibility of an area, high-resolution readings are required. The resolution has to be a function of the size of the feature being measured. In the end, apparent magnetic susceptibility was derived from TMI, which had a smaller sample spacing of 10m intervals, which provides greater reliability and increased probability of resolving the zones of alteration.

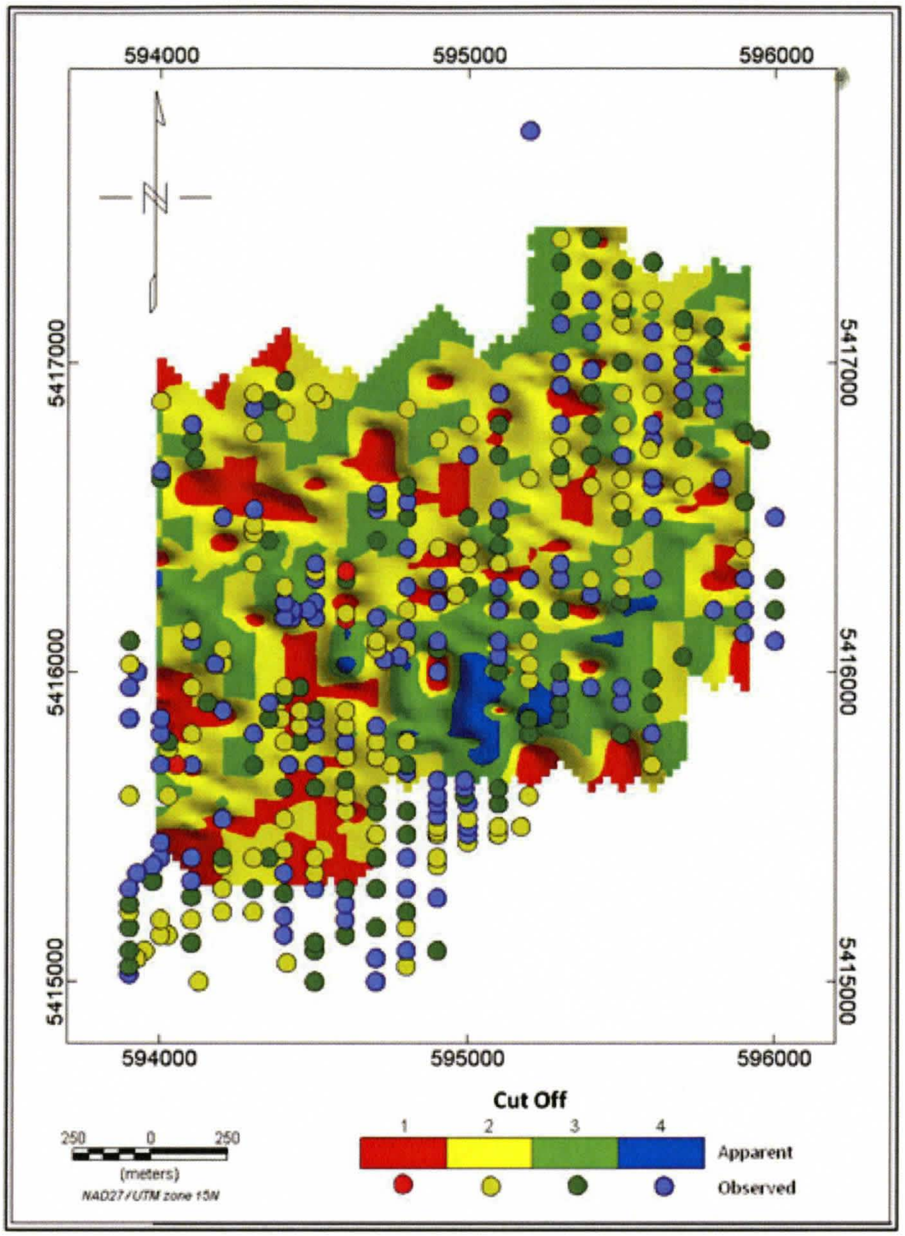
594000
595000
596000
5417000
5416000
5415000
Cut Off
1
2
3
4
Apparent
Observed
250 0 250
(meters)
NAD27 / UTM zone 15N

Figure 3-11.

Distribution of apparent and observed susceptibilities. Apparent susceptibility grid with observed susceptibility symbols overlaid both using a colour table based on four defined cut off levels. Based on this plot, there appears to be a visible spatial correlation in cut off levels 2 and 3 between apparent and observed susceptibilities; however, there is less visible correlation in cut offs 1 and 4 of the apparent and observed susceptibilities.

Aside from a sampling problem, there were other conditions that may have contributed to the DC shift. First, the outcrops on which in-situ magnetic susceptibility readings were conducted, will have likely undergone some form of weathering which causes the in-situ readings not to be representative of the true property of the whole rock. Furthermore, TMI surveys measure the amplitude of the summation of all magnetic minerals within a specified range; this summation includes both a constant ambient field and a varying magnetic susceptibility value. Second, that these alteration zones may have remanent magnetization and since remanence was not incorporated into the modelled magnetics, the modelled susceptibility values were higher than their true value.

Conclusion

A common method of delineating fractures is through alteration mapping. Zones of alteration are often associated with magnetic lows due to a decrease in the overall titanium-oxide mineral. Through magnetic susceptibility mapping, fracture configurations may be deduced. However, in a previous study conducted during the eighties, the interpreted magnetic datasets were not corrected for a varying source-sensor separation due to an undulating terrain. As such, terrain corrections using Taylor Series expansion were applied using known ground topography and a newly calculated bathymetry to view the effects of the varying source-sensor distance. However, in this case it was shown that the unaccounted bathymetry did not cause a significant change in the recorded magnetic intensity (less than 10nT). Ultimately, the presence of the lake is likely caused by a fracture in which the lake depevloped over time. In which case, the lake is underlain by fracture in-filled mineralizations that have overall lower magnetic susceptibility values causing the magnetic anomaly low in Figure 2A. However, it is still stressed that to derive a magnetic dataset that is completely influenced by geology, terrain corrections must be accomplished.

Furthermore, it was shown through a modified Nettleton method, that magnetic susceptibility values may be derived from total magnetic field intensity. Magnetic susceptibility is often measured in-situ, however this causes a limitation in the survey sample spacing and the overall resolution of geological features. In this case study, the sample spacing of the in-situ magnetic susceptibility survey was too limited to ideally resolve most alterations. As an alternative method, apparent magnetic susceptibility was calculated using total magnetic intensity, which had a smaller sample spacing and therefore a greater ability to resolve smaller fracture patterns. In the end, through qualitative and quantitative analyses, populations of NW-SE striking magnetic susceptibility populations were delineated. This supported previous studies that the Eye-Dashwa Lakes Pluton is not homogeneous in respect to structure.

CHAPTER FOUR

Application of high-resolution electromagnetic, magnetic, radiometric and gravity surveys in geological map evaluations:

A case study from the Bathurst Mining Camp, New Brunswick, Canada

Summary

In order to develop Canada's base metal reserves the Geological Survey of Canada implemented two collaborative initiatives: the EXTECH and the TGI. Both initiatives focused on the Bathurst Mining Camp in New Brunswick, Canada, which as of 2001 was responsible for 70% of New Brunswick's mineral production. As part of these initiatives, multi-parameter geophysical surveys over the entire camp were completed between 1995 and 2007. These surveys included high-resolution airborne electromagnetic, magnetic, radiometric survey data along with ground gravity survey data. This chapter presents an integrated study using these four geophysical datasets to re-evaluate the presently accepted geological map. Due to the large spatial extent of the Bathurst Mining Camp only one section will be discussed in detail, the Sheephouse Brook Block located in the southern portion of the camp. This block is recognized for complex folding and thrusting, most of which is unfortunately hidden by vegetation and glacial overburden. Furthermore, this block hosts the oldest known massive sulfide deposits within the Bathurst Mining Camp, which includes the Chester deposit. The Chester deposit which was discovered in 1955 by an airborne electromagnetic survey may act as a template for future geophysical exploration methods.

Introduction

The Bathurst Mining Camp (BMC) has 45 known massive sulfide deposits and 95 significant occurrences. The BMC became publicly recognized when the discovery of the Brunswick 6 deposit occurred in 1952. Shortly thereafter, the Brunswick 12 deposit was discovered, which as of 1998, had produced 88,806,500 tons. Due to these two major discoveries the area was heavily explored and staked, with a number of further discoveries occurring, like for example Heath Steele and Chester deposits. As of 1998, Heath Steele had processed 130 million metric tonnes of massive sulfide, gossan, and supergene ores (McCutcheon, 2003). Subsequently, the area underwent extensive geological and drillcore investigation which lead to the further discovery of disseminated sulfides. The Chester deposit was discovered in 1955 courtesy of an airborne electromagnetic survey flown by Kennco Explorations (Canada) Limited (Fyffe, 1995).

In 2001, the BMC accounted for 70 percent of New Brunswick's total mineral production and whose production value exceeded $500 million dollars. The BMC accounts for the employment of over 2000 personnel, however due to a decline in Canada's mineral resources these positions are threatened (Goodfellow, 2003). In response to the decline in production, a number of Government interdisciplinary projects were carried out, including: EXTECH (**Ex**ploration and **Tech**nology) and TGI (Targeted Geoscience Initiative) - both aimed at extending Canada's base metal reserves. The specific program components, EXTECH-II and TGI-3, focused on the BMC and involved a variety of high-resolution geophysical surveys.

The first project EXTECH-II, initiated in 1994 was a collaboration between the Geological Survey of Canada, the Department of Natural Resources and Energy of New Brunswick, and a number of non-governmental organizations, including mining companies and universities (Goodfellow, 2003). The purpose of this project was to develop an understanding of regional and local scale geological models. In 1995, a multi-parameter helicopter-borne geophysical survey was completed over the entire BMC. This survey consisted of high-resolution magnetic, electromagnetic and radiometric data acquisition (Keating, 2003). From these datasets an improved geological understanding of the BMC was accomplished along with the identification of a few non-economic deposits. EXTECH-II provided insight into surface indirect geological mapping through geophysics; however this was limited in the understanding of subsurface structure (Rogers, 2008). In order to derive further subsurface geological detail on the Bathurst region a second project was completed close to a decade later.

The TGI-3 project was initiated by the Government of Canada in 2005 as a 5-year integrated geoscientific investigation into Canadian base metal reserves (Geological Survey of Canada, 2007). This project aims to develop new and existing mapping methods of deep-seated base metal deposits through geological, geophysical, and geochemical methodologies. As part of the TGI-3 project a ground surface gravity survey was collected in 2007 by Geomatics Canada (Rogers, 2008).

The objective of this case study is to integrate the geophysical datasets acquired from the EXTECH-II and TGI-3 initiatives into a re-evaluated geologic map. This geologic map represents the boundaries and geological structures that are readily resolved by strictly by these geophysical datasets.

General Geology

The Bathurst Mining Camp (BMC), originally termed the Bathurst-Newcastle district, is located in northeastern New Brunswick and is part of the Miramichi Highlands (Figure 1) (McCutcheon, 2003). The BMC is underlain by primarily Cambrian and Ordovician sedimentary and volcanic rocks units. These units are subdivided into five blocks: the Miramichi, Tetagouche, California Lake, Sheephouse Brook, and Fournier. The first of these blocks is Cambrian to Ordovician of age while the latter four are Ordovician in age. These blocks are the remnants of the ancient Tetagouche-Exploits back-arc basin and were thrust into juxtaposition during the closure of the back-arc basin (van Staal, 2003). The BMC hosts a very complex assemblage of multi-generational folds, structures, and deformation of volcanic and sedimentary rocks. The most well known fold structures are the Tetagouche Antiform and the Nine Mile Synform (Figure 1).

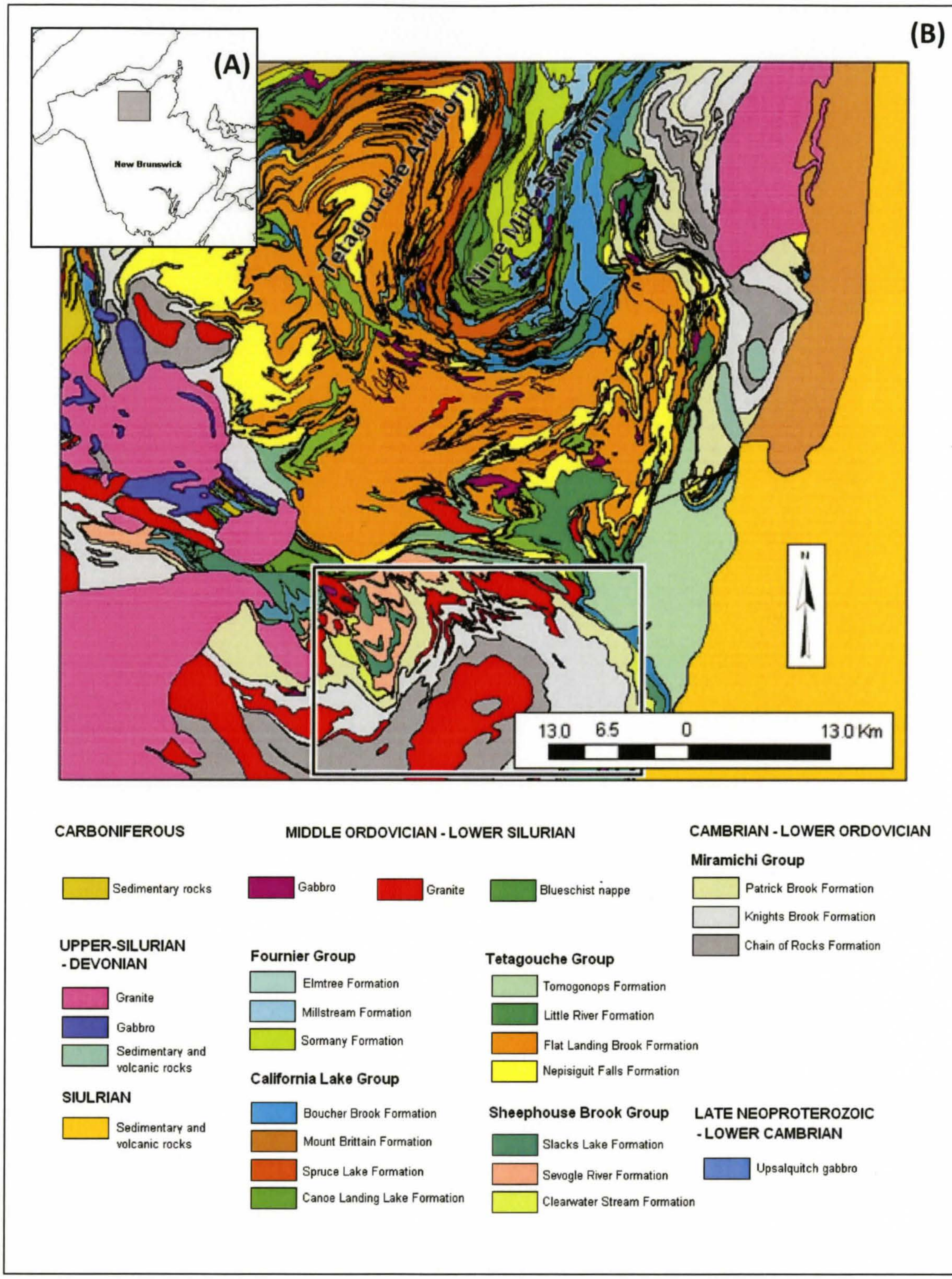
(A)
New Brunswick
(B)
Tetagouche Antiform
Nine Mile Synform
N
13.0 6.5 0 13.0 Km
CARBONIFEROUS
Sedimentary rocks
UPPER-SILURIAN - DEVONIAN
Granite
Gabbro
Sedimentary and volcanic rocks
SIULRIAN
Sedimentary and volcanic rocks
MIDDLE ORDOVICIAN - LOWER SILURIAN
Gabbro
Granite
Blueschist nappe
Fournier Group
Elmtree Formation
Millstream Formation
Sormany Formation
California Lake Group
Boucher Brook Formation
Mount Brittain Formation
Spruce Lake Formation
Canoe Landing Lake Formation
Tetagouche Group
Tomogonops Formation
Little River Formation
Flat Landing Brook Formation
Nepisiguit Falls Formation
Sheephouse Brook Group
Slacks Lake Formation
Sevogle River Formation
Clearwater Stream Formation
CAMBRIAN - LOWER ORDOVICIAN
Miramichi Group
Patrick Brook Formation
Knights Brook Formation
Chain of Rocks Formation
LATE NEOPROTEROZOIC - LOWER CAMBRIAN
Upsalquitch gabbro

Figure 4-1.

Geological Map of Bathurst Mining Camp. Generalized geology of the Bathurst Mining Camp and location within New Brunswick, Canada (A: ESRI, 1997; B: after van Staal, 2003). Nine Mile synform and Tetagouche antiform have been indicated. The Sheephouse Brook Block is located in the inset box in the south-central portion of the camp.

However, outcrop availability is less than 2% due to vegetation and glacial overburden (van Staal, 2003), which makes geological interpretation difficult, thus the importance of indirect mapping methods such as geophysics and remote sensing. One block in particular that displays multi-scale folding and has very limited geological information is the Sheephouse Brook block.

The Sheephouse Brook block, located in the southern portion of the BMC (Figure 2) is compiled of two groups – the sedimentary Miramichi Group and the overlying volcanic Sheephouse Brook Group (van Staal, 2003). The former is divided into three formations: Chain of Rocks, Knights Brook, and Patrick Brook. The latter is divided into the Clearwater Stream, Sevogle River, and Slacks Lake Formations. A large Ordovician aged granite, known as the Mullin Stream (MS) granite intruded the sedimentary units of the Miramichi Group. Furthermore, in this region the geologic feature that controls the fabric is the Moose Lake Shear Zone. North of this shear zone, the structures are steeply dipping to the north with ENE foliation. However, south of the Moose Lake Shear Zone the structures are more shallow-dipping with varying foliation (NW and NNE) (Fyffe, 1995). There are a series of early (F1-F2) and late (F3-F4) folds molding the block ranging from upright isoclinal F2 folds, open recumbent F3 folds and a large southwest plunging F4 fold in the north section of the block. It has been proposed by Fyffe (1995) and Rogers (2008) that the east limb of this F4 fold has been truncated by a thrust fault. Evidence cited in support of this hypothesis is the lack of the Clearwater Stream Formation on the eastern limb but is prominent on the west limb.

The Sheephouse Brook Block hosts the oldest known occurrences of massive sulfides and are typically found in early Arenig (ca. 478 Ma) dacites of the Clearwater Stream Formation (van Staal, 2003). The Sheephouse Brook block also hosts a number of other massive sulfide deposits found in coeval feldspar-porphyritic rhyolites (Sevogle River Formation). The most well-known deposit of the Sheephouse Brook block is the Chester deposit. The Chester deposit is located on the west limb of the large late F4 fold structure and is hosted in plagioclase-crystal tuff, which is part of the Clearwater Stream Formation.

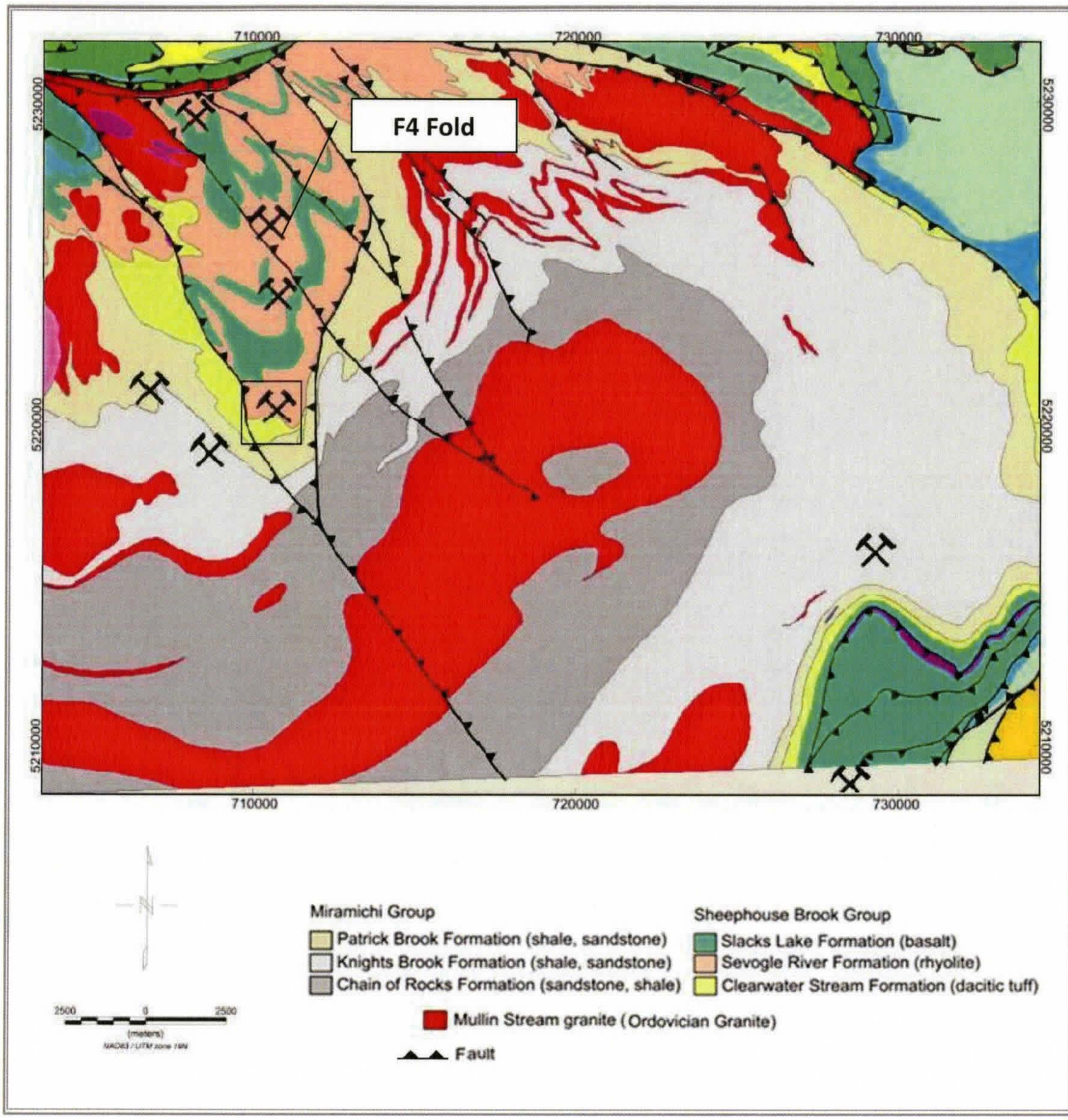
F4 Fold
710000
720000
730000
5230000
5220000
5210000
N
2500
0
2500
(meters)
Miramichi Group
Patrick Brook Formation (shale, sandstone)
Knights Brook Formation (shale, sandstone)
Chain of Rocks Formation (sandstone, shale)
Sheephouse Brook Group
Slacks Lake Formation (basalt)
Sevogle River Formation (rhyolite)
Clearwater Stream Formation (dacitic tuff)
Mullin Stream granite (Ordovician Granite)
Fault

Figure 4-2.

Geology of the Sheephouse Brook Block. The Sheephouse Brook Block with distribution of massive sulfide deposits and the fault locations. The Chester deposit is located within the inset box.

The Chester deposit is subdivided into West, Central, and East zones, where the Central and East Zone are exposed at surface. The East zone is composed of inter-mixed massive and disseminated sulfides, the Central Zone is a thick massive sulfide lens, and the West zone is composed of stringer and disseminated sulfides (Fyffe, 1995).

Data Sources

All data used in this project were acquired from the airborne and ground geophysical surveys conducted during the EXTECH-II and TGI-3 projects (NGD, 2008). The EXTECH-II program was flown in four separate blocks - A, B, C, and D. For the purpose of this study, only data from blocks B and D were used since they would guarantee total coverage of the Sheephouse Brook block (Keating, 2003).

Total Magnetic Intensity

In previous studies processed products of magnetic datasets have shown strong correlation to the location of fold structures, faults, and lithologies (Keating, 2003). Most lithological units in the BMC are weakly magnetic due to being either a felsic igneous intrusion or non-magnetic sediments. In order to delineate more specific geological structures (folds, faults, contacts) marker horizons are used. This marker horizon is to have a strong magnetic signal and is to be located within a weakly magnetic background. The most influential units are those that are primarily basalt, specifically alkali-basalts that are known to overlie many economic deposits including the Brunswick 12 deposit (Keating, 2003).

The magnetometer used in the helicopter-borne survey was flown at a height of 50m above surface. The flight lines were 200m apart while tie lines were 7km apart. A differential geographical positioning system was used that allowed for a positioning accuracy of ± 10m. A split-beam cesium vapour magnetometer with a sensitivity of 0.0005nT was used at a sampling frequency of 0.1s (Keating, 2003).

Electromagnetic Survey

Electromagnetic methods are amongst the most commonly used geophysical tool in mineral exploration. This is especially useful in the BMC setting where there is a strong conductive contrast between base metal deposits and resistive host rocks or due to a thin glacial overburden (Keating, 2003). Often conductivity anomalies may be due to non-mineralized sources, including graphitic slabs. As such, additional geophysical surveys, either magnetic or gravity, are used to help isolate the source of the conductive anomaly. As discussed by Keating (2003), mid- to high-frequency coils typically resolve anomalies well within the BMC.

An electromagnetic (EM) bird was suspended below the magnetic sensor underneath the helicopter at a height of 30m above the ground and contained three coplanar coils operating at 835, 4433, and 32290Hz and two coaxial coils operating at 914 and 4786 Hz. Sampling rate was 0.1s with a time constant of 0.1s. Flight line spacing was identical to the magnetic survey at 200m apart and 7km separated tie lines.

Radiometric Survey

Radiometric surveys provide insight into lithological variations of thorium, uranium, and potassium due to differences in primary lithochemical content. Variations are typically well defined along boundaries of the felsic volcanic rock units of the BMC. The region has undergone extensive metamorphism and zones of hydrothermal alteration, which are resolved well in radiometric contents like potassium (Shives, 2003). A drawback to radiometric surveying is that it will only capture the top 20-60cm of rock so it is used explicitly for surface mapping (Shives, 2003). Furthermore, radiometric surveys are strongly influenced by many surficial factors: topography, erosion, weathering, and water bodies, so any interpretation should take these into consideration (Shives, 2003).

The 256 channel helicopter- mounted spectrometer included a 16-L main detector and a 4-L upward looking NaI detector with a sampling rate of 1s. The spectrometer was mounted on the same system (60m above ground surface) that conducted the EM and magnetic surveys therefore, the survey parameters are the same.

Gravity Survey

Because of their higher cost and lower productivity per day when compared with airborne magnetic or EM surveys, gravity surveys are not used for direct exploration purposes but rather as follow up to previous surveys to determine the direct cause of electromagnetic and magnetic anomalies. That being said, gravity surveys work well in the BMC due to alternating lithologies of felsic sedimentary and volcanic rocks with high density mafic rocks. Additionally, if these felsic volcanic rocks host a sulfide deposit, which is composed of dense minerals, a gravity high will be generated. Gravity will typically resolve sulfides that are within a few meters of the overlying overburden; however deposits up to 180m below surface have been discovered through gravity surveys (Thomas, 2003).

A ground gravity survey was conducted in summer of 2007 by Geomatics Canada. LaCoste and Romberg gravimeters were used with an accuracy of sub-meter courtesy of a differential GPS system. The average sample spacing was 1 to 2km, however the sampling was constrained by accessibility, which included roads and water features.

Topography

Topographic data was obtained from the Service New Brunswick Geographic Data and Maps Website (Service New Brunswick, 2007) and is from the 1998 Digital Topographic database. The location of each sample point was referenced to a 1:10 000 base map. The resolution is 1m in the x and y directions and 0.1m in the z direction with an overall accuracy of ± 2.5m.

Data Processing

There are a number of processing schemes that may be applied to geophysical data in order to isolate anomalies generated by near-surface features. All received datasets had already undergone initial aircraft-related corrections along with other necessary corrections which will be discussed here.

Topographic and Terrain Corrections

There are a number of standard corrections for gravity data processing. These include free-air, Bouguer, and terrain corrections. Both free-air and Bouguer corrections were completed on the data prior to having been received. Terrain correction was deemed unnecessary since the topography is not very rugged, therefore Bouguer corrections are typically sufficient in this situation.

In-flight variations, seen in the grid as high-frequency corrugations, were corrected through microlevelling on all electromagnetic, magnetic and radiometric survey data. In addition to microlevelling, in an attempt to minimize magnetic anomaly contributions created by varying source-signal separations (terrain effects) related to flying over undulating terrain, a Taylor Series expansion method was applied previous to the application of the reduce-to-pole filter. This Taylor Series expansion corrected for the height between the magnetometer and the ground surface. This was accomplished through the summation of the first and second vertical derivatives that had each undergone a non-linear filter of 5 fiducials.

Regional-Residual Separation

A residual magnetic field was first derived by subtracting the appropriate International Geomagnetic Reference Field (reference year of 1995) from the total magnetic field signal. Both the gravity and the residual magnetic field underwent regional-residual separation in order to isolate the remaining high-frequency signal. The grid cell segregation routine developed in Chapter 2 was implemented. A desampled coarse grid equal to ten times the original grid size was initially generated. This coarse grid was re-gridded at the equivalent original grid cell size, which was finally subtracted from the original grid. It is important to note that prior to regional-residual separation, reduction-to-pole was completed on the residual magnetic field dataset to locate the anomalies directly over their respective sources.

Gridding

Each processed dataset was gridded using the standard ¼ line spacing, which for all airborne survey datasets was a 50m grid cell size. The mid- and high-frequency electromagnetics along with the residual magnetic field were gridded using a minimum curvature interpolation method and displayed using a equal area colour scheme (Figure 3-4). In the case of the radiometric survey dataset, separate grids for equivalent Thorium, equivalent Uranium, and Potassium were generated for composition in a ternary diagram. A Red-Green-Blue (R-G-B = K-eTh-eU) ternary diagram of all three radiometric counts was produced in order to assess their spatial variability (Figure 5). Since the ground gravity survey was conducted in a more random distribution pattern, the grid cell size chosen was slightly larger than the standard ¼ spacing - 2km grid cell size was chosen (Figure 6). This was done to compensate for large areas of no data.

Derivatives and Tilt-Depth

In order to enhance gravity anomalies and marker horizons in the residual magnetic field data, the first vertical derivatives were calculated (Figure 7-8). To further amplify geological contacts and marker horizons tilt-depth method was applied to both the regionally-reduced gravity and residual magnetic datasets (Figure 9). No further enhancement products were applied to the radiometric and electromagnetic datasets as it was deemed unnecessary due to the quality of already prominent near-surface features in the original grids.

(A)

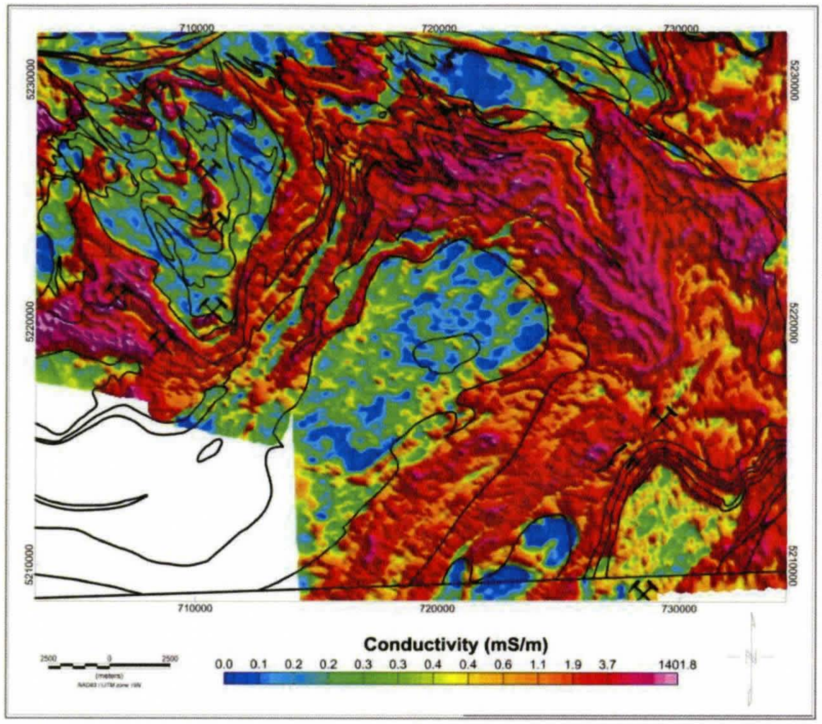
710000
720000
730000
5230000
5220000
5210000
Conductivity (mS/m)
0.0 0.1 0.2 0.2 0.3 0.3 0.4 0.4 0.6 1.1 1.9 3.7 1401.8

(B)

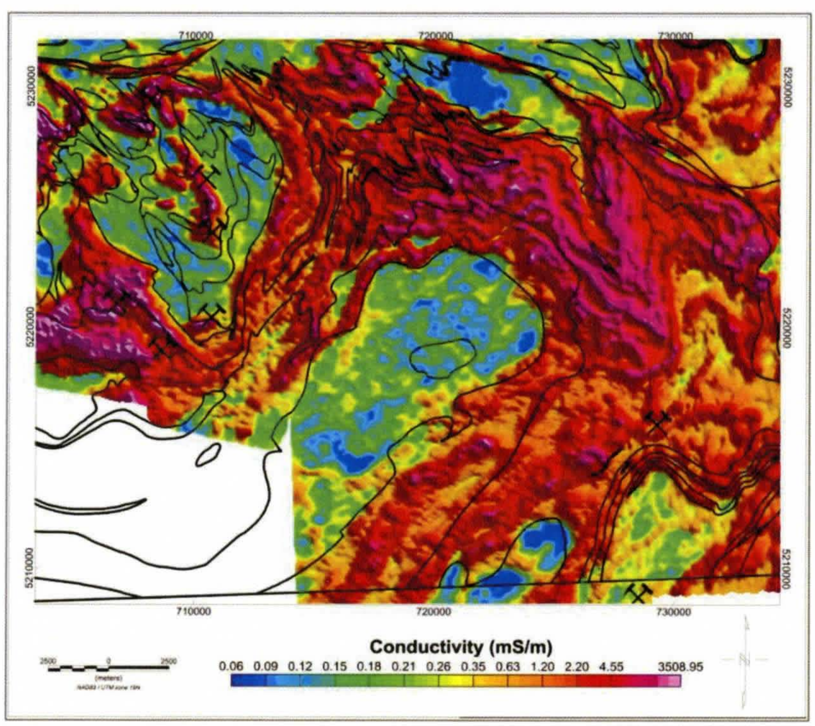
710000
720000
730000
5230000
5220000
5210000
Conductivity (mS/m)
0.06 0.09 0.12 0.15 0.18 0.21 0.26 0.35 0.63 1.20 2.20 4.55 3508.95

Figure 4-3.

Grid results of mid- and high-frequency electromagnetics. Electromagnetic grids of 835 Hz (A) and 4433Hz (B). Geologic boundaries and known mineral occurrences overlaid. Equal area distribution colour scheme used.

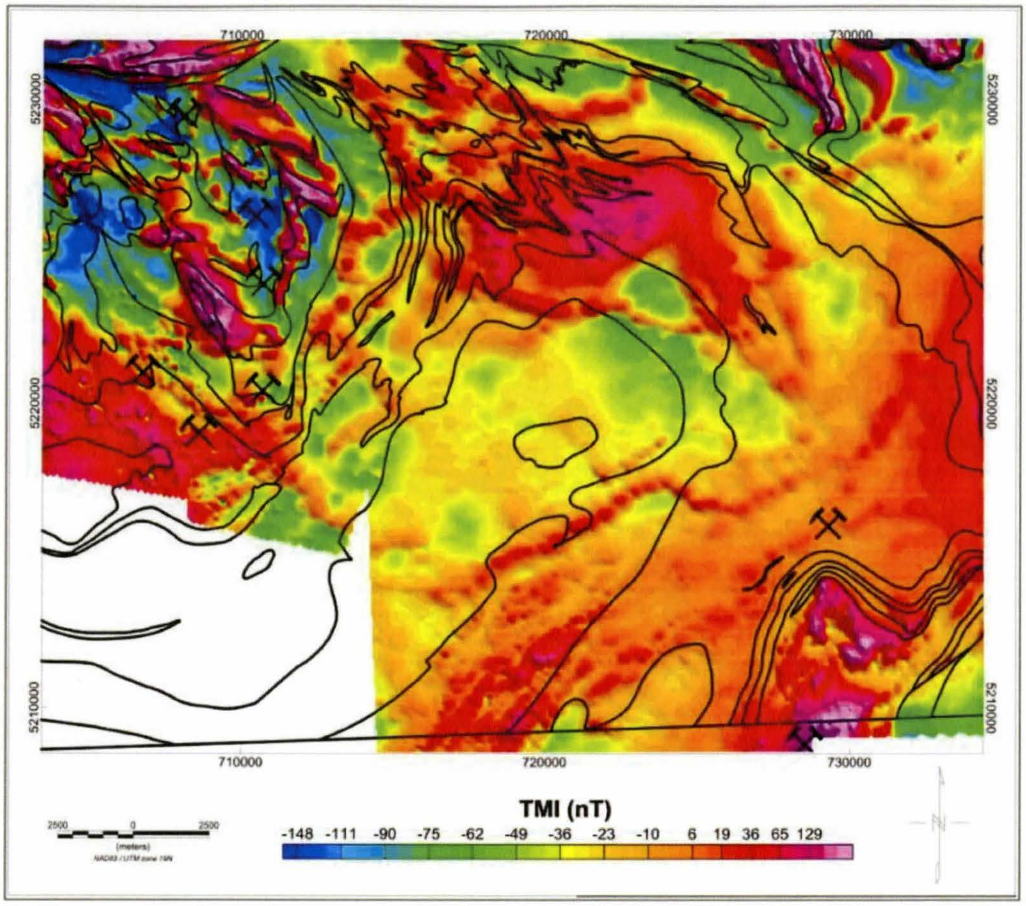
710000
720000
730000
5230000
5220000
5210000
TMI (nT)
-148 -111 -90 -75 -62 -49 -36 -23 -10 6 19 36 65 129
2500 0 2500
(meters)
N

Figure 4-4.

Grid results of residual magnetic field. Magnetic survey data post IGRF, reduction-to-pole, and terrain corrections. Geologic boundaries and known mineral occurrences overlaid. Equal area distribution colour schemed used.

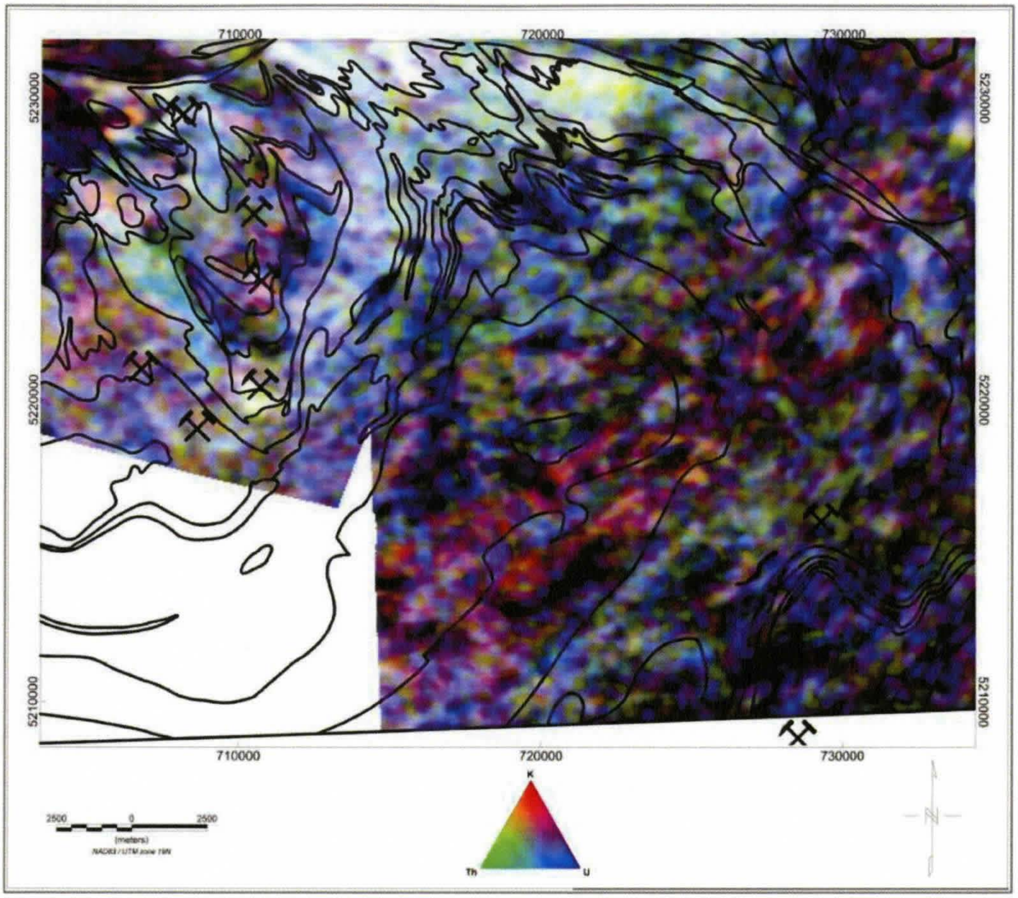
710000
720000
730000
5230000
5220000
5210000
2500
0
2500
(meters)
NAD83 / UTM zone 19N
K
Th
U

Figure 4-5.

Radiometric ternary diagram. Ternary diagram of microlevelled radiometrics using a Red-Green-Blue (K-eTh-eU) colour scheme. Geologic boundaries and known mineral occurrences overlaid. Black regions in grid correspond to water bodies.

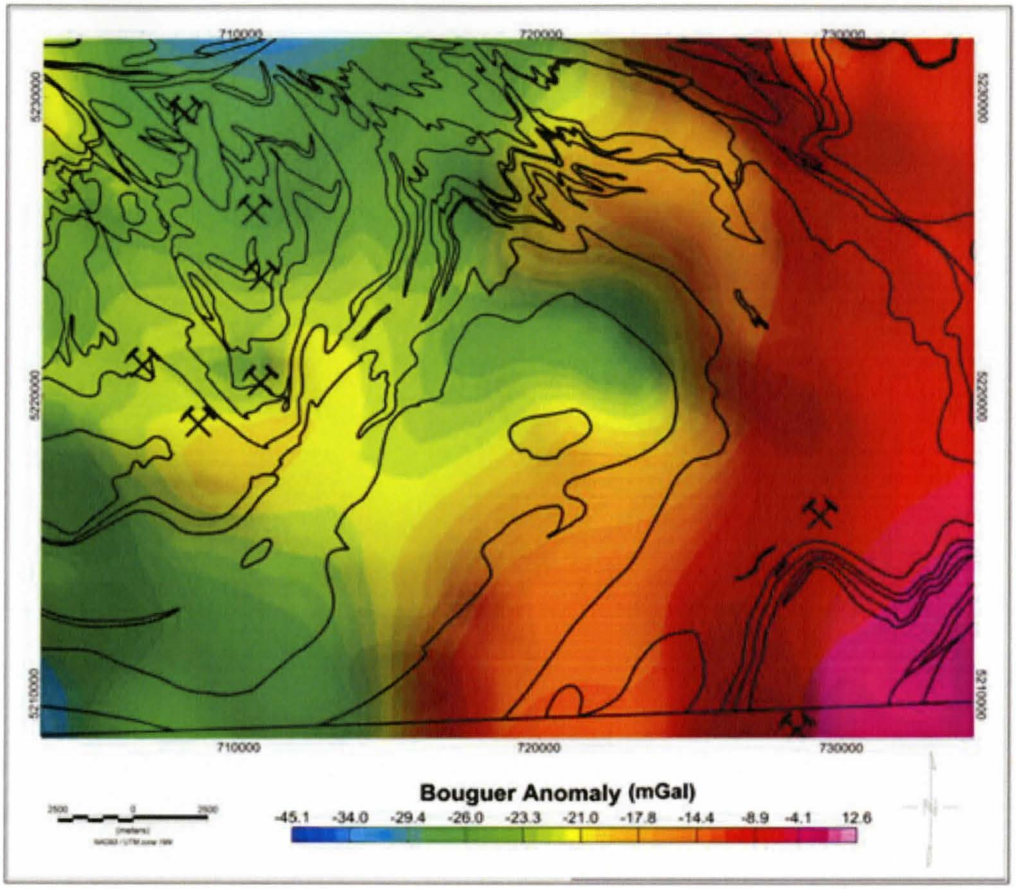
710000
720000
730000
5230000
5220000
5210000
Bouguer Anomaly (mGal)
-45.1 -34.0 -29.4 -26.0 -23.3 -21.0 -17.8 -14.4 -8.9 -4.1 12.6

Figure 4-6.

Grid results of Bouguer anomaly. Bouguer anomaly grid with geological boundaries and known mineral occurrences overlaid. Equal area distribution colour scheme used.

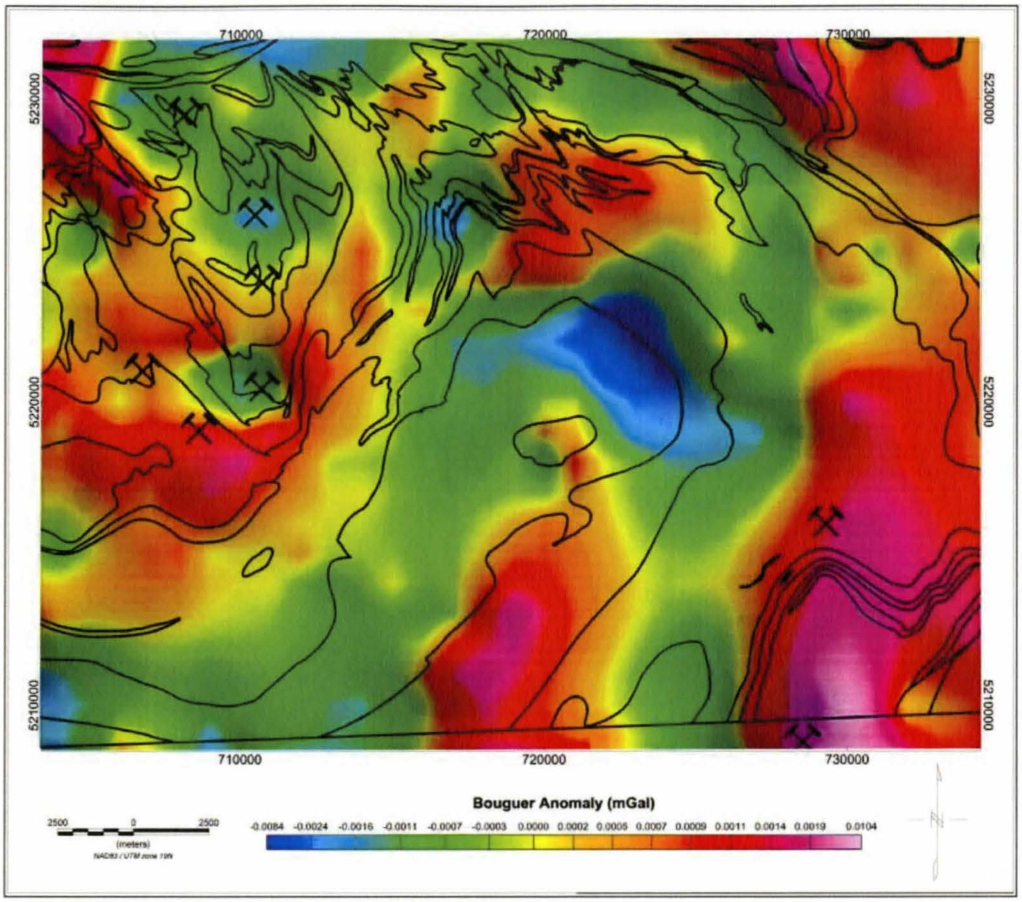
710000
720000
730000
5230000
5220000
5210000
Bouguer Anomaly (mGal)
2500
0
2500
(meters)
NAD83 / UTM zone 19N
-0.0084 -0.0024 -0.0016 -0.0011 -0.0007 -0.0003 0.0000 0.0002 0.0005 0.0007 0.0009 0.0011 0.0014 0.0019 0.0104

Figure 4-7

First vertical derivative of Bouguer anomaly. The first vertical derivative of Bouguer anomaly with geologic boundaries and known mineral occurrences overlaid. Equal area distribution colour scheme used.

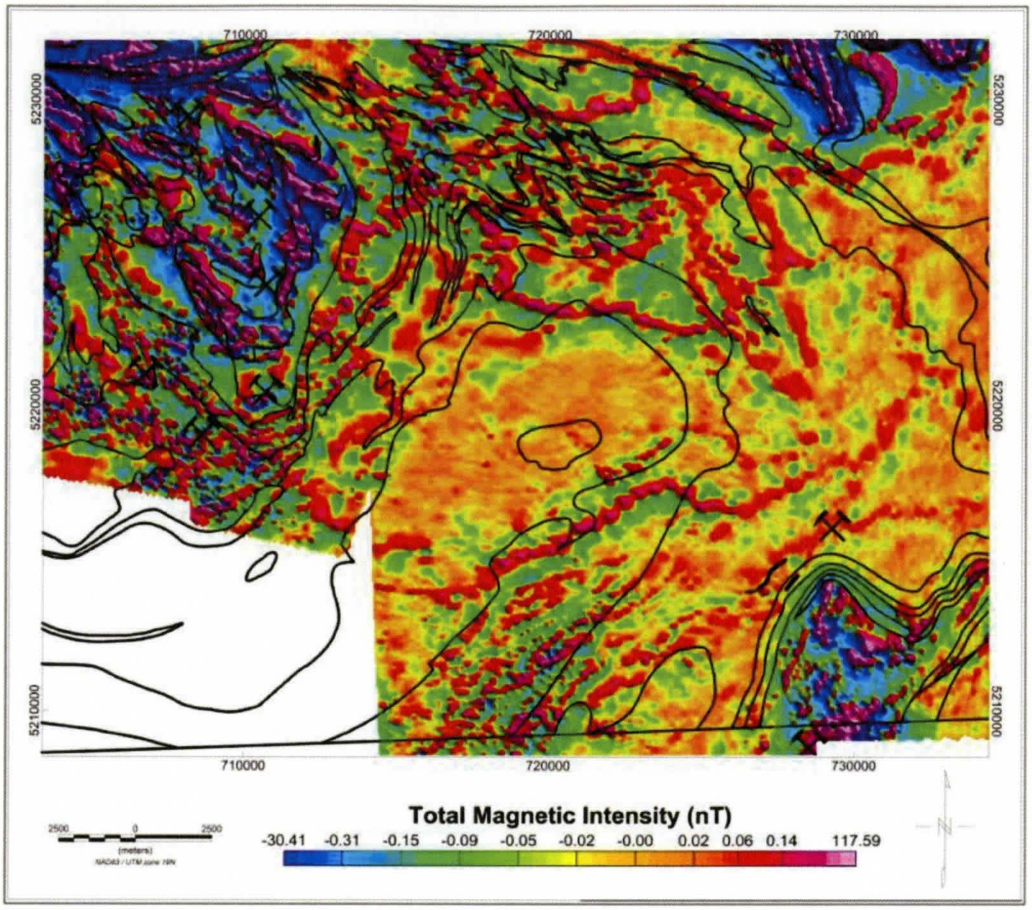
710000
720000
730000
5230000
5220000
5210000
Total Magnetic Intensity (nT)
-30.41 -0.31 -0.15 -0.09 -0.05 -0.02 -0.00 0.02 0.06 0.14 117.59
2500 0 2500
(meters)

Figure 4-8.

First vertical derivative of residual magnetic field. The first vertical derivative of the magnetic field post IGRF, reduction-to-pole, and terrain corrections. Geologic boundaries and known mineral occurrences overlaid. Equal area distribution colour scheme used.

(A)

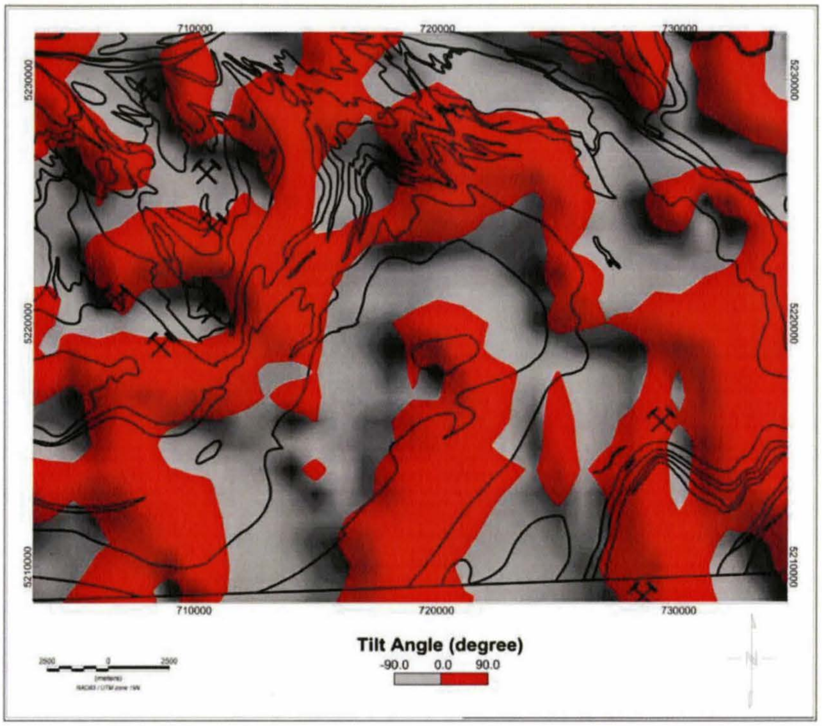
710000
720000
730000
5230000
5220000
5210000
Tilt Angle (degree)
-90.0 0.0 90.0

(B)

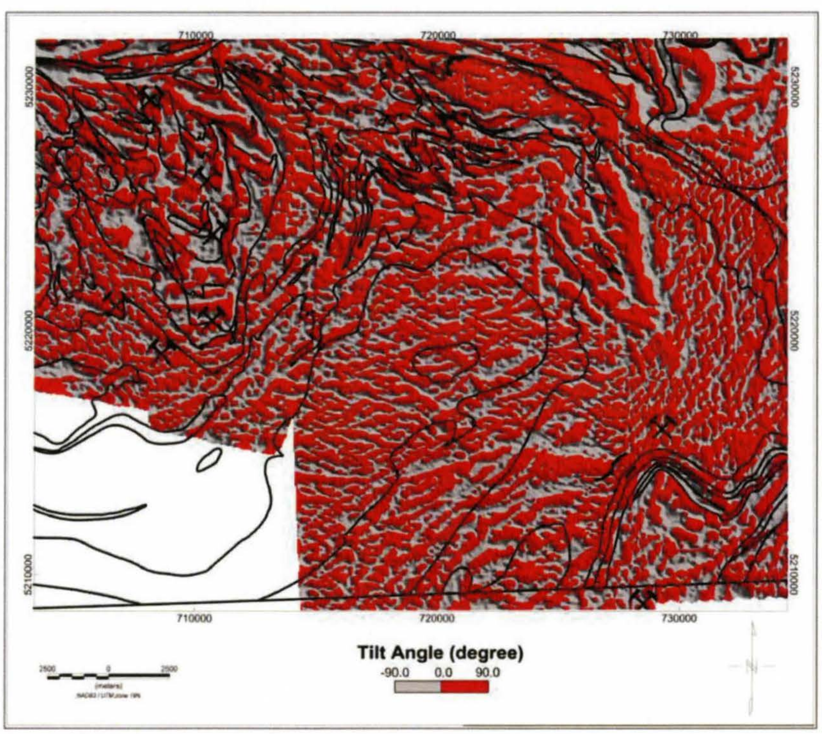
710000
720000
730000
5230000
5220000
5210000
Tilt Angle (degree)
-90.0 0.0 90.0

Figure 4-9.

Comparison of tilt-angle results of gravity and magnetic survey data. Tilt-angle results of regional-residually separated Bouguer anomalies (A) and residual magnetic field (B). Red represents positive tilt-angle values over the geologic source and grey represents negative tilt-angle values beyond the source. The intersection point of red and grey indicate the source edge.

3D Structure

A primary objective of this study was to determine if interpretation of geophysical data in detail could provide any insight into the subsurface structure of this area to better constrain the geometry of possible thrust surfaces and the structural relationship between the massive granitic intrusion, the Miramichi Group, and the Sheephouse Brook Group. Recently, it has been proposed that a thrust fault exists along the geological contact between the Miramichi Group and the Sheephouse Brook Group (Fyffe, 1995; Rogers, 2008), causing the Patrick Brook Formation to be thrusted upon the Clearwater Stream Formation. This would support why there is no occurrence of Clearwater Stream formation on the western limb of the F4 structure.

A 3D representation of the subsurface geology of the Sheephouse Brook block was generated by integrating individual 2D models along six profiles (Figure 10). Three profiles ran sub-parallel to the hinge lines of the late F4 fold, while the other three profiles run sub-perpendicular to the first three profiles. For each of the profiles, the TGI-3 gravity dataset and the high-resolution magnetic survey were imported into Geosoft's GM-SYS modelling software. The subsurface structure of the units was estimated by computing 2.75D forward models for each of the pre-determined profiles. Simultaneous optimized matches between the observed and computed magnetic field and gravity field for each survey line were derived through the introduction of a preliminary subsurface geology that was based on previous studies and surface geological contacts (Figure 11).

Knowing topography, TMI, and the local Earth's magnetic field the only remaining variables are: a) geometrical, that is the location of a contact and the orientation of that contact near surface, and b) physical property variations. With very limited outcrop the position of a geological contact on the surface is only weakly constrained. The spatial resolution associated with each of the geophysical datasets also permits some variance in the placement of a contact. All general trends and significant anomalies were compared to the most recent 1:50 000 geology map (van Staal, 2003).

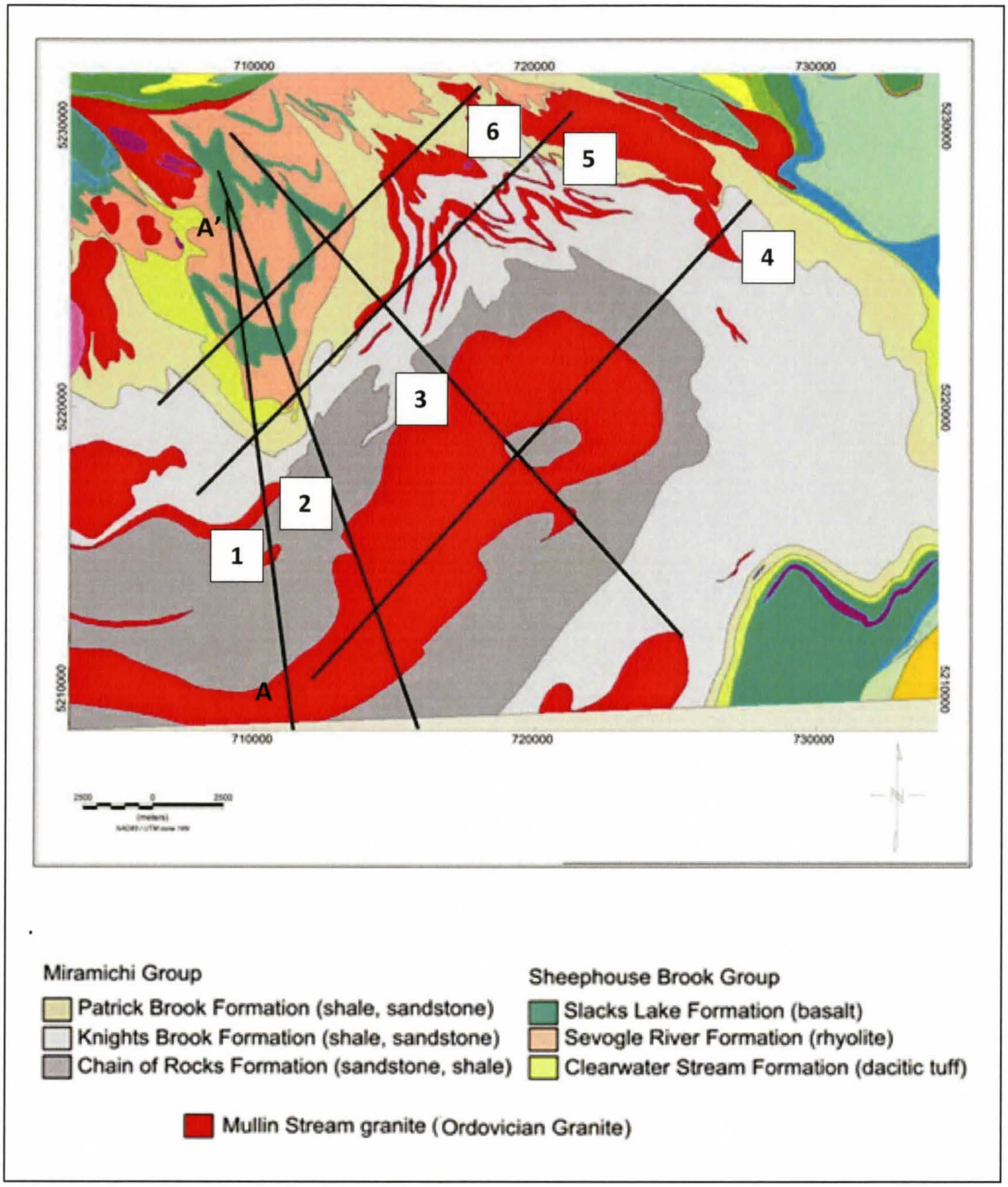
710000
720000
730000
5230000
5220000
5210000
1
2
3
4
5
6
A
A'
Miramichi Group
Patrick Brook Formation (shale, sandstone)
Knights Brook Formation (shale, sandstone)
Chain of Rocks Formation (sandstone, shale)
Sheephouse Brook Group
Slacks Lake Formation (basalt)
Sevogle River Formation (rhyolite)
Clearwater Stream Formation (dacitic tuff)
Mullin Stream granite (Ordovician Granite)

Figure 4-10.

Geological map with sectional profile locations. 1:50 000 geology map (after van Staal, 2003) with location of the six 2D profiles. Profiles were chosen to optimally resolve the most amount of geologic structure.

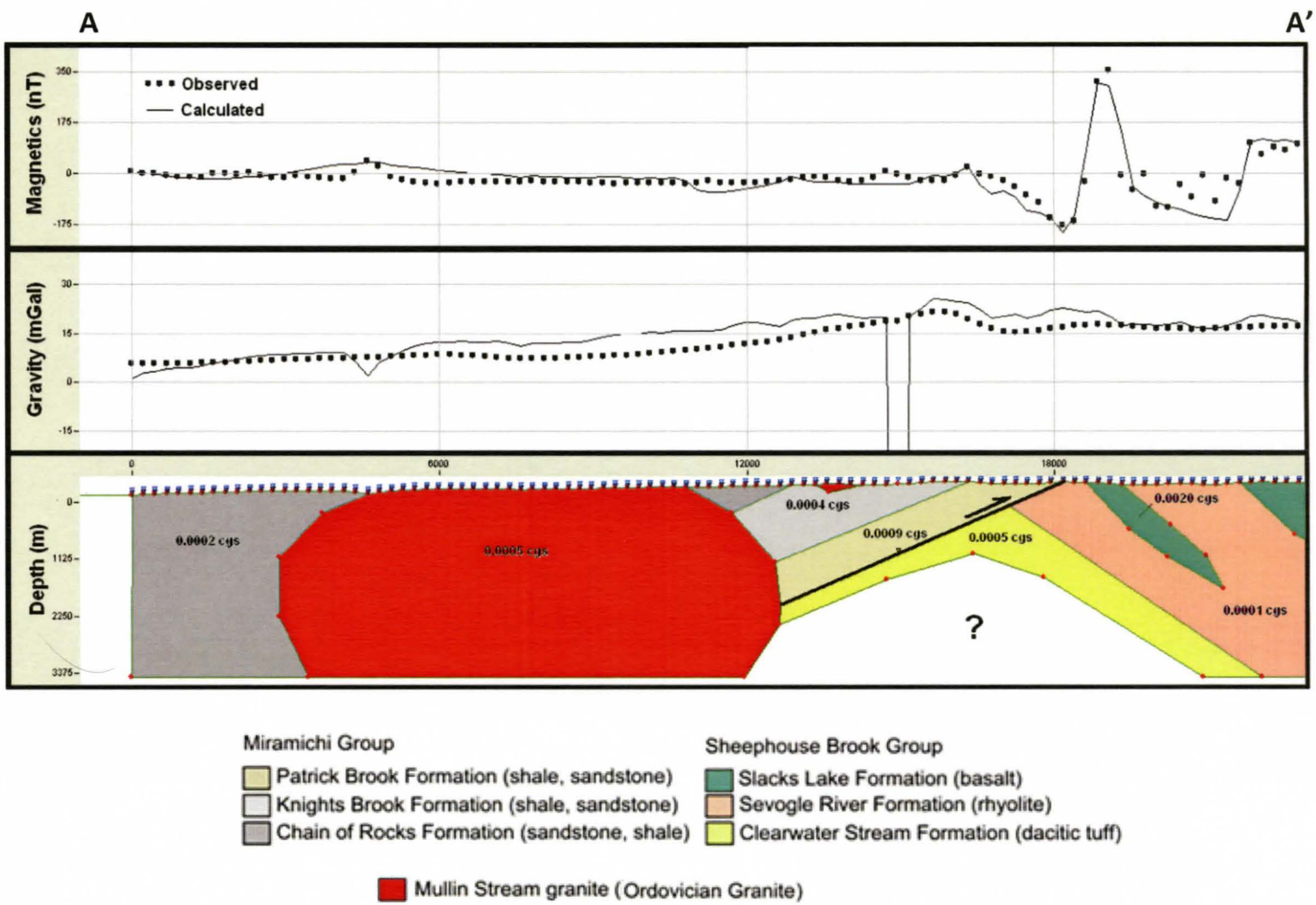
A
A'
Observed
Calculated
Magnetics (nT)
350
175
0
-175
Gravity (mGal)
30
15
0
-15
Depth (m)
0
1125
2250
3375
0
6000
12000
18000
0.0002 cgs
0.0005 cgs
0.0004 cgs
0.0009 cgs
0.0005 cgs
0.0020 cgs
0.0001 cgs
?
Miramichi Group
Patrick Brook Formation (shale, sandstone)
Knights Brook Formation (shale, sandstone)
Chain of Rocks Formation (sandstone, shale)
Sheephouse Brook Group
Slacks Lake Formation (basalt)
Sevogle River Formation (rhyolite)
Clearwater Stream Formation (dacitic tuff)
Mullin Stream granite (Ordovician Granite)

Figure 4-11.

GM-SYS result along profile 1. Cross-sectional along profile 1 of thrust surfaces between Miramichi and Sheephouse Brook Groups using the residual magnetic data.

The general dip of the individual lithologies on any geological map can be derived from the geometrical relationship between a geological contact and the local topography (Figure 12). The more shallow the dip of a geological unit, the more the unit's surface contacts will mimic topographic contours. With steeper dips, geological contacts will display less correlation with varying topography. By draping the known geology on topography, it was shown that the geological contacts in the north section of the Sheephouse Brook Block were highly influenced by varying topography, which would mean the lithological rock units of the Miramichi Group had a shallow dip. However, the geological units to the south, more specifically the Millen Stream granite, were not as highly influenced by topography which would mean that the dip is quite steep, if not sub-vertical. However, it is important to note that the topography in the southern portion of the Sheephouse Brook Block is not very rugged, so the interpreted dip of the Miramichi Group rocks is difficult to determine based solely on topography and delineated geologic contacts.

The final 2.75D profiles were imported into Encom's Profile Analyst software. This allowed for the 3D analysis of the thrust fault, granitic intrusion and complex folds. The individual profiles were fine tuned based on intersection points of the profiles with each other, so that all units were coherent in direction and dip between all six profiles. Screen captures of the six profiles in perspective can be seen in Figure 13. The variations determined from all gridded and enhanced datasets along with the profiles in 3D were to adapt previously accepted geological boundaries and incorporated to produce an enhanced geological map of the Sheephouse Brook Block (Figure 14).

No prior physical property data was available to help restrict possible models that might be generated before the forward modelling procedure. Consistent relative physical property contrasts between lithological units were derived through optimized match of observed and computed and used throughout all six profiles.

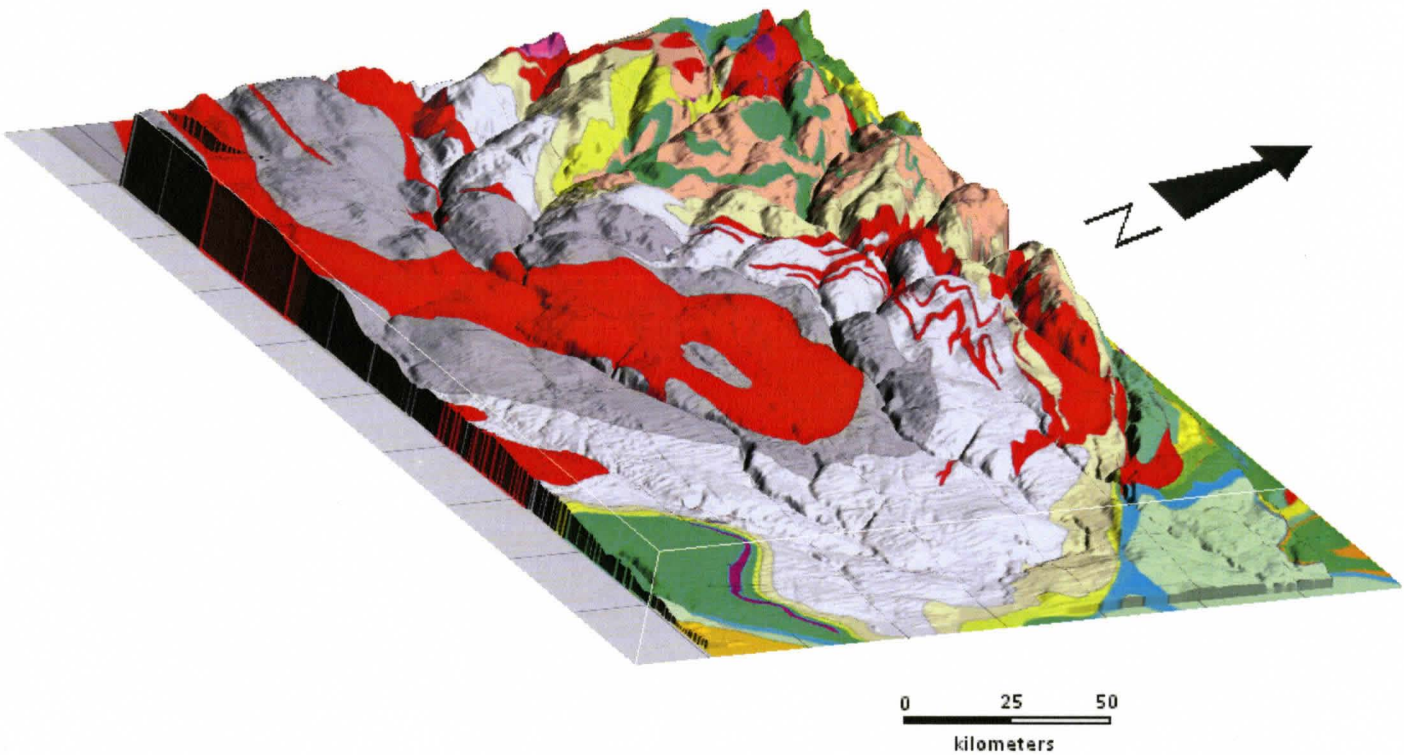
N
0
25
50
kilometers

Figure 4-12.

3D perspective of topography and geology. Geology draped on topography. 1:50 000 geology map (after van Staal, 2003) draped on topography.

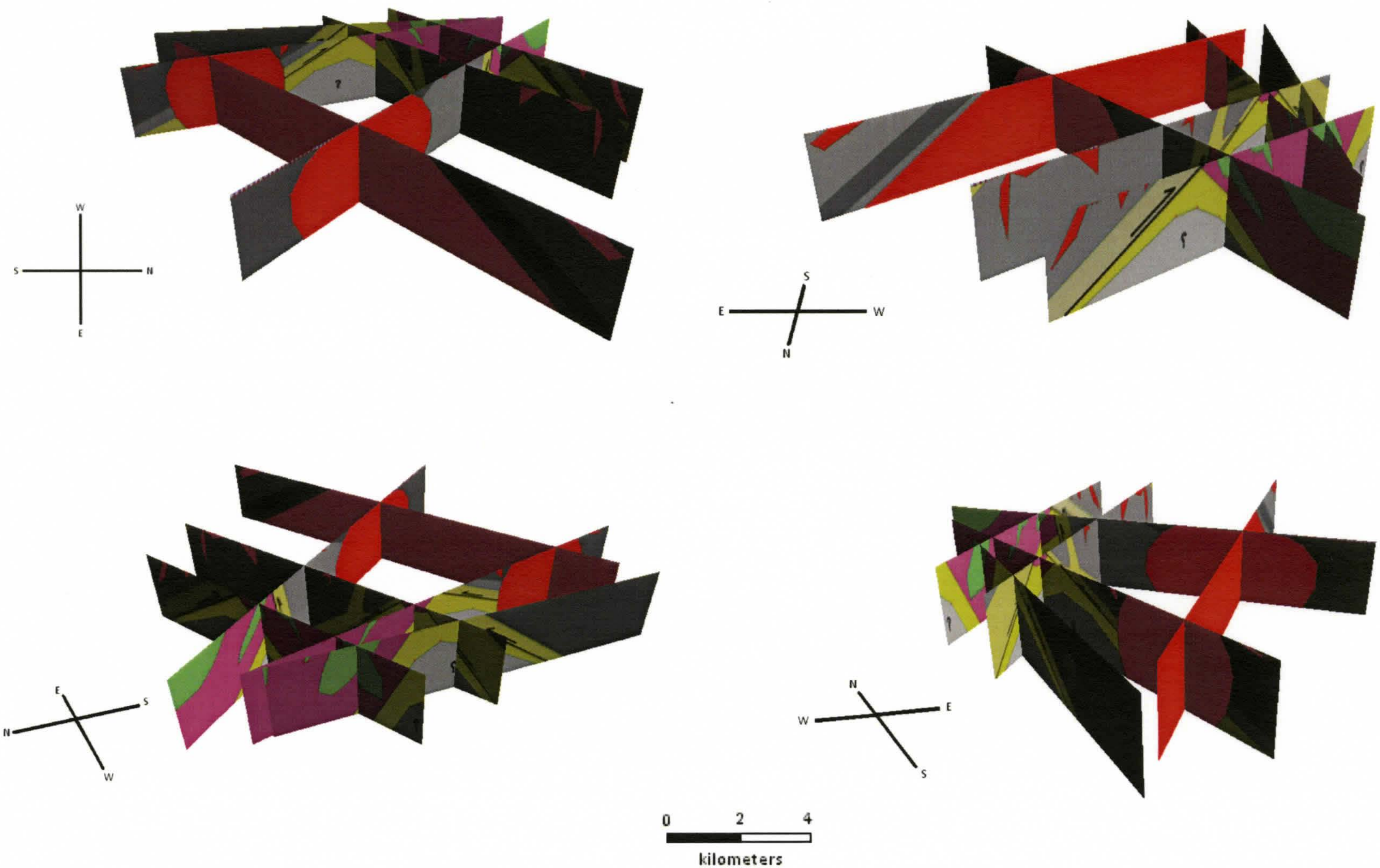
W
S
N
E
S
E
W
N
E
S
N
W
N
W
E
S
0
2
4
kilometers

Figure 4-13.

Screen captures of intersecting profiles. Different perspectives of modelled 2.75D geological sections. Key geologic features, such as the thrust fault, Millen Stream granite, and Slacks Lake Formations are resolved very well and coherent between profiles.

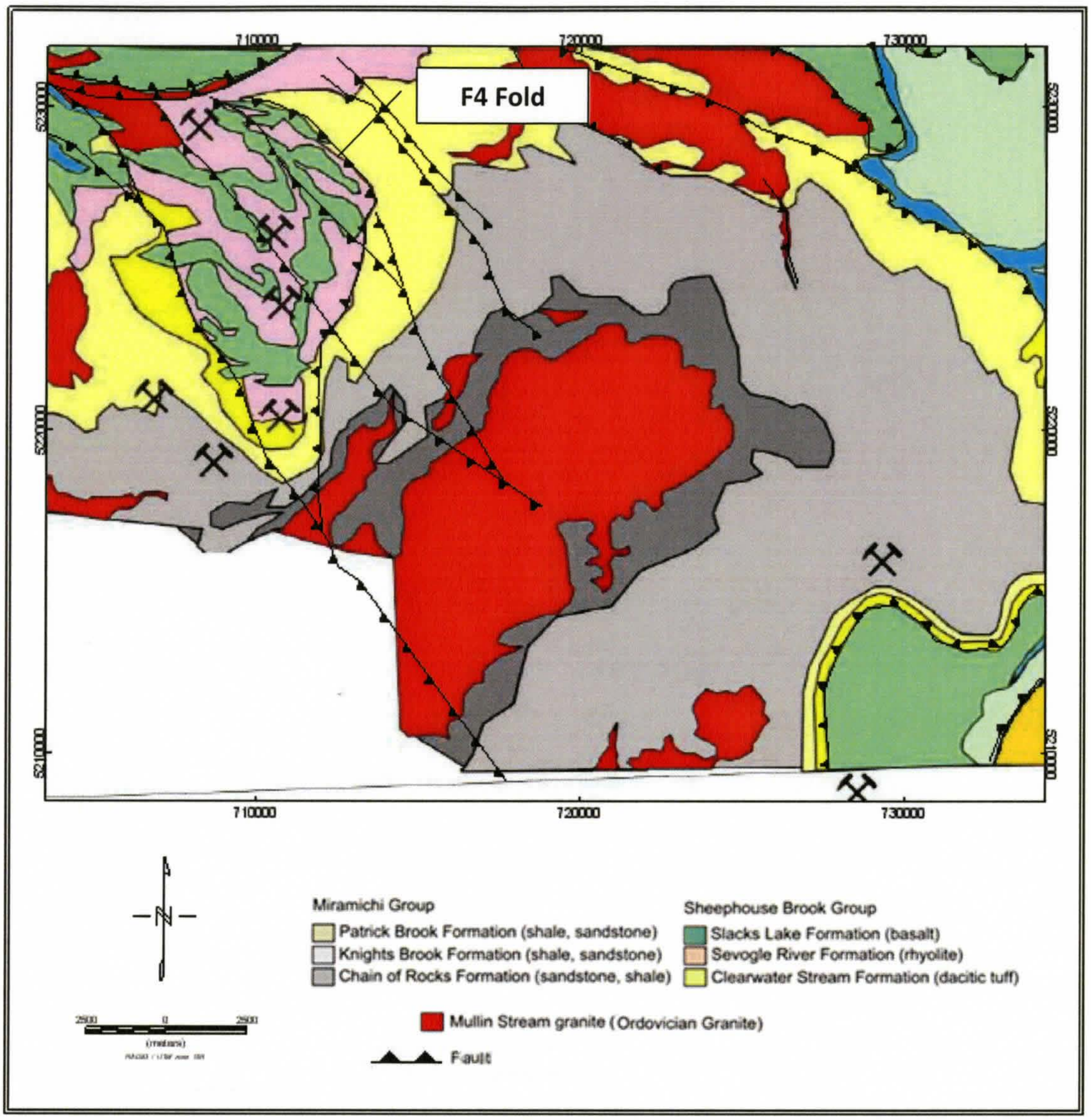
F4 Fold
710000
720000
730000
Miramichi Group
Patrick Brook Formation (shale, sandstone)
Knights Brook Formation (shale, sandstone)
Chain of Rocks Formation (sandstone, shale)
Sheephouse Brook Group
Slacks Lake Formation (basalt)
Sevogle River Formation (rhyolite)
Clearwater Stream Formation (dacitic tuff)
Mullin Stream granite (Ordovician Granite)
Fault
2500
0
2500
N

Figure 4-14.

Final geological map. Revised Sheephouse Brook Block geology map based on results from interpreted geophysical data. Known deposits and re-evaluated faults are indicated. Faults have been relocated from previous map (Figure 2) based on the interpreted geological contacts.

Results

Certain geophysical methods optimally resolve near-surface sources, including electromagnetic and the radiometric survey dataset. Low-, mid- and high-frequencies may be implemented in electromagnetic surveys. Based on the principle of skin depth, which is the depth below surface to which a frequency can penetrate, states that as frequency decreases skin depth increases and vice versa. On this notion, by processing and interpreting the high-frequency (4433Hz) EM data, near surface features are resolved. An initial assessment indicates that there is some agreement between the geological boundaries shown by the 1:50 000 map and the sharp conductivity contrasts, where updated boundaries only require minor location readjustment.

Both the EM (Figure 3) and radiometric (Figure 5) datasets support the contact surface between the felsic Slacks Lake Formation and the mafic Sevogle River Formation. This is done through the strong conductivity contrast between the two Sheephouse Brook units and lack of all radiometric occurrences (shown as white) in the Slacks Lake Formation.

The lithological units of the Miramichi group are conductive sedimentary rocks and therefore produce a strong signal EM signal. Furthermore, when the high-frequency EM grid is compared to topography, many conductivity highs are based along topographic lows (Figure 3A). Water saturated rocks and sediments, irrespective of mineralogical composition are likely to be imaged as conductivity highs. This point can be further developed once again through the analysis of the radiometric data (Figure 5). When the radiometric data is compared to topography (Figure 15), a high occurrence of potassium occurs in this basin region, which is consistent with documentation that transported sediment will often display a strong occurrence of potassium (Shives, 2003). Furthermore, along these sediment transport channels and other point locations, complete absorption of all three elements occur (seen in black) (Figure 5). When compared to orthophotographs these black regions are caused by water features. This is because gamma signal is attenuated by the presence of water bodies.

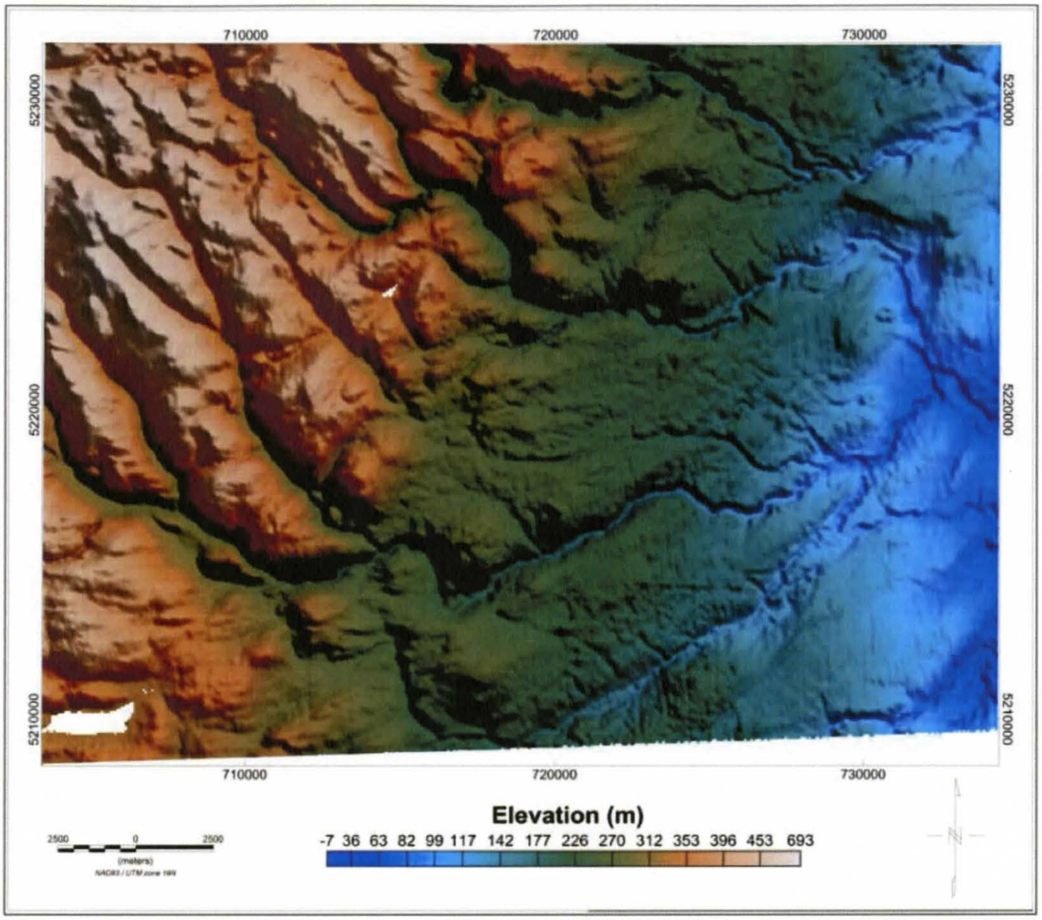
710000
720000
730000
5230000
5220000
5210000
Elevation (m)
-7 36 63 82 99 117 142 177 226 270 312 353 396 453 693
2500 0 2500
(meters)

Figure 4-15.

Topography of Sheephouse Brook Block area. A grid representing the elevation data over the Sheephouse Brook Block of the Bathurst Mining Camp.

Deep seated structures are well resolved in magnetics, gravity and low-frequency electromagnetics. The Mullin Stream granite intruding the Miramichi Group is distinctly resistive relative to surrounding units. In the mid-frequency range (Figure 3a), the area over the MS granite shows an even stronger conductive low than at the high-frequency range (Figure 3b), which indicates a stronger presence of resistivity at depth. Furthermore, the EM conductivity boundary between the Millen Stream granite intrusion and the Miramichi group aligns near perfectly with existing geological boundaries. However, when this contact between the Millen Stream granite and the Miramichi Group is examined in the magnetics image, the same does not hold true. Both residual magnetic field (Figure 4) and the first vertical derivative (Figure 8) show a more complex geometry to the granite than previously presented in geological maps. This is not only true for the Millen Stream granite but many smaller intrusions. The gravity dataset also displays this large scale trend due to the MS granite, which is less dense than the surrounding felsic sedimentary and volcanic rocks, which is producing a gravity low (Figure 6).

For the Sheephouse Brook Block, the Slacks Lake Formation, a transitional tholeiite-alkali basalt, is the most suitable candidate for a magnetic marker horizon. The Slacks Lake Formation is juxtaposed against the Sevogle River Formation, which is a rhyolite and has a very weak magnetic signature (Figure 4). This horizon was easily delineated with the residual magnetic field and the first vertical derivative. It can be seen that the complexity of folding is different than that previously mapped. This holds true for the small occurrences in the most northeast section of the Sheephouse Brook Block where there is a small unit of Slacks Lake Formation according to existing maps. However, upon inspection of the magnetics, the nature of the folding of the Slacks Lake Formation appears to have a different spatial layout than proposed by previous maps (van Staal, 2003).

A number of gravity lows are resolved in the first vertical derivative of the Bouguer anomaly (Figure 7). These gravity lows conveniently occur at the same position as known mineralizations such as the Chester and Sheephouse Brook deposits. However, following further investigation on the distribution of gravity readings, these low gravity anomalies are recorded by only one station reading (Figure 17). This raises the important point that a gravity dataset must be carefully interpreted due to large spatial separation between most points and in this case the sample spacing not tight enough to resolve any mineralized deposit (Figure 16C). Rather, concurrent anomalies in mid- to low-frequency electromagnetic and magnetic datasets support the occurrence of mineralization. As can be seen in Figure 16A, the Chester deposit produces a 3000 mS/m elliptical anomaly in the mid-frequency EM data and a near circular 300nT anomaly in the residual magnetic field (Figure 16A).

Modelling

In the end, no emphasis was placed on acquiring an optimized match for the gravity dataset. This was because most of the geologic features that were being modelled were significantly smaller than the average spacing of gravity readings and as such were not resolved in the gravity signals. Instead, the residual magnetic dataset had a tighter sample spacing and could readily resolve more geologic lithologies. Therefore, the modelling was strictly conducted on the magnetic dataset. Each 2.75D profile was modelled with an interpreted thrust fault occurring between the Clearwater Stream Formation and the Patrick Brook Formation. With consistent magnetic susceptibilities used in all profiles (Table 1), the modelled thrust fault produced magnetic and gravity signals that corresponded well with the recorded datasets. Furthermore, the Millen Stream granite intrusion was modelled to occur subsequent to the Miramichi and Sheephouse Brook Groups, as well to the thrust fault. When the individually modelled profiles where imported into Profile Analyst software, they displayed significant geological coherency between all profile intersections.

(A)

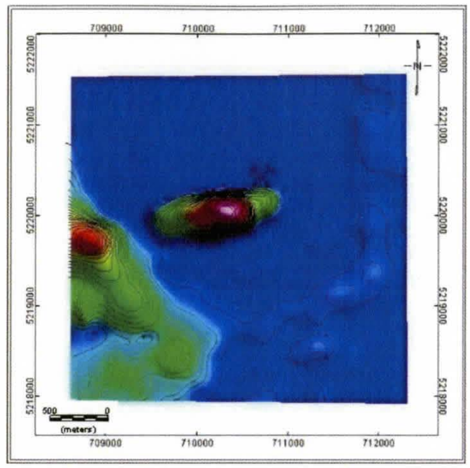
709000
710000
711000
712000
5222000
5221000
5220000
5219000
5218000
N
500 0
(meters)

(B)

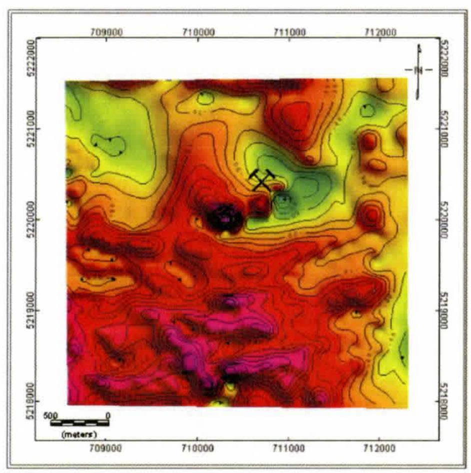
709000
710000
711000
712000
5222000
5221000
5220000
5219000
5218000
N
500 0
(meters)

(C)

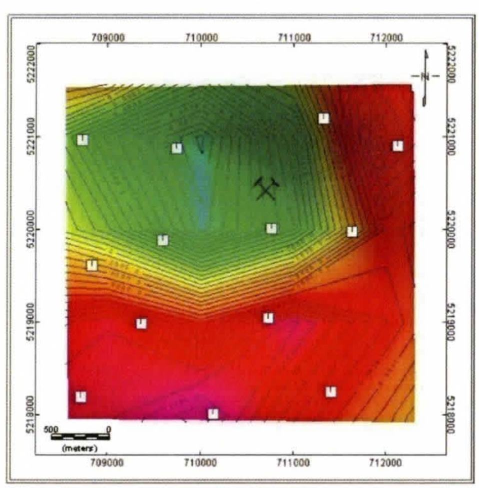
709000
710000
711000
712000
5222000
5221000
5220000
5219000
5218000
N
500 0
(meters)

Figure 4-16.

Geophysical response variability over the Chester deposit. Log contoured EM conductivity at a frequency of 835Hz (A); contoured (10nT increments) residual magnetic field (B); and contoured Bouguer anomaly (0.0001mGal increments) with observation points □ (C).

(A)

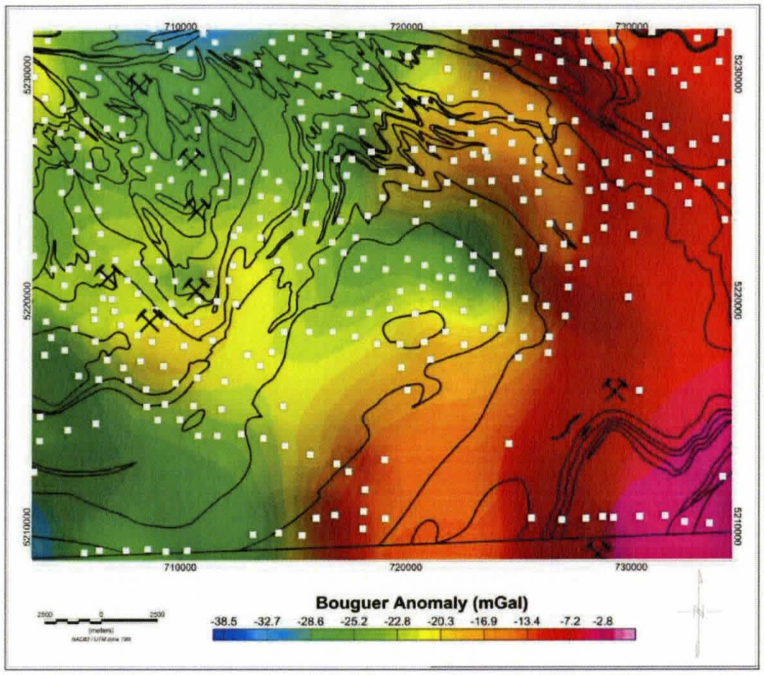
710000
720000
730000
5230000
5220000
5210000
Bouguer Anomaly (mGal)
-38.5 -32.7 -28.6 -25.2 -22.8 -20.3 -16.9 -13.4 -7.2 -2.8

(B)

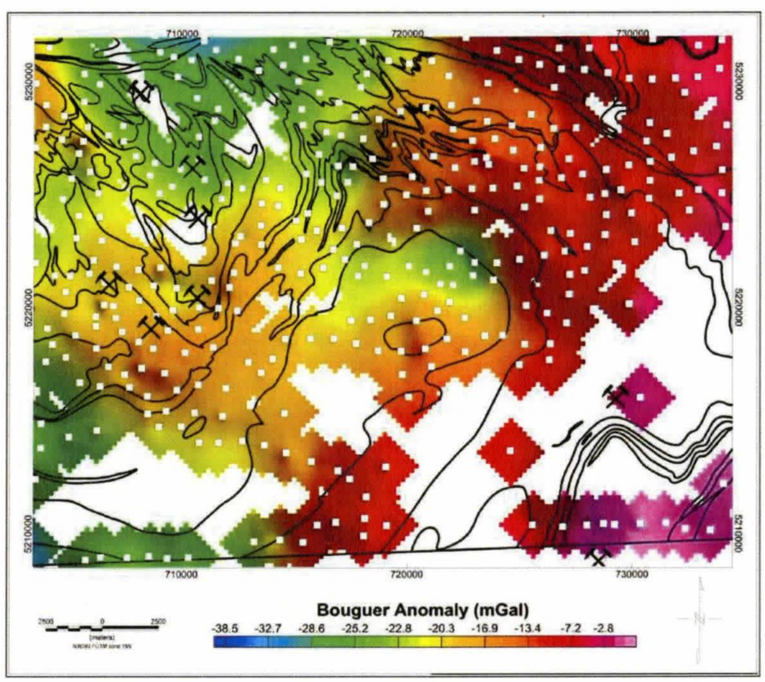
710000
720000
730000
5230000
5220000
5210000
Bouguer Anomaly (mGal)
-38.5 -32.7 -28.6 -25.2 -22.8 -20.3 -16.9 -13.4 -7.2 -2.8

Figure 4-17.

The influence of sample spatial distribution in the ground gravity dataset. (A) The results of over gridding at 500m grid cell size with no blanking distance and (B) a grid cell size of 200m based on average sample space and a blanking distance of 1km.

Lithological Unit/ Formation	Magnetic Susceptibility (cgs)
Chain of Rocks	0.0002
Knights Brook	0.0005
Patrick Brook	0.0004
Mullin Stream Granite	0.0009
Clearwater Stream	0.0005
Sevogle River	0.0001
Slacks Lake	0.0020

Table 4-1.

Magnetic susceptibilities used in profile sections. A table of the constant magnetic susceptibilities used for all lithological units in each individual profile.

The complex south dipping thrust fault modelled across all profiles permitted a view into the unknown lithology below the Clearwater Stream and Patrick Brook Formations (Figure 11 and Figure 13). Based on the occurrence of the Chester deposit in the exposed Clearwater Stream Formation on the west limb, this could potentially mean similar 'Chester type' mineralization at greater depths now that there is further information on the potential nature of the down-thrusted Clearwater Stream Formation along the east limb. Furthermore, the modelled profiles provided a crude view into the potential subsurface structure of individual units, such as the small intrusive units of tholeiitic-basalt of the Slacks Lake Formation and the Millen Stream granite intrusion.

Discussion

Previous geological maps (van Staal, 2003) have suggested a roof pendant composed of the Chain of Rocks Formation to be present in the center of the massive Millen Stream granite. However, as can be seen from the proposed geological map (Figure 14), there is no geophysical evidence to support the existence of this isolated rock unit. The roof pendant may exist but be of another rock unit that has a similar geophysical signature to that of the granite, and causing no geophysical contrast. This may be solved through more thorough geological subsurface sampling or borecore investigations. On the other hand, this individual rock unit may be an erratic displaced during the last glacial movement.

In the south and south-east section of the Sheephouse Brook Block, a network of magnetic highs can be delineated (Figure 4). These magnetic highs correlate with extreme sharp topographic lows, such as stream channels (Figure 15). These magnetic highs are likely an artefact of the terrain correction process completed on the residual magnetic dataset. Terrain correction is based on the Taylor Series expansion equation which implements some aspect of the first and second vertical derivatives. During an airborne survey the magnetometer collects the magnetic field from a footprint below (not a single point directly below). In the case of a sharp topographic gradient, this footprint is too large to resolve the change in topography. Therefore, when the vertical gradient is calculated, and incorporated into the Taylor Series expansion, this unaccounted steep topography creates a magnetic high. At the moment, there is no means in order to correct for this issue and can merely be taken in to consideration during interpretation.

Recently there has been a greater push towards alternative enhancement methods, one of which is tilt-angle. Tilt-angle is most commonly used in potential field interpretation such as gravity and magnetic datasets. Tilt-angle has been applied to both the Bouguer anomaly and to the residual magnetic field datasets. The results can be seen in Figure 9. Unfortunately, tilt-angle does not produce the same reliability in both datasets. The sample spacing in the gravity dataset is once again strongly distorting anomalous responses. Although, there is a strong correlation between the Bouguer tilt-angle and the first vertical derivative, the tilt-angle clearly displays a linear biasing affect. The tilt-angle produced through the residual magnetic dataset on the other hand has clearly displayed a more detailed insight into the geological fabric of the sediment packages and volcanic intrusions. It particularly highlights well the results earlier, where there is to be high consideration towards the actual location of all granite intrusions and the complex folding associated with the marker horizon, the Sevogle River formation.

All this being said it has been shown that previous geological maps that incorporated many geoscientific datasets, including geophysical datasets, placed most of the interpretation emphasis on the electromagnetic results. This is because thus far, the mid- and high-frequency results have shown the greatest amount of correlation between known anomalies and mapped geological contacts. Therefore, at the end of this project that the final geological map be the resultant of all geophysical datasets, with no emphasis placed on any one dataset.

Based on these results, the geophysical data supports the tectonic model that suggests a thrust surface between the Clearwater and the Knights Brook Formations. Unfortunately, due to the limited subsurface physical data, it is yet to be determined the exact sequence of geological events. The model presents the intrusion of the Millen Stream granite occurring after the placement of the thrust fault. However, through additional studies, it may be shown that the

Millen Stream granite intrusion occurred pre-thrust and the granite intrusion is actually displaced below surface along the thrust fault.

A re-evaluated geological map of the Sheephouse Brook Block has been presented in Figure 14. Although this map has taken into consideration the results from all processing methods and analytic routines of the geophysical datasets, there is still opportunity for further refinement. It is important to note that there is a lot of uncertainty around certain contacts, including the contact between the Knights Brook and the Patrick Brook Formations. This is because they both have very similar geophysical signatures which makes them hard to differentiate in all datasets. Therefore, additional constraints become critical. This can be accomplished best through subsurface investigations, more specifically borecore studies. Furthermore, with TGI-3 still being conducted at this time, new high-resolution airborne and ground geophysical surveys may be conducted. In conjunction with advancing processing and analytic routines, these high-resolution surveys will provide greater insight into geological structure. Finally, additional multi-parameter geological, geophysical, and geochemical data may be used to support current models, such as geochemical and drillcore analyses. Geology offers concrete evidence on the spatial location and more importantly provides structural information, which is often very difficult to derive from geophysical datasets. On the other hand, geophysics permits alternative means to derive information in areas that have restricted access for geological information, whether it be due to remote location, overburden, or vegetation. This is to say that geophysics is not the final say and in order to develop the most reliable model possible, additional information is necessary.

Conclusion

The Bathurst Mining Camp hosts a complex geology that is hidden due to limited outcrops. Many studies have contributed to the 1:50 000 geological map proposed by van Staal (2003) including geological, geophysical, and geochemical analyses. The objective of this chapter was to re-evaluate the proposed geological boundaries proposed by this most current map on a purely geophysical basis. Geophysical data, which included electromagnetics, magnetics, radiometrics, and gravity from two government initiatives (the EXTECH-II and the TGI-3) were incorporated into a re-evaluated geologic map of the Sheephouse Brook Block. Evaluations of the geophysical datasets were conducted using standard gridding practices and select analytic routines. Furthermore, throughout the data processing, the limitations addressed in Chapters 2 and 3 were incorporated. The final enhanced map offers new light into the location of geological contacts and most importantly supports previous discussions on the occurrence of a thrust fault between the Miramichi and Sheephouse Brook Groups. In the end, geophysics cannot provide all the answers and this map may be further refined through the addition of new geophysical, geological, and geochemical studies that are currently and will be conducted in the future.

CHAPTER FIVE

Conclusion

The primary objective of this thesis was to address limitations imposed by current geophysical processing and interpretations methods. With geophysical surveys becoming more widely used, these limitations need to be regarded with the upmost importance in order to derive the most geologically sound model possible. A few important limitations were discussed and their effects were exhibited through the analysis of three case studies. Furthermore, in some instances, alternative measures were successfully applied to both synthetic and real-world datasets to minimize these limiting effects.

Chapter 1 presented the intended project objectives alongside an overview of all appropriate acquisition, processing, and correction methods used throughout this thesis. Emphasis was placed on magnetic survey datasets since that was the primary data source in all chapters.

Chapter 2 presented limitations imposed by the preferred processing domain, Fast Fourier Transforms (FFT), for geological interpretations. Although, there are many advantages associated with frequency domain processing such as rapid analysis of large datasets, there are disadvantages to the method. These disadvantages, such as induced corrugation effects, prevent the interpretation of a geologically sound model. A spatial domain filter, based on the curvature analysis of a potential field signal was proposed as an alternative to FFT. This method was applied to both synthetic and real-world situations. In the case of shallow, near-surface structure, the curvature routine successfully separated high frequency signal generated by the depth to bottom. However, when analytic routines such tilt-depth method and Euler deconvolution were applied to this filtered dataset, it was apparent that despite regional-residual separation, there was remaining signal interference that tainted the solution depths. That being said, the results were more accurate than the depth solutions produced by the unfiltered dataset. This stresses the importance that a segregation routine needs to be implemented prior to any sort of interpretation. And although the solution depths were not perfect, they did reduce the amount of associated error in depth calculations. When the segregation routine was applied to the field dataset over the Porcupine Destor-Pipestone Fault area, all high-frequency signatures related to dykes, kimberlites, and faults were very well isolated. When depth estimators were applied, the expected results were achieved - the filtered dataset produced on average more shallow/near-surface depths compared to the depths produced by the unfiltered dataset.

Chapter 3 presented the effects of varying source-signal separation in magnetic surveys. In the case of a ground magnetic survey conducted over the Eye-Dashwa Lakes pluton near Atikokan, Ontario, initial magnetic lows were interpreted as being produced zones of alteration. However, in hindsight to the original survey, proper terrain corrections were not applied. This chapter conducted the necessary terrain corrections using a Taylor Series expansion method. It was shown that these previous linear zones of alteration were actually generated by unaccounted bathymetry in the study area. Post-terrain analysis, the valid zones of alteration could be distinguished at this point and it was shown that there are still NW-SE running alteration zones and that the granite is not homogeneous. This supports the results from those acquired in previous borecore studies, which to date are the most reliable means of fracture mapping since they are not limited by outcrops or by interference of signal from nearby rock lithologies.

Finally, **Chapter 4** presented a re-assessment of the 1:50 000 geologic map over the Bathurst Mining Camp in New Brunswick, Canada. With an increase pressure on Canada's base metal preserved, a more thorough understanding of potential mineralized regions is necessary. This is possible through an integrated geological map. It became evident that previous geological maps were primarily based on limited in-situ field samples and the electromagnetic datasets. However, through the careful consideration of additional airborne and geophysical datasets many of these geological boundaries could be refined. One significant change is the lack of geophysical evidence supporting the occurrence of roof-pendant in the large granitic intrusion cutting the Sheephouse Brook block. As such, this small occurrence of Chain of Rocks has been removed; however through future studies, like borecore, it may be shown that an outlier does exist at this location of a same geophysical signature as the surrounding granite intrusion. Furthermore, through an integration of local and large scale trends, a thrust fault was interpreted to occur along the contact between the Miramichi and Sheephouse Brook Groups.

Limitations

It will always be impossible to avoid all limitations in geophysical processing and interpretation. Even in this project, the processing and final interpretations were still influenced by imposed restrictions by the respective geophysical survey method. The primary dataset used in all chapters was magnetics, which, along with gravity, suffer the drawback of there being an infinite number of solutions for all anomalies. As mentioned, a short wavelength can only be produced near-surface features; however, a long wavelength may be produced features at any varying depth. This causes a limitation in the attempt at wavelength separation dependant on finding features at a specific depth. Unfortunately, there is no quantitative way in which to accurately solve the infinite solution problem. That is why multi-parameter investigations are key to a reliable and accurate geological model. Similarly, multi-parameter investigations aid in another limiting affect. All interpretations were calculated on the basis of some physical property contrast. However, if two juxtaposed rocks have the same physical properties, no contacts will be resolved.

Finally, magnetic remanence was not considered in all case studies due to time constraints and to maintain simplicity. However, magnetic remanence is an important consideration when conducting interpretations on any magnetic dataset. It is recommended that in any future studies developing on the discussed case studies should be addressed.

Significance

This thesis offers straight forward recognition of the problems faced with contemporary geophysical processing and interpretations, which are often not fully appreciated or completely ignored. In the case of the curvature based filtering, this methodology may be further refined on a more quantitative level where depths may be more reliably measured. This can be accomplished in a number of different ways including histogram analysis. Ultimately, this crude curvature based filtering method acts as a precursor to the future development of spatial domain filters.

It was the aim of this project to bring awareness to the effects of terrain magnetic survey data and that it should become a standard step in magnetic data processing. It is interesting to note that in spite of terrain induced effects tainting final interpretation results, the effect of source-signal has been shown to be useful in determining bathymetry in field areas where measurements may not be feasible.

Finally, with an offered re-evaluation of the geologic structure of the Sheephouse Brook block, the methodologies used may be implemented in other areas of the Bathurst Mining Camp. This should be especially in areas of greatest economical potential, such as the Brunswick 12 deposit. Furthermore, since the TGI-3 project is still in progress, once new data is acquired, whether it be geological, geophysical, or geochemical, further assessment on the geology should be conducted using inter-disciplinary methods.

BIBLIOGRAPHY

Barnett, C. T., 1976. Theoretical modeling of the magnetic and gravitational of an arbitrarily shaped three-dimensional body. Geophysics, 41 : 1353.

Blakely, R.J., 1995. Potential Theory in Gravity and Magnetic Applications. Cambridge University Press, 441 pp.

Brown, P.A., Kamineni, C., Stone, D., and Thivierge, R.H., 1980. General Geology of the Eye-Dashwa Lakes Pluton, Atikokan, Northwestern Ontario. Atomic Energy of Canada Limited Technical Record, TR-108, 14 pp.

Brown, P. A., Stone, D., and Rey, N., 1984. Criteria for Selecting New Areas for Geological Investigation within the Eye-Dashwa Lakes Pluton, Atomic Energy of Canada Limited Technical Record, TR-237, 26 pp.

Chomyn, B.A., Lapointe, P., Morris, W.A. and Coles, R.L., 1986. Application of magnetic susceptibility within crystalline rocks, *In:* Borehole Geophysics for Mining and Geotechnical Applications, ed. P.G. Killeen. Geological Survey of Canada, 85 (27) : 227-236.

Coles, R., 1981. Magnetic properties of rock: assessment of geoscience methods of rock mass evaluation. Earth Physics Branch, Energy Mines and Resources, internal report.

Cowan, D.R., Cooper, G.R.J., and Cowan, S., 2001. Reducing cross-profile aliasing in aeromagnetic data. ASEG Extended Abstract, 15

Dugal, J.J.B., Hillary, E.M., Kamineni, D.C., and Sikorsky, R.I. 1981. Drilling and core logging programs at the Atikokan research area, Atomic Energy of Canada Limited Technical Record, TR-174, 62 pp.

Environmental Systems Research Institute Canada Inc. (ESRI Canada), 1997. ArcCanada CD-ROM, Schools and Libraries Edition, version 1.0

Flis, M.F. and Cowan, D.R., 2000. Aeromagnetic drape corrections applied to Turner valley Syncline, Hammersley Basin, Exploration Geophysics, 31 : 84-88.

Fyffe, L.R., 1995. Regional geology and lithogeochemistry, in the vicinity of the Chester VMS deposit, Big Bald Mountain area, New Brunswick, Canada. Exploration Mining Geology, 4 (2) : 153-173.

Geological Survey of Canada, 2007. EXTECH: Exploration Science and Technology Initiative. EXTECH II: Bathurst Mining Camp N.B. http://gsc.nrcan.gc.ca/extech/extech2_e.php. October 20, 2007.

Grauch, V.J.S. and Campbell, D.L., 1984. Does draping aeromagnetic data reduce terrain-induced effects? Geophysics, 49 (1) : 75-80.

Goodfellow, W.D., McCutcheon, S.R., and J.M. Peter, 2003. Massive Sulfide Deposits of the Bathurst Mining Camp, New Brunswick, and Northern Maine: Introduction and Summary of Findings. Economic Geology, Monograph 11 : 1-16

Harding, K.A., Morris, W.A., Balch, S.J., Lapointe, P., and A. G. Latham, 1988. A comparison of magnetic character and alteration in the three granitic drill cores from eastern Canada. Canadian Journal of Earth Sciences, 25 : 1141-1150.

Hearst, R. B., and Morris, W.A., 2001. Case History: Regional gravity setting of the Sudbury Structure. Geophysics, 66 (6) : 1680-1690.

Hildenbrand, T. G., Rosenbaum, J. G., and J. P. Kauahikaua, 1993. Aeromagnetic Study of the Island of Hawaii. Journal of Geophysical Research, 98 (B3) : 4099-4119.

Hillary, E.M., 1982. Geometric representation of subsurface fracturing in boreholes ATK-1, ATK-2, ATK-3, ATK-4 and ATK-5, Atikokan, Northwestern Ontario (RA 4), Atomic Energy of Canada Limited Technical Record, TR-182 : 38 pp.

Hillary, E.M., McEwen, J.H. and Rey, N.A.C., 1985. The evaluation of fracture zones at the Atikokan Drill site and their geophysical response, Atomic Energy of Canada Limited Technical Record, TR-299 : 26 pp.

Kamineni, D. and Stone, D., 1983. The ages of fractures in the Eye-Dashwa Pluton, Atikokan, Canada. Contributions Mineral Petrology, 83 : 237-246.

Keating, P., and Pilkington, M., 2004. Euler deconvolution of the analytic signal and its application to magnetic interpretation. Geophysical Prospecting, 52 : 165-182.

Keating, P., Thomas, M., and Kiss, F., 2003. Significance of a High-Resolution Magnetic and Electromagnetic Survey for Exploration and Geologic Investigations. Bathurst Mining Camp, Economic Geology, Monograph 11 : 783-798.

Lapointe, P., Morris, W.A., and Harding, K.L., 1986. Interpretation of magnetic susceptibility: a new approach to geophysical evaluation of the degree of rock alteration. Canadian Journal of Earth Sciences, 23 : 393-401.

Li, Y., and Oldenburg, D.W., 1996. 3-D inversion of magnetic data. Geophysics, 61 (2) : 394-408.

McCutcheon, S.R., Luff, W.M., and Boyle, R.W., 2003. The Bathurst Mining Camp, New Brunswick, Canada: History of Discovery and Evolution of Geologic Models. Economic Geology, Monograph 11 : 17-35.

Mickus, K.L., Aiken, C.L.V., and Kennedy, W.D., 1991. Regional-residual gravity anomaly separation using the minimum-curvature technique. Geophysics, 56 (2) : 279-283.

Miller, H. G., and Singh, V., 1994. Potential field tilt - a new concept for location of potential field sources. Applied Geophysics, 32 : 213-217.

Morris Magnetics Inc., 1985. Identification of Fracture/Alteration Zones Using Ground-Based Magnetic Surveys in the Atikokan Research Area (1984-1985). Unpublished report available from Morris Magnetics Inc., RR#2, Lucan, Ontario.

Morris, W. A., Leblanc, G., and Prevac, L., 2002. An alternative simple procedure to identify magnetic and other geophysical anomalies due to kimberlite pipes. SEG Expanded Abstracts, 21 : 712-715.

National Geophysics Database (NGD), 2008. Geoscience Data Repository, Geological Survey of Canada, Earth Sciences Sector, Natural Resources Canada, Government of Canada.

Nettleton, L. L., 1940. Geophysical prospecting for oil. New York, McGraw-Hill : 1-444.

Ontario Geological Survey (OGS), 2004: Ontario airborne geophysical surveys, magnetic data, Central Abitibi Destor Porcupine – Pipestone Faults Area; Ontario Geological Survey, Geophysical Data Set 1049.

Pfeiffer, K., Direen, N.G., and Sexton, M., 2004, Exploration under regolith cover, and the problem of remanent magnetism: An example from the Tanami au Province. Regolith 2004 : 269-272.

Parasnis, D.S., 1962. Principles of Applied Geophysics. London, Chapman and Hall Limited : 1-214.

Pilkington, P. and Thurston, J.B., 2001. Draping corrections for aeromagnetic data: line- versus grid-based approaches. Exploration Geophysics, 32 : 95-101.

Phillips, J.D., Hansen, R.O., and Blakely, R.J., 2007. The use of curvature in potential-field interpretation. Exploration Geophysics, 38 : 111-119.

Reid, A.B., Allsop, J.M., Granser, H., Millet, A.J., and Somerton, I.W., 1990. Magnetic Interpretation in 3 dimensions using Euler deconvolution. Geophysics, 55 (1) : 80-91.

Rogers, N., 2008. TGI-3 Appalachians. Presentation at Geological Association of Canada, Newfoundland 2008.

Roberts, A., 2001. Curvature attributes and their application to 3D interpreted horizons. First Break, 19.2 : 85-100.

Salem, A., William, S., Fairhead, D., Ravat, D., and Smith, R., 2007a. Tilt-depth method: A simple depth estimation method using first-order magnetic derivatives. The Leading Edge, December : 1502-1505.

Salem, A., William, S., Fairhead, D., Smith, R., and Ravat, D., 2007b. Interpretation of magnetic data using tilt-angle derivatives. Geophysics, 73 (1) : L1-L10.

Service New Brunswick, 2007. Geographic Data and Maps – Products and Services. http://www.snb.ca/gdam-igec/e/2900e_1.asp. October 18, 2007

Sharma, P.V., 1997. Environmental and engineering geophysics. Cambridge University Press, 475 pp.

Shives, R.B.K., Ford, K.L., and Peter, J.M., 2003. Mapping and Exploration Applications of Gamma Ray Spectrometry in the Bathurst Mining Camp, Northeastern New Brunswick. Economic Geology, Monograph 11 : 819-840.

Smith, R.S., Thurston, J.B., Dai, T., and MacLeod, I.N., 1998. iSPI™ – the improved source parameter imaging method: Geophysical Prospecting, 46 : 141-151.

Spector, A., and Grant, F.S., 1970. Statistical Models for Interpreting Aeromagnetic Data. Geophysics, 35 (5) : 293-302.

Stone, D., 1980. Distribution of Near-vertical fractures in the Dashwa Pluton, Atikokan, Ontario, Atomic Energy of Canada Limited Technical Record, TR-125 : 43 pp.

Stone, D. and Kamineni, D., 1981. Fractures and fracture infillings of the Eye-Dashwa lakes pluton, Atikokan, Ontario. Canadian Journal of Earth Sciences, 19 : 789-803.

Telford, W.M., Geldart, L.P., Sheriff, R.E., and Keys, L.P., 1976. Applied Geophysics. Cambridge University Press, 860 pp.

Thomas, M.D., 2003. Gravity Signatures of Massive Sulfide Deposits, Bathurst Mining Camp, New Brunswick, Canada. Economic Geology, Monograph 11 : 799-817.

Thomson, V.L., 2004. Integrating aeromagnetics, remote sensing, and magnetic modelling to understand 3D geologic structure – applications to mineral exploration, McMaster University, Hamilton, xi + 171 pp.

Thurston, J. B., and Smith, R.S., 1997. Automatic conversion of magnetic data to depth, dip, and susceptibility contrast using the SPI (TM) method. Geophysics, 62 (3) : 807-813.

Ugalde, H. and Morris, B., 2008. An assessment of topographic effects on airborne and ground magnetic data. The Leading Edge, January : 76-79.

van Staal, C.R., Wilson, R.A., Rogers, N.A., Fyffe, LR., Langton, J.P., McCutcheon, S.R., McNicoll, V., and Ravenurst, C.E., 2003. Geology and Tectonic History of the Bathurst Supergroup, Bathurst Mining Camp, and Its Relationships to Coeval Rocks in Southwestern New Brunswick and Adjacent Maine – A Synthesis. Economic Geology: Monograph 11 : 37-60